



**A MODEL ANALYSIS OF AN ACTIVE VEHICLE
SUSPENSION SYSTEM USING HYDRAULIC CONTROL**

A THESIS SUBMITTED FOR THE DEGREE OF
MASTER OF ENGINEERING SCIENCE

MECHANICAL ENGINEERING FACULTY
DEPARTMENT OF ENGINEERING,
UNIVERSITY OF ADELAIDE

BY

PETER CHAPLIN B.Eng.

13 APRIL 1996

SYNOPSIS

The aim of this study was build and evaluate the performance of a laboratory active suspension. Much has been published on active suspension theory but relatively few have actually been built and reported on. This study examines the performance of two types of active suspension controllers and the performance of a hydraulic control system used to generate the active force.

A quarter car model is used to represent the major dynamic modes for a simple active suspension. A Linear Quadratic Regulator (LQR) controller is designed with a weighted performance index. Two variants of this controller are studied: an optimal and a sub-optimal type with reduced state variable feedback. Of particular note is that an optimal controller is able to be produced without measuring the road input to the suspension. The controllers are optimised by minimising the performance index using the Ricatti equation.

A "frequency shaped" LQR controller is also studied. This employs a conceptual filter with an output made up from system state variables. The filter is included as a cost function in the weighted performance index. Thus the conceptual filter characteristics influence the calculated optimum feedback gains and effectively implement a filter without the physical hardware and without the disadvantages of time delays that a physical filter would introduce.

A laboratory suspension was built and tested. A main area of interest was the performance of the inner loop, which generates the active force required by the controller. This loop must faithfully reproduce the required force from an electrical signal. The loop did not perform as expected due to inadequate system gain available from the servo valve. This is despite the valve being aduadtely sized for the pressure and maximum flow rate demands of the system.

A model of the system was developed and used to predict the performance and to analyse potential system improvements. The results show that a redesigned servo valve with much greater flow gain is required in order to achieve a satisfactory performance.

TABLE OF CONTENTS

Section.	Page
CHAPTER 1 - INTRODUCTION	
1.1 Background	1
1.2 Fully Active Suspension Controller Summary	8
1.3 Conclusions	10
1.4 Objectives of Present Work	10
CHAPTER 2 - DESIGN OF AN ACTIVE SUSPENSION CONTROL LAW	
2.1 Considerations in the Design Process	11
2.2 Road Surface Models	11
2.3 Model Characteristics	13
2.4 Selection of Performance Measurement Criteria	21
2.5 Determination of a Control Law	23
CHAPTER 3 - CONSTRUCTION OF THE EXPERIMENTAL SUSPENSION	
3.1 General Layout of the Experimental Suspension	35
3.2 Design of Hydraulic Servo and Actuator	42
3.3 Instrumentation	45
3.4 Parameter Measurement and Calibration	54
CHAPTER 4 - CALCULATIONS AND COMPUTER SIMULATION	
4.1 Calculation of Optimum Feedback Gains	58
4.2 Computer Simulation of Suspension Theoretical Performance	62
CHAPTER 5 - RESULTS	
5.1 Theoretical Suspension Performance	73
5.2 Experimental Results	76
5.3 Computed Results	85
5.4 Discussion	88
5.5 Summary and Conclusions	93
5.6 Recommendations for Future Study	94

LIST OF FIGURES AND ILLUSTRATIONS

Figure.	Page
CHAPTER 1	
1.1 1/4 Car passive suspension model.	2
1.2 1/4 Car active suspension model	5
CHAPTER 3	
3.1a Experimental 1/4 car active suspension test rig.	36
3.1b Experimental 1/4 car active suspension test rig. Close up photograph showing hydraulic actuator and servo valve assembly.	37
3.1c Experimental 1/4 car active suspension test rig. Analogue computer and instrumentation amplifiers.	38
3.1d Experimental 1/4 car active suspension test rig. Summary of physical data.	39
3.2 Hydraulic system and actuator arrangement.	41
3.3 Servo valve frequency response; operating at 100% design current.	43
3.4 Servo valve load pressure versus output flow performance.	43
3.5 Integrator design.	47
3.6a Integrator gain performance.	48
3.6b Integrator phase performance.	49
3.7 Low pass filter design and performance.	50
3.8 Analogue computer circuit design.	53
3.9 LVDT calibration curve.	54
3.10 String potentiometer calibration curve.	55
3.11 Load cell calibration curve.	57
CHAPTER 4	
4.1a Pascal code for the derivatives subroutine used in computer simulation program.	63
4.1b Variables and constants used in computer simulation program.	65
CHAPTER 5	
5.1 Theoretical suspension performance for the optimal and sub-optimal LQR controllers.	73
5.2 Theoretical suspension performance for the 'frequency shaped' controller.	74
5.3 Comparison of frequency response of theoretical and modelled laboratory suspension with sub-optimal controller.	75

Figure.	Page
5.4 Comparison of frequency response of theoretical and modelled laboratory suspension with frequency shaped controller.	76
5.5 Typical recorded response with step input, sub-optimal LQR controller.	78
5.6 Typical recorded response with sinusoidal input, sub-optimal LQR controller.	79
5.7 Typical recorded displacement for a step response, showing body and axle motion prior to and after the step input, sub-optimal LQR controller.	80
5.8 Body and axle frequency responses for the original set-up of the laboratory suspension; sub-optimal LQR controller.	82
5.9 Body and axle frequency responses for the laboratory suspension with servo loop gain doubled; sub-optimal LQR controller.	84
5.10 Comparison of typical simulated and recorded step responses, LQR controller.	85
5.11 Modified section of the derivatives subroutine to include internal actuator leakage.	86
5.12 Simulated axle step responses with increasing C_{sp} .	87
5.13 Simulated body step responses with increasing C_{sp} .	88
5.14 System block diagram.	91
5.15 Simplified system block diagram.	92

STATEMENT OF ORIGINALITY

This work contains no material which has been accepted for the award of any other degree or diploma in any university or other tertiary institution and, to the best of my knowledge and belief, contains no material previously published or written by another person, except where due reference has been made in the text.

I give consent to this copy of my thesis, when deposited in the University Library, being available for loan and photocopying.

PETER CHAPLIN
13 APRIL 1996

ACKNOWLEDGEMENTS

I wish to express sincere appreciation to my supervisors Dr. A.G. Thompson and Dr. M. Wahab of the Faculty of Mechanical Engineering, University of Adelaide in providing guidance and support. Thanks also to the Defence Science and Technology Organisation, Bridgestone Australia Pty. Ltd., Dr. B.R. Davis of the Faculty of Mathematics, University of Adelaide and to Mr. H. Bode of Mechanical Engineering, University of Adelaide for assistance with the building of the laboratory suspension.

GLOSSARY OF TERMS AND VARIABLES

a	wave number (cycles/metre).
A, B, C, D, F, G	constant matrices which contain the system characteristics.
b ₁ , b ₂	arrays containing system characteristics.
λ	tyre spring rate (Newtons/metre)
F _a	matrix of system characteristics, frequency shaped suspension.
G _a	array of feedback gains, frequency shaped suspension.
H	array defining system output.
i	drive current to servo-valve.
J	performance index.
K, K _a	array of feedback gains which minimises J.
K _p	PID filter proportion feedback gain.
K _d	PID filter damping feedback gain.
K _i	PID filter integral feedback gain.
K _v	constant for servo-valve.
k _a	acceleration feedback gain.
k _b	acceleration feedback gain.
k _s	relative displacement feedback gain.
k _d	damping feedback gain.
k _v	velocity feedback gain.
k ₁ , k ₂ , k ₃ , k ₄	feedback gains.
m ₁ , M ₁	axle mass
m ₂ , M ₂	body mass
P	positive definite symmetric solution to Riccati equation.

ΔP	pressure difference across actuator.
Q	weighting matrix.
q_1, q_2	weighting factors.
r, R	weighting factor.
$S(a)$	road profile vertical displacement spectral density (metre ³ /cycle).
$u_n(t)$	n dimensional external input to the system.
u, u_{opt}	active force, produced by suspension actuator.
V	vehicle forward velocity (metre/second).
$\Psi, \Psi(t)$	road profile frequency (radians/second).
$x_n(t)$	n dimensional vector of system state variables.
x_0	road input displacement
x_1	axle displacement
x_2	body displacement
\dot{x}_1, \dot{x}_3	axle velocity
\dot{x}_2, \dot{x}_4	body velocity
\ddot{x}_1, \ddot{x}_3	axle acceleration
\ddot{x}_2, \ddot{x}_4	body acceleration
$Y_1(s)$	PID filter input.
$Y_2(s)$	PID filter output.
$y_n(t)$	n dimensional system output, ie: the response of the system.
∂, n	values representing the road surface condition, determined experimentally for each type of road profile.



A MODEL ANALYSIS OF AN ACTIVE VEHICLE SUSPENSION SYSTEM USING HYDRAULIC CONTROL

CHAPTER 1

INTRODUCTION

1.1 Background

Vehicle suspension systems have developed from the need to isolate passengers or cargo from vibrations caused by the vehicle's wheels as it rolls over a road surface. The development began in the days of the horse drawn carriage and made little significant progress until the advent of the motor vehicle. Around the time that motor vehicles began to be mass produced, in the early 1900s, the problem of improving the performance of the suspension systems became of interest. Suspension systems' development has progressed to where three broad classes can be defined; passive, semi-active and active.

Passive type suspensions are those where all of the energy imparted to the suspension components is from the forward motion of the vehicle over the road surface; the components of the suspension only dissipate or store energy. Active suspensions have the same overall aims as passive suspensions but use an externally generated force to influence or supplement the vertical motion of the vehicle. In order to do this, these suspension systems use an actuator which either directly applies forces within the suspension or alternatively provides a small force to actuate a variable rate spring or damper. The former is said to be fully active and the latter type, semi-active suspensions.

Vehicle suspensions have virtually always been of the passive type. They use a spring and damper between the axle and body. The complete system is then comprised of the unsprung mass of the wheel and axle assembly (supported by the tyre) through which the road surface undulations are transmitted to the sprung mass of the vehicle body via the main spring and damper arrangement. A simple model of this suspension at each wheel is one where the body and axle are represented by lumped masses, and is effectively a two

degree of freedom dynamic system, if only the vertical motions are considered. This is shown in Figure 1.1.

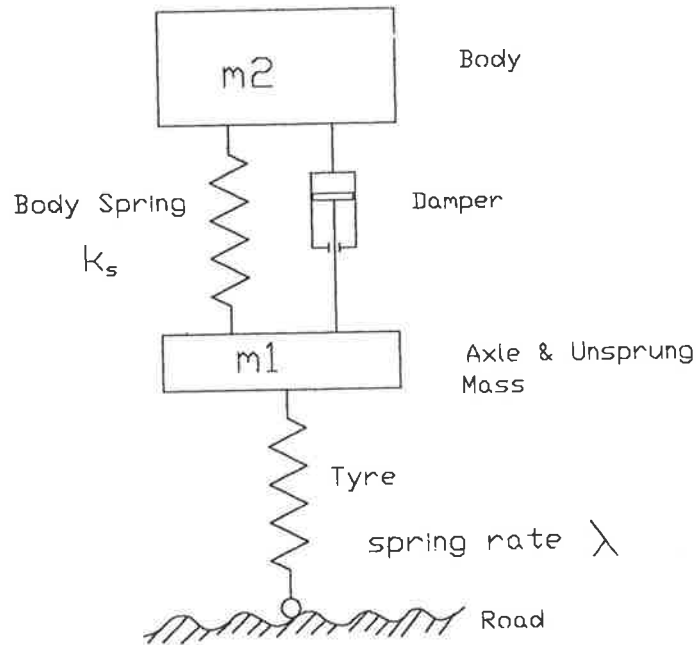


Figure 1.1 1/4 car passive suspension model.

The tyre stiffness is such that for practical motor vehicle suspensions the resonant frequency of the tyre and axle, sometimes referred to as the "wheel hop" frequency, is in the range of five to ten times greater than that of the body on the main suspension spring. Road inputs are attenuated through tyre and spring compliance, providing ride comfort. Inputs near the wheel hop frequency are amplified in the motion of the axle, creating high dynamic tyre deflections which significantly influence the vertical forces of the tyre on the road and so limit the lateral forces applicable to the tyres without slipping on the road surface.

The suspension damping is provided to limit the body and axle amplitude response near system resonances. Dampers typically used are hydraulic and produce a damping force proportional to the relative velocity of the body and axle. Additionally, some Coulomb (dry) friction is always present, which has a serious detrimental effect on the suspension performance. Friction prevents suspension movement until overcome by the disturbing force, implying that there is a minimum level of roadway force input which will always be transferred to the body. The choice of spring and linkage mechanism in a suspension has a major effect on the amount of inherent friction in the system. Morman & Giannopolous (1982) reported that the inherent friction in practical suspension systems can be as high as 5-10% of static load in coil sprung independent front suspensions and 15-30% for a leaf sprung rear axle arrangement. This has a significant effect on the performance of a suspension and is one reason why coil springs have supplanted leaf springs in most passenger vehicle suspension applications.

The original suspension requirement of smoothing the ride for occupants was soon extended to include provision of an acceptable level of vehicle handling. This includes control of body roll, maintenance of adequate tyre to road contact to prevent slippage, control of body pitching during braking and acceleration and response to disturbances such as lateral wind gusts and road camber changes. Invariably the selection of suspension characteristics that best suits a smooth ride for the occupants does not provide the best handling capabilities. This is because high spring stiffness and damping are required to limit deflections of the axle at the axle resonant frequency whereas much lower stiffness and damping are necessary in order to allow greater axle and body deflections to limit the level of force transmitted to the body for a smooth ride.

Additionally, typical road vehicle suspensions are not designed for optimum performance at a unique and well defined condition. They must instead be designed to provide acceptable performance over a wide range of road conditions, vehicle load states and vehicle speeds.

Large variations in vehicle load causes static deflection of the suspension, consuming some of the available suspension displacement. The available displacement is limited by external factors such as overall vehicle height and vehicle body styling. Additional spring stiffness can be added by supplementary springs to keep the vehicle body static deflection within acceptable levels. One example of these are "load leveller" pressurised gas springs mounted in parallel with the primary vehicle springs, where the spring rate is determined by the air pressure employed by the vehicle operator.

Further to the requirements of providing smooth ride and adequate handling, the suspension must also provide an acceptable response to extreme disturbances such as potholes, when the tyre loses contact with the road surface. This requirement leads to the use of much higher rebound damping rates (Sharp & Crolla, 1987), although the actual rates selected by motor vehicle manufacturers appears to be highly subjective. It is understood that this gives the suspension an improvement in the pothole response by either improving the vertical acceleration response (subjectively judged as better) or by reducing the longitudinal forces input into the vehicle by limiting the vertical travel of the wheel into the pothole. This asymmetry could lead to additional difficulty in modelling of the suspension systems, however Thompson (1969-70) reports that even quite large asymmetries have little effect on the response to random road inputs, when the average damping values are assumed.

In summary it is evident that a typical vehicle suspension system's design is a compromise of a number of characteristics:

- i) the ride comfort, or vibration isolation provided to the occupants.
- ii) the handling qualities imparted.
- iii) the available suspension travel, set by physical constraints of the vehicle.
- iv) the static deflection of the vehicle body when varying loads are applied ie: the static stiffness of the springs.

The intended application of the vehicle will dictate the bias placed on each of the above characteristics in order to reach the desired compromise.

A fully active suspension system employs an actuator placed to exert a controlled force, velocity or displacement between the body and the axle. This is shown diagrammatically in Figure 1.2.

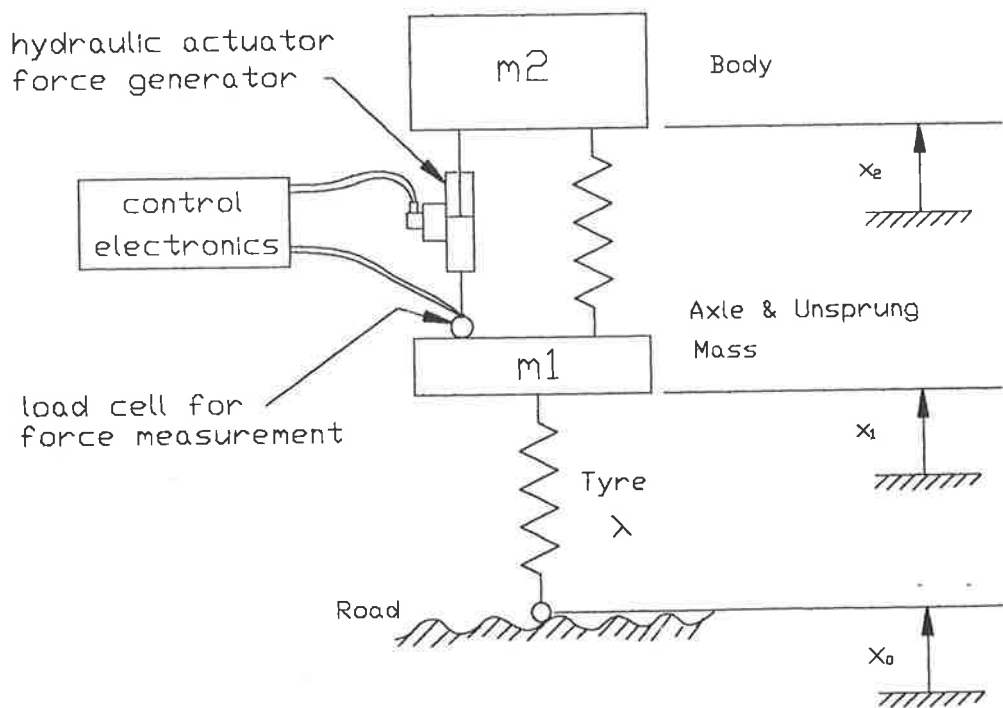


Figure 1.2 1/4 car active suspension model.

Hydraulic actuators are typically assumed to be the most suitable due to the high power output being readily produced. When controlled by a servo valve, these actuators are able to provide the required motions at frequencies covering the body/spring and tyre/wheel resonances. This enables the choice of a control law which is able to directly influence the motions of both the body and the axle. Control of the body resonance is required to limit

the accelerations induced in the body and reducing ride comfort. Control of the axle resonance minimises the dynamic tyre forces which reduce the wheel to road surface contact forces and thereby reduce road holding capability and also braking distances.

Ideally an active suspension would be able to achieve an improvement in the trade-off between vehicle handling, wheel travel and ride comfort by controlling resonances of the body and axle in a way that is not possible to achieve with a passive suspension (Margolis, 1982). For instance, a passive suspension can only provide damping according to the relative velocity between the body and axle whereas an active system can provide 'skyhook' damping (that is damping which is based upon the absolute velocity of the body or axle). This produces the characteristic of being able to specify the damping of the sprung and unsprung masses independently, unlike the passive suspension where the damping for both masses is not independent (Gordon et al., 1991). Another potential advantage of an active suspension is the ability to provide frequency dependant damping. Mitschke (1986) proposed that damping could be as high as possible over the ranges 0 to 2 Hertz and 10 to 12 Hertz. Damping should be zero at all other frequencies. This would give high damping at the body and axle resonant frequencies, where amplitude control is required. Zero damping at other frequencies provides improved ride comfort.

Thompson and Davis have suggested (Thompson & Davis, 1988) that an active suspension will exhibit a lower natural frequency for the vehicle body. Since active and passive systems show similar characteristics for any particular application, if the same limits are placed upon dynamic tyre deflections and suspension travel, an advantage of the active system is that it can be designed with a lower body resonant frequency but still retain excellent static stiffness to resist variations in vehicle load and manoeuvring forces (Karnopp, 1986; Thompson & Davis, 1988; ElMadany, 1990). This will lower body accelerations and improve ride comfort in a way which is not realisable with a passive suspension. Thus one of the constraints limiting suspension design can be dealt with

without compromising the system performance as is required in the case of a passive suspension.

A further advantage offered by active systems is that of adaptability, where the suspension characteristics can be altered in real time to allow virtually instantaneous adjustments under control of an on-board computer, to optimise the suspension to allow for the exact conditions of vehicle speed, road surface condition cornering force, desired body reactions due to cornering and braking, the level of comfort desired by the occupants or any other parameter which can be measured or estimated by on board sensors or directly controlled under command of the vehicle occupants (Fruehauf et al, 1985). Thus the vehicle could be made to provide optimum handling characteristics when cornering and a smooth ride at other times. Whether such schemes are worth the additional complexity incurred is not clear and in fact the methodology used to develop an adaptive scheme which optimised system performance under all conditions may not yet be fully explored (Gordon et al 1991). For example, an active suspension system can be made to effectively simulate a passive suspension but allow real time adaptive control, as apparently used on Lotus Formula 1 racing cars for several years (Thompson & Davis 1991). While this is of course feasible it may not present the optimum active system control laws.

Only relatively few fully active suspensions appear to have been successfully operated, even in the laboratory. Several Formula 1 racing car types are well known to have used active suspensions. Lotus have also been developing active suspensions for road vehicles. Other examples are Yamaguchi et al (1993), Alleyne et al (1993), Yamashita (1993), Acker et al (1989), Williams (1985) and Sutton (1978), while Federspiel-Labrosse (1954) must have made one of the earliest attempts at producing an active vehicle suspension.

1.2 Fully Active Suspension Controller Summary

The active element of an active suspension system must be controlled to perform the designer's requirements by some type of controller. This may be designed using classical control theory such as root locus analysis or by employing modern control techniques based on state variable analysis. In general there is no particular method which is uniquely suited to active suspension control law design, since there are inevitable trade-offs to be made with any method regarding controller performance, robustness (ie: the degree of sensitivity of the controller to changes in system parameters or imperfections of the model), number of required sensors for measuring system parameters and the complexity of the design process. Williams (1985) made comparisons between a number of active suspension control laws including position control of the body, 'skyhook' damping and several linear controllers based on Kalman filtering and observers, where some of the state variables used for feedback control are estimated by the system rather than being measured directly. de Jager (1991) has performed a theoretical study comparing the performance of Linear Quadratic Regulator (LQR), Linear Quadratic Gaussian (LQG), Linear Quadratic Output Feedback (LQOF) and H_{∞} controllers. This appears to be the only study to date of H_{∞} control for this type of vehicle suspension. LQR theory uses directly measurable system state variables as the system feedback and employs an optimisation process to ensure a reasonable balance is found between the system output performance and the amount of active force produced by the actuator. This technique is commonly used by suspension researchers to formulate full state feedback control laws. LQG and LQOF are variants of the basic LQR technique. LQG is a generalisation of the LQR method to allow design using system states which are not sensed directly and LQOF is a simplified LQR controller where the feedback is restricted to be only a partial set of the system output states. LQG is a relatively more complex design procedure than LQR and LQOF requires fewer transducers for feedback but has a slightly inferior performance to LQR. Whereas the linear control methods mentioned minimise a performance index made up of system outputs in the time domain, the H_{∞} controller requires a search for the optimum controller in the frequency domain. H_{∞}

control systems are of interest because of robust performance in the presence of noise (Yamashita et al, 1993) and has certain advantages in choosing optimisation criteria over other LQR variants (de Jager, 1991), although their design is substantially more complex than for the linear methods.

Williams (1985) concluded that the most effective controller was skyhook damping which has a theoretically lower performance than the mathematically more sophisticated types. It gave the best actual improvement in performance when tested however, since it was more robust than the other methods investigated. Some further development of the modal observer controller may prove to provide the best performance. Modal control has also been investigated by Sutton (1978) which allows system eigenvalues to be readily placed as desired. This design method does not incorporate any optimisation procedure and so, as with classical methods, the design may not readily produce acceptable compromises in the key performance parameters that the modern optimal methods provide.

The study by de Jager (1991) concluded that there was only small differences in performance between the LQR, LQG and LQOF controllers, however the LQR is the simplest computationally and is the most robust of the LQR variants. The initial implementation of a H_{∞} controller performed poorly and additional studies would be necessary to further investigate this before any proper comparison could be made. Yue et al (1988) have proposed that the best overall designs for an active suspension were achieved using an LQG compensator with relative suspension deflection as the only feedback variable.

Non-linear control design methods have been studied, such as bilinear modelling of a system using varying spring and damping rates. This has been shown to provide significantly improved performance over a time invariant LQR system (Gordon et al,

1991 & Kimbrough, 1986). Alleyne et al (1993) have trialed a non-linear method to overcome the effects of actuator friction with good results.

1.3 Conclusions

Active suspensions can be designed to provide characteristics not realisable with a passive suspension, although the fundamental limitations of passive suspensions also affect the performance of active suspensions. Active suspension theory is still developing rapidly. A number of different design methods have been proposed, based on classical control methods, modern control theory and newly developing mathematical techniques. Currently there is no clear method that provides uniquely superior results.

No evidence was found of a standard method accepted amongst researchers for comparing the performance of various suspension control methods.

There are very few practical results reported in detail. It appears that there are working active suspensions where the status is unpublished due to commercial secrecy. The results that have been reported suggest that relatively simple active control schemes are likely to be the most effective despite theoretical advantages from more complex controllers.

1.4 Objectives of Present Work

The objectives of this study are to:

- a. Model the theoretical performance of an active vehicle suspension system.
- b. Experimentally measure the actual suspension performance of the active system.
- c. Evaluate the performance of the 'inner feedback loop' for force control.
- d. Compare the measured performances of the system against that predicted.
- e. Evaluate the validity of the control law of the active suspension and propose modifications to overcome any problems found.

CHAPTER 2

DESIGN OF AN ACTIVE SUSPENSION CONTROL LAW

2.1 Considerations in the Design Process

The design of the control is based on a mathematical model of an actual suspension, since this allows the suspension performance to be evaluated and altered with relative ease. There are many factors which must be considered in the design of an active suspension control law:

- a. The road surface. This is the primary input to the suspension and it must be modelled to reasonably represent true road surfaces.
- b. The type of model must be chosen. A simple model, such as the two degree of freedom quarter car type, may be used for basic evaluation of active control laws. Model complexity must increase to provide a more accurate performance prediction of a real vehicle. A model will be selected to incorporate only sufficient detail to validate the control law design as applied to a laboratory experimental suspension. The model must ensure that measurements of system performance parameters, used as inputs to the control law, should be able to be made readily and preferably without sophisticated devices.
- c. Selection of the performance measurement criteria. These must represent critical performance characteristics to provide a basis on which to compare the performance of a particular control law.

These considerations are discussed in detail in sections 2.2 to 2.6.

2.2 Road Surface Models

Many studies have shown that the profile of formed roadways can be satisfactorily described in terms of the vertical spectrum only, reports on this topic including Robson (1979), Bulman (1979) and Sayers (1986). A study by Kamash (1978) confirms this concluding that road surface irregularities mainly exhibit themselves as vertical displacements. Roadway induced longitudinal and lateral forces input to the vehicle are

primarily due to the design of the suspension linkages which cause coupling of the vehicle motions in all three axes. Aurell and Edlund (1989) also confirm that vertical vibrations are the most important roadway inputs with regard to the vibrations transmitted to the vehicle. The road models suggested by researchers such as Robson (1979) are of the form:

$$S(a) = \partial(a)^{-n} \quad (2.1)$$

where:

- $S(a)$ is the profile vertical displacement spectral density ($m^3/cycle$).
- a is the wave number (cycles/metre).
- ∂, n are values representing the road surface condition, determined experimentally for each type of road profile.

Equation 2.1 is equivalent to:

$$S(w) = \partial(2\pi V)^{n-1} (\Psi)^{-n} \quad (2.2)$$

where:

- V is the vehicle forward velocity (metres/second).
- Ψ is the profile frequency (radians/sec).

The actual measured values for ∂ and n vary considerably with the type of surface being evaluated. Measurements typically are made over the range of 0.01 to 10 cycles/metre with values for ∂ reported by Sharp & Crolla (1987) from 3×10^{-8} to 3000×10^{-8} with $n = 2.5$, while Bulman (1979) reports measurements of smooth and cross country profiles with ∂ in the range 0.6×10^{-5} to 60×10^{-5} with $n = 2$. Aurell & Edlund found values for ∂ of 3 for smooth roads and 2.5 for rough surfaces. The differences here are no doubt partly due to the diverse range of road surfaces being measured. Mitschke (1986) suggests that improvements in road construction have resulted in ∂ becoming smaller while n has become larger. Morman & Giannopolis (1982) conclude that from various reported data the exponent n seems to be about 2. A profile where $n = 2$ corresponds to a road surface with a white noise vertical velocity spectrum, which is of significant mathematical convenience and is hence often assumed by researchers. In reality the spectral density of road surfaces does not approach infinity at low frequencies as suggested by equation (2.2) so it is evident that

road surfaces may be better described by a coloured noise velocity spectrum ie: n not equal to 2. Thompson (1976) reports that the performance of a suspension optimised for a white noise input would only be slightly inferior in this case.

Whichever road spectrum is assumed, a practical difficulty arises in calculating the mean values of the system states or outputs. It is impractical to choose a pseudo-random time "segment" for repeatably applying the system input. The segment must be long and is unlikely to have a non-zero mean. Assuming that a white noise velocity spectrum is sufficiently representative has a unique mathematical property, in that the mean squared values of system state variables can be calculated instead by applying a step input and integrating the squared state variables to infinity. This feature is exploited when developing the system model in section 2.5.

2.3 Model Characteristics

2.3.1 Considerations.

Contemporary vehicle suspensions typically utilise a spring and viscous damper at each road wheel, retained by one of a variety of linkages and mechanisms. The springs and dampers have approximately linear characteristics, that is the spring deflections are directly proportional to applied axial loads and damping rates are proportional to the relative velocity between the body and axle. As discussed in section 2.1, vertical vibrations input from the road surface are the primary source of roadway induced disturbance to a moving vehicle. The suspension linkages have the primary design aim of controlling wheel movement to be (ideally) purely vertical. In practice, suspension systems possess many characteristics which influence the system performance to varying degrees and are required to cope with numerous other influences. The primary influences on suspension system performance are discussed in sections 2.3.2 to 2.3.10.

2.3.2 Horizontal force inputs.

The major horizontal forces affecting vehicle handling and ride are applied to the vehicle body during cornering or by cross winds. The centre of gravity of the body is above the roll centres for the front and rear suspensions due to practical considerations. This applies a rolling moment to the body as a result of the cornering force, which results in a weight transfer from the inner wheel track to the outer track. The rolling motion is uncomfortable for passengers and the weight transfer reduces the ability of the inner track tyres to maintain contact with the road and increases the tyre to road contact forces on the outer track which eventually will exceed the lateral capability of the tyre. Thus the lateral cornering loads that may be applied to either track without slippage on the road surface are reduced.

An active suspension seeks to control the vertical responses of the body and axle and conventional linkages will control the horizontal loads. Horizontal load input through the wheel hence need not be considered in the design of the suspension at a single wheel station, although the effect of horizontal loads from body motion should be considered.

2.3.3 Available suspension working space.

In order to produce vehicles with an acceptable coupling between pitch and bounce road inputs, it is advantageous that the front suspension natural frequency be lower than that of the rear suspension (Bastow, 1980). To facilitate this, passenger vehicles typically move the front mounted engine as far forward as possible. This means that the engine is mounted astride the front suspension and forces the suspension components outwards, severely limiting the available space. As a result, suspension control arm dimensions are limited. This often produces linkage arrangements which cause the disc of the wheel to move out of the desired vertical plane of movement. The limiting allowable value for the relative wheel movement is controlled by the amount of bump-stop clearance and by the amount of rebound clearance provided in the system.

2.3.4 Structural stiffness of the vehicle and suspension components.

This may influence the ride comfort and handling. It is unlikely that a typical motor car will demonstrate structural frequencies within the range of interest (0.5 to 10 Hertz). Structural stiffness is relevant in larger vehicles such as semi-trailers where ElMadany (1988) reported that the active suspension system could be used to control the resonances of the vehicle structure to improve ride quality. The axle, wheel and associated mechanism components for common passenger vehicle suspension systems may be considered as effectively rigid masses for the purposes of primary suspension component design since any natural modes of vibration are at frequencies substantially higher than those of interest in the design of the primary suspension characteristics.

2.3.5 Suspension spring characteristics.

When leaf springs are used with a rigid axle, the spring provides the location control of the axle as well as the spring element. This leads to a number of additional characteristics:

- a. The details of the mounting of the spring can provide a non-linear characteristic, which is sometimes used to stiffen the suspension in order to limit body static deflections when the vehicle is carrying additional loads.
- b. The twisting and sideways bending that the spring is subjected to when cornering increases the effective anti-roll spring rate substantially over what would be expected.
- c. The application of torque to the axle while accelerating and braking induces changes of body attitude.

Coil sprung suspensions avoid all of these characteristics at the expense of providing linkages to control the wheel movement in all directions other than vertical. The model for this study will use coil springs for simplicity.

2.3.6 Influence of the vehicle's engine assembly on suspension system response.

The engine/transmission assemblies constitute a significant portion of a typical vehicle mass and they are virtually always mounted on soft rubber mounts for noise isolation. This

arrangement can have a dramatic effect on the suspension system response over the front wheels (for a front mounted engine). Mitschke (1986) reports that the peak body vertical acceleration response can be approximately three times higher at the engine mounting frequency than would be predicted assuming that the engine was rigidly connected to the body, although lower accelerations result at the axle natural frequency. The problem is aggravated by low damping of the engine assembly and the trend for body weights to be reducing more rapidly than engine weights. The suspension vertical acceleration performance for the body at the rear axle is however little affected whether the engine assembly is resiliently mounted or fixed to the body.

Since the objective of this study is to analyse the fundamental control of the axle and body dynamics, the influence of engine mounting dynamics will not be further investigated, although it is clearly evident that for an accurate prediction of suspension performance these influences must be taken into account.

2.3.7 Tyre characteristics.

Tyres are complex to mathematically model in detail and exhibit non-linear and time dependent behaviour, by virtue of their construction from rubber compounds supported by a matrix of fabrics with highly directional properties. Further complicating the modelling of a rolling tyre is the changing contact patch of the tyre on the road surface, which varies depending on the vertical and lateral loads and also the shape of the road surface.

The 'envelopment' by the tyre of the roadway profile is reported by Captain et al (1979) to provide filtering of the input forces of wavelength shorter than 0.75m, which corresponds to approximately 22 Hertz and 37 Hertz at typical vehicle forward velocities of 60km/h and 100km/h respectively. These speeds are of prime interest in suspension design and so it can be considered that tyre envelopment limits the frequency range of roadway inputs which need be considered. Most importantly, this implies that the tyre transmits roadway forces effectively unfiltered at frequencies for which body and axle resonances occur.

Sharp & Crolla (1987) report that measurements on pneumatic tyres show that for most loads, radial force is directly proportional to deflection. This is supported by the measurements attached in Appendix 1, made by Bridgestone Australia Ltd on one type of commercially available tyre, where static and rolling measurements were made at a number of combinations of tyre pressures, rim sizes and rolling speeds. The static tests were made against a flat loading surface. The rolling tests were run against a drum of diameter 1.7 metres with a cleat on the drum causing the tyre excitation. In all cases the tyre stiffness can be considered as being very closely approximated by a linear relationship. Sharp & Crolla (1987) also report that tyre stiffness is considerably less when rolling and increases slightly with an increase of speed. The results in Appendix 1 support the latter point in that there is an increase of between 3% and 8% in stiffness between 60km/h and 100km/h, with the degree of increase apparently being dependent on tyre pressure. The results also show that the stiffness of the tyre tested is virtually the same at 60kph as when stationary. This may be because of the difference in tyre contact patch between the static and rolling tests and the effect of lower stiffness when rolling have been approximately cancelled out by the effect of the drum shape. It is apparent that making allowance for the changes in tyre stiffness would require either considerable complexity in a practical active suspension, or the design of a robust control system.

The damping rate of tyres is known to be significant in comparison to the damping rate of the suspension dampers, however the location of this damping within the suspension system means that it has little effect on active or passive suspension system performance (Sharp & Crolla, 1987; Lee & Hedrick, 1989). Thompson (1989) reports that for conventional type passive suspensions the tyre damping has negligible effect on suspension performance. For active suspensions, where the body is better isolated and forces transmitted from the axle are lower, tyre damping may become significant and could improve the overall system performance.

If accurate predictions of the performance of an active suspension were to be made it appears that the damping would need to be considered. It is also apparent that the considerable differences in tyre stiffness due to inflation pressure and vehicle speed would need to be included. However it is clear that the fundamental control of the suspension is not dependent on tyre damping and an undamped linear, coil spring will be used to simulate tyre stiffness.

2.3.8 Model type.

A representative model of a vehicle body and suspension is a 'full car' model which provides for pitch, bounce and heave of the vehicle body and the independent vertical displacement of each of the four axle and wheel assemblies, ie: seven degrees of freedom. This should allow a detailed study to be performed of suspension performance and so would provide a reasonably accurate representation of a real vehicle suspension performance (Barak & Sachs, 1985). As discussed in section 2.3.6, the addition of an extra degree of freedom would ideally be included to account for the significant effect of the engine. Such a model would certainly enable the major dynamic modes of the suspension system and their interaction to be studied. Lateral loads due to cornering could also be applied. The disadvantage of using this model though is the complexity of designing it and analysing the effect of changes on system performance. There is also additional complexity in the provision of two representative parallel roadway inputs which are time delayed between the front and rear wheels.

The quarter car model, as shown in Figure 1.1 is a significant simplification of a vehicle suspension. Only two degrees of freedom are considered, since the model represents the vertical motion of the axle and body supported by a tyre and a suspension spring at one corner of a vehicle. Although very simple, this is adequate since the purpose of this study is to analyse the effects of various control strategies for an active suspension on the resonances of the axle and body without coupling to other road wheels (Chalisani, 1982; Sharp and Crolla, 1987).

2.3.9 Inherent constraints.

Suspension performance has some defined limitations dependent only on the relative masses and the tyre stiffness. The control of body and axle motions are linked through the actuator or suspension forces being applied between the two masses, giving rise to 'invariant' relationships (Thompson, 1970-71; Lee & Hedrick, 1989; Yue et al, 1988) which define the compromises which must be made between body acceleration, dynamic tyre deflection and axle working space. For the quarter car model shown in Figure 1.1 it can be shown that:

- a. The frequency response of the body displacement will pass through a point at the axle resonant frequency $\sqrt{k_t/m_1}$ with amplitude $20 \cdot \log_{10}(m_1/m_2)$, regardless of the control law used for the active suspension.
- b. With a design change producing a reduction in dynamic tyre deflection, the body acceleration is reduced at low frequencies but increased at high frequencies and the suspension travel increases.
- c. With a design change producing a reduction in body acceleration, tyre deflection is reduced at low frequencies but is increased as the wheel hop frequency and suspension travel are increased.

Lee & Hedrick (1989) also show that similar relationships exist for a half car model and conclude that a full car model would also demonstrate similar characteristics.

2.3.10 Non-ideal actuator characteristics.

The control force required of an actuator in an active suspension, as dictated by the control laws used, is ideally reproduced accurately and without friction losses or phase lags. Real actuators suitable for a fully active suspension typically are a hydraulic cylinder controlled by a servo valve with some type of load sensing device in series with the cylinder to provide a feedback signal for the control loop. Pneumatic and electric actuators could conceivably be used although pneumatic actuators with sufficient bandwidth are not readily available and

permanent magnet direct current motors are available where the performance and weight approach that available from hydraulic systems, however they are not often used.

The typical hydraulic actuator does have significant levels of friction, does incur a phase lag and may introduce additional resonances into the system. Common engineering design practice allows for 5-15% of the actuator force to be lost as seal friction. This, in combination with friction introduced through the suspension springs and mechanisms is enough to severely affect the performance of a control system. Sharp & Crolla (1987) report that friction forces should be less than 40N for a medium sized car which would require special efforts to be made to ensure that actuator friction was below this value. Actuators may be designed with negligible friction at the expense of additional manufacturing cost and greater hydraulic fluid consumption. The actuator design described in Chapter 3 is an example of such a type.

Typical servo valves for controlling hydraulic actuators are of the two-stage type where the output flow rate or output pressure is proportional to the input current. These are readily available with bandwidths suitable for an active suspension application. The effect of non-linearities in the valve response such as phase lag increasing with frequency, varying flow gain near the null position and any interdependence of output flow with load pressure may need to be accounted for in the control system design. Sutton (1978) built a laboratory active suspension where an hydraulic actuator was used as an open loop 'block' in the control system. Many practical difficulties were found with this arrangement. Drift problems were encountered due to minor variations in hydraulic oil temperature and the difficulty with precisely centering the servo valve spool. Additional effects were the non linear flow range of the servo spool near the null position, the non-linear response of the valve in each direction and non-linear inherent damping within the hydraulic cylinder. These problems can be overcome by using the valve and actuator as a "force generator" in a closed loop. The measured actuator force output is compared to a desired force and an appropriate feedback signal is generated to minimise the error. This of course requires a control law

which produces a "desired force" as its output. An electro-rheostatic fluid hydraulic actuator may prove to be superior although electro-rheostatic fluids are currently in developmental form only, (Sturk et al., 1995).

2.4 Selection of Performance Measurement Criteria

In order to make comparisons between various selections of spring and damper rates and to carry out an optimisation process to select the 'best' combination, some specific physical criteria must be chosen. Each of these criteria then uniquely represents the measure of a particular suspension system characteristic. Sections 2.4.1 to 2.4.3 discuss the physical parameters to represent the ride comfort, the road holding and the suspension travel in the evaluation of the suspension model.

2.4.1 Representation of Ride Comfort.

One of the prime purposes for a suspension is for the comfort of human passengers, however the judgement of performance of a suspension by humans is clouded by the many other factors which also apply during a journey such as tiredness, fatigue, mood and any distractions present. There have been many studies performed which have attempted to characterise the susceptibility of humans to specific frequencies of vibration by excluding the influence of these other factors. Early attempts were reported in 1907 by F.W. Lanchester (1907-08) which suggested that a suspension frequency of less than 1.5 Hertz was desirable. Since then many studies have been made which report on the sensitivity to specific frequency vibrations of whole body or various parts of the human body often with varying results. The Australian Standard, AS2670-1983 is stated to be a compromise between results of available data. This standard is based on International Standards Organisation Standard, ISO 2631, and defines levels for acceptable durations for transverse and vertical vibrations and might be used to objectively evaluate a vehicle suspension performance. Note that Clarke (1979) casts doubt upon the validity of ISO 2631, concluding that there is no evidence that discomfort due to whole body vibrations is time dependent, at least for durations up to two and a half hours and probably even longer.

Sharp and Crolla (1987) state that it is widely accepted that frequency weighting of the passenger root mean square (rms) acceleration data should be made to allow for frequency dependent discomfort. Lee & Salman (1989) do introduce a frequency weighting based on passenger comfort. It is clear though that many investigations on active suspension performance use a non-weighted body acceleration as the ride comfort indicator.

The seating of a passenger vehicle provides an additional source of dynamics which plays an important role in isolating the passenger from roadway inputs. The vibration inputs to various parts of the occupant must also be considered since the perception of ride comfort is heavily dependent upon which part of the body is being vibrated. Additionally the dynamics of the seat itself are influenced significantly by the dynamics of the occupant. Studies on seat dynamics, such as that by Rakheja et al. (1994), usually include a dynamic model of the human body.

It is evident that there are no clear guidelines or accepted practices for evaluating the perception of human comfort when exposed to vibrations. The standards: ISO 2631 and AS2670 appear to be the best compromise, although they apply only to whole body vibration. These standards show frequency dependent acceleration limits and their adaptation to a vehicle study should include the effect of seating dynamics to be realistic. The suspension design might then be made to maintain body accelerations within a limiting envelope, based on a prescribed random roadway roughness and at a particular vehicle speed. It is doubtful however that the 1/4 car model would be sufficiently accurate for such an evaluation to be valid.

The alternative is the simple approach of assuming that unweighted root mean square, vertical acceleration of the vehicle body adequately represents the passenger ride comfort. This is useful when comparing various system designs, without evaluating the actual performance for a particular vehicle under prescribed roadway and vehicle speed conditions.

The body acceleration is proportional to the forces applied to it by the actuator and hence these forces can be used for comparative purposes to represent ride comfort.

2.4.2 Representation of Road Holding Capability.

Another purpose which a suspension must serve is to provide good road holding capability. Tyre to road surface contact forces will reach a minimum with large dynamic tyre forces, leading to the conclusion that high dynamic tyre forces reduce the ability to resist lateral loads and so limit the road holding capabilities of the vehicle. Hence dynamic tyre forces are an indicator of road holding. Since the tyre is assumed to possess linear force versus deflection characteristics, the dynamic tyre deflection may be used as a measure of the road holding capability of the suspension. For the quarter car model, dynamic tyre deflections are the only measure of road holding. For more complex models other additional criteria such as body roll would need to be considered.

2.4.3 Suspension Travel Limitations.

The suspension travel or 'rattle' space is the relative deflection between the axle and the vehicle body and will always be limited by the practical considerations of vehicle styling and the space available for the suspension components. The design process therefore must include some constraints placed on the suspension travel to ensure that the final design will operate within the available space.

2.5 Determination of a Control Law

Section 1.2 summarised that LQR controllers are relatively simple to design with similar performance to other design methods. LQR is based upon a dynamic system which is described by:

$$\begin{aligned}\dot{x}_n &= Ax_n + Bu_n \\ y_n &= Cx_n + Du_n\end{aligned}\tag{2.3}$$

where:

$x_n(t)$ is an n dimensional vector of system state variables.

$u_n(t)$ is the n dimensional external input to the system.

$y_n(t)$ is the n dimensional system output, ie: the response of the system.

A, B, C and D are constant matrices which contain the system characteristics.

The controlled variable, $u(t)$ is constructed from a linear combination of the system state variables:

$$u = K x_n \quad (2.4)$$

where: K is a constant $n \times 1$ dimensional array. The values of K are chosen to provide optimum performance of the controller. This requires minimisation of a weighted, quadratic performance index, defined:

$$J = \int_{-\infty}^{\infty} (x_n^T Q x_n + u^T R u) dt \quad (2.5)$$

Q and R contain the desired weighting factors; Q is constructed to penalise dynamic tyre deflection and suspension travel. R is a scalar that weights the applied body force. Note that there is no method known for precise selection of appropriate weighting factors to achieve a specified performance, however there are some guidelines which can be adopted to enable some control of system performance (Anderson & Moore, 1990). Thompson (1976) discusses initial values which may be used for suspension system modelling.

The choice of which system states would be used to represent critical aspects of the performance is discussed in sections 2.4.1 to 2.4.3. These can be incorporated into equation (2.5). The value of the performance index is equivalent to ∂V times that determined from the integral squares for a step input to the system (Thompson, 1973).

Equation (2.5) then becomes:

$$J_m = \partial V J \quad (2.6)$$

where:

$$J = 1/2 \int_0^{\infty} (ru^2 + q_1(x_0-x_1)^2 + q_2(x_1-x_2)^2) dt \quad (2.6a)$$

V = the vehicle forward velocity,

∂ is defined in equation (2.1) and the initial conditions, $x_n(0) = [0]$.

The standard solution to the minimisation of the performance index problem results in an optimum controller given by:

$$K = -(R)^{-1} B^T P \quad (2.7)$$

where:

B and R are as previously defined,

P is the positive definite symmetric solution to the matrix Riccati equation:

$$P A + A^T P - P B B^T P R^{-1} + Q = 0 \quad (2.8)$$

where Q is positive semi-definite and symmetric and R is positive definite and symmetric.

One method for solution of this problem is given by Davis and Thompson (1986).

Two implementations of LQR controller were studied, one using the standard form and one where a frequency shaping 'conceptual' filter was added to the performance index.

2.4.1 LQR Standard Form Controller

Thompson (1976) presents a procedure for developing state variable differential equations for the quarter car model in Figure 1.2 about the steady state position (ie: zero initial conditions):

$$\dot{x}_0 = w(t)$$

$$\dot{x}_1 = x_3$$

$$\dot{x}_2 = x_4$$

$$\dot{x}_3 = (\lambda(x_0 - x_1) - u)/M_1$$

$$\dot{x}_4 = u/M_2$$

This may be expressed in vector matrix form:

$$\dot{x}_n = A x_n + b_1 u + b_2 w \quad \text{and}$$

$$y = K x_n \quad (2.9)$$

where:

$$A = \begin{bmatrix} 0 & 0 & 1 & 0 \\ 0 & 0 & 0 & 1 \\ \lambda/M_1 & 0 & 0 & 0 \\ 0 & 0 & 0 & 0 \end{bmatrix} \quad b_1 = \begin{bmatrix} 0 \\ 0 \\ -1/M_1 \\ 1/M_2 \end{bmatrix} \quad b_2 = \begin{bmatrix} 0 \\ 0 \\ k_1/M_1 \\ 0 \end{bmatrix}$$

In terms of the standard controller expressed in equation (2.3):

$$C = \begin{bmatrix} 1 & 0 & 0 & 0 & 0 \\ 0 & 1 & 0 & 0 & 0 \end{bmatrix}$$

$$D = [0]$$

The road displacement input $w(t)$ is a unit step, as was discussed in section 2.2. Making the transformation:

$$\hat{x}_1 = x_1 - x_0$$

$$\hat{x}_2 = x_2 - x_0$$

$$\hat{x}_3 = x_3$$

$$\hat{x}_4 = x_4$$

(2.10)

and applying the unit step input to x_0 , at time $t = 0$ the initial conditions are:

$$\hat{x}_1(0) = \hat{x}_2(0) = -1 \quad \text{and}$$

$$\hat{x}_3(0) = \hat{x}_4(0) = 0.$$

Equation (2.9) is then re-written:

$$\dot{\hat{x}}_n = A \hat{x} + b_1 u \quad \text{and}$$

$$\hat{y} = K \hat{x}$$

(2.11)

The weighting matrix Q is then:

$$Q = \begin{bmatrix} q_1 + q_2 & -q_2 & 0 & 0 \\ -q_2 & q_2 & 0 & 0 \\ 0 & 0 & 0 & 0 \\ 0 & 0 & 0 & 0 \end{bmatrix} \quad \hat{x} = \begin{bmatrix} \hat{x}_1 \\ \hat{x}_2 \\ \hat{x}_3 \\ \hat{x}_4 \end{bmatrix}$$

and
$$J = \int_0^{\infty} (ru^2 + q_1(x_0 - x_1)^2 + q_2(x_1 - x_2)^2) dt \quad (2.12)$$

Note that the component terms of J represent ride comfort, dynamic tyre deflection and suspension travel, as discussed in section 2.3.

From the scheme derived above an expression for the optimal control force, u_{opt} can be derived from a linear combination of the state variables:

$$u_{opt} = k_1 \hat{x}_1 + k_2 \hat{x}_2 + k_3 \hat{x}_3 + k_4 \hat{x}_4 \quad (2.13)$$

This can be written in the following equivalent form:

$$u_{opt} = k_1(\hat{x}_1 - \hat{x}_2) + k_3(\hat{x}_1 - \hat{x}_2) + (k_1 + k_2)\hat{x}_2 + (k_3 + k_4)\hat{x}_2 \quad (2.14)$$

which is apparently realisable by using a conventional spring in parallel with an actuator, where the component term: $k_1(\hat{x}_1 - \hat{x}_2)$ is contributed by the spring and the remaining terms generated by the actuator. The values for k_1 to k_4 are determined by application of equation (2.7) The relationship in (2.14) still implies that measurements relative to x_0 are available which presents considerable practical difficulties on a real suspension system. An alternative to alleviate this problem is to substitute x_1 for x_0 . This is justifiable since the displacement spectrum of the axle will approximate that of the road surface up to the cut-off frequency. Thus the measurement of \hat{x}_2 (ie: $x_2 - x_0$) can be replaced with $x_2 - x_1$. When this is substituted into (2.14):

$$u = -k_2(x_1 - x_2) + k_3(\dot{x}_1 - \dot{x}_2) + (k_3 + k_4)\dot{x}_2 \quad (2.15)$$

The control force u is however no longer optimal except for the case when $k_2 = -k_1$, which can be demonstrated by re-introducing x_0 into (2.15) and rearranging to obtain:

$$u = -k_2(x_1 - x_0) + k_2(x_2 - x_0) + k_3\dot{x}_1 + k_4\dot{x}_2 \quad (2.16)$$

and similarly for equation (2.13) to give:

$$u_{opt} = k_1(x_1 - x_0) + k_2(x_2 - x_0) + k_3\dot{x}_1 + k_4\dot{x}_2 \quad (2.17)$$

Comparing coefficients it is evident that $u = u_{opt}$ only when $k_2 = -k_1$. Equation (2.15) appears to be a reasonable basis on which to implement a practical active suspension. The

actual values calculated for the gains k_2 to k_4 are entirely dependent upon the weighting factors applied. Instead of using equation (2.15) directly, let the control force be given by:

$$u = k_s(x_1 - x_2) + k_d(\dot{x}_1 - \dot{x}_2) + k_v \dot{x}_2 + k_a \ddot{x}_2 \quad (2.18)$$

Then by substituting $\ddot{x}_2 = u/M_2$ and equating coefficients with equation (2.15):

$$k_a = (1 + k_s/k_2)/M_2 \quad (2.19)$$

$$k_d = (1 - k_a/M_2)k_3 \quad (2.20)$$

$$k_v = (1 - k_a/M_2)(k_3 + k_4) \quad (2.21)$$

This then allows the spring stiffness to be arbitrarily chosen and the other gains calculated accordingly. The performance index for this system is as per equation (2.12). The values obtained for k_a , k_d and k_v are of course dependent on the weighting factors used. The increase in the performance index from the optimal solution will indicate how close the overall performance is to the optimal. In order to implement this system, an actuator must be placed in parallel with a load cell. The difference between the actual force developed and the desired force calculated by equation (2.18), is suitably amplified and used as the error signal in an "inner loop" to control the actuator. The gain of this loop is required to be sufficient to produce negligible error between the actual and desired forces.

It is possible to obtain a completely optimal control by using a sufficient number of feedback variables. In place of equation (2.15), instead assume that the control force can be expressed as a linear combination of five state variables (ie: one more than the number of Kalman gains calculated in order to allow the spring stiffness to be arbitrarily selected):

$$u = k_s(x_1 - x_2) + k_d(\dot{x}_1 - \dot{x}_2) + k_v \dot{x}_1 + k_a \ddot{x}_2 + k_b \ddot{x}_1 \quad (2.22)$$

Substituting $x_2 = u/M_2$:

$$u = k_s(x_1 - x_2) + k_d(\dot{x}_1 - \dot{x}_2) + k_v \dot{x}_1 + k_a(u/M_2) + k_b \ddot{x}_1$$

$$(1 - k_a/M_2)u = k_s(x_1 - x_2) + k_d(\dot{x}_1 - \dot{x}_2) + k_v \dot{x}_1 + k_b \ddot{x}_1$$

rearranging:

$$u = (k_s/(1 - k_a/M_2))(x_1 - x_2) + (k_d/(1 - k_a/M_2))(\dot{x}_1 - \dot{x}_2)$$

$$+ (k_v/(1-k_a/M_2)) \dot{x}_1 + (k_b/(1-k_a/M_2)) \ddot{x}_1 \quad (2.23)$$

Equation (2.13) may be re-written:

$$u = k_2(x_2 - x_1) + k_4(x_4 - x_3) + (k_1 + k_2)(x_1 - x_0) + (k_3 + k_4)x_3$$

and from equations (2.9):

$$\begin{aligned} x_1 - x_0 &= -(M_1 \ddot{x}_1 + u)/\lambda \quad \text{and} \\ u &= M_2 \ddot{x}_2 \end{aligned}$$

Hence:

$$\begin{aligned} u &= k_2(x_2 - x_1) + k_4(\dot{x}_2 - \dot{x}_1) - (k_1 + k_2)(M_1 x_1 + u)/\lambda + (k_3 + k_4)\dot{x}_1 \\ (1 + (k_1 + k_2)/\lambda) &= -k_2(x_1 - x_2) - k_4(\dot{x}_1 - \dot{x}_2) - (k_1 + k_2)(M_1 \ddot{x}_1)/\lambda + (k_3 + k_4)\dot{x}_1 \\ u &= (-k_2 \lambda)(x_1 - x_2)/\phi - (k_4 \lambda)(\dot{x}_1 - \dot{x}_2)/\phi - (k_1 + k_2)M_1 \ddot{x}_1/\phi + (k_3 + k_4)\lambda \dot{x}_1/\phi \end{aligned} \quad (2.24)$$

where: $\phi = \lambda + k_1 + k_2$

Comparing coefficients with equation (2.23) gives:

$$\begin{aligned} k_a &= (1 + k_s \phi/k_2 \lambda)M_2 \\ k_b &= (k_1 + k_2)M_1 k_s/k_2 \lambda \\ k_d &= k_4 k_s/k_2 \\ k_v &= -(k_3 + k_4)k_s/k_2 \end{aligned} \quad (2.25)$$

Where k_s is an arbitrary spring stiffness. The practical implementation of this is to minimise the actuator force required by using the existing body spring to provide the k_s feedback if the coefficients k_a to k_v according to equation (2.25).

2.4.2 Frequency Shaped Controller

Frequency shaped controllers can be seen as a combination of classical and modern control methods. The classical concept of filtering to produce desired effects in the frequency domain are combined with modern time domain state variable techniques. Frequency shaped controllers have been applied to active suspensions by Lee & Salman (1989) and Thompson & Davis (1992). Lee & Salman used the concept to enable the susceptibility of human discomfort to motion in particular frequency ranges to be incorporated to provide improved ride comfort. The vertical acceleration component of the performance index is directly frequency weighted by use of a filter such that the optimum feedback gains calculated

include the effect of the filter. The dynamic tyre deflection and suspension travel cost terms were not frequency weighted. The filter is a conceptual one only as far as the system is concerned since it exists as a concept with which to modify the state variable feedback gains and not as an explicit filter included in the system hardware. Thompson & Davis (1992) also use a conceptual filter in a similar way, as developed below.

Assuming a suspension system as per Figure 1.2, the motion is described by:

$$\begin{aligned}\dot{x}_1 &= x_3 \\ \dot{x}_2 &= x_4 \\ \dot{x}_3 &= \lambda(x_0 - x_1)/M_1 - u/M_1\end{aligned}\tag{2.26}$$

$$\dot{x}_4 = u/M_2\tag{2.27}$$

where x_0 is the input which is integrated white noise. As for the LQR controller, transform the system to a standard LQR form by including x_0 as a known disturbance to the system.

Hence substitute the following:

$$\begin{aligned}\hat{x}_1 &= x_1 - x_0 \\ \hat{x}_2 &= x_2 - x_0 \\ \hat{x}_3 &= x_3 \\ \hat{x}_4 &= x_4 \\ \hat{u} &= u\end{aligned}\tag{2.28}$$

As discussed previously, a more convenient and equivalent problem is to study the unit step response of the system. Immediately after the application of the step input at the tyre contact point:

$$\begin{aligned}x_0(0) &= 0 \\ \hat{x}_1(0) &= -1 \\ \hat{x}_2(0) &= -1\end{aligned}\tag{2.29}$$

The relative body to axle displacement is nominated as the system output, ie: $y_1 = \hat{x}_2 - \hat{x}_1$

$$= [-1 \ 1 \ 0 \ 0] \hat{x}$$

$$= H' \hat{x} \quad (2.30)$$

where $H = \begin{bmatrix} -1 \\ -1 \\ 0 \\ 0 \end{bmatrix}$

The system may now be described as a standard LQR problem:

$$\dot{\hat{x}} = F\hat{x} + G\hat{u}$$

$$y_1 = H' \hat{x}$$

with:

$$F = \begin{bmatrix} 0 & 0 & 1 & 0 \\ 0 & 0 & 0 & 1 \\ \lambda/M_1 & 0 & 0 & 0 \\ 0 & 0 & 0 & 0 \end{bmatrix} \quad G = \begin{bmatrix} 0 \\ 0 \\ -1/M_1 \\ 1/M_2 \end{bmatrix} \quad (2.31)$$

The output of y_1 being the relative body to axle displacement is easily measured on a

practical suspension. In addition, define:

$$\hat{x}_5 = y_1 = H' \hat{x} \quad (2.32)$$

where: \hat{x}_5 is the integral of the relative displacement between the body and axle. Noting that

$H'G = 0$, we obtain:

$$\begin{aligned} \dot{y}_1 &= H' \dot{\hat{x}} \\ &= H'F\hat{x} + H'G\hat{u} \\ &= H'F\hat{x} \end{aligned} \quad (2.33)$$

The augmented system is now defined by:

$$\begin{bmatrix} \dot{\hat{x}} \\ \dot{\hat{x}}_5 \end{bmatrix} = \begin{bmatrix} F & 0 \\ H' & 0 \end{bmatrix} \begin{bmatrix} \hat{x} \\ \hat{x}_5 \end{bmatrix} + \begin{bmatrix} \hat{x} \\ \hat{x}_5 \end{bmatrix} \hat{u}$$

and the optimal control will be a linear combination of the system states:

$$\begin{aligned} \hat{u} &= K\hat{x} + K_5\hat{x}_5 \\ &= K\hat{x} + K_5 \int H' \hat{x} dt \end{aligned} \quad (2.34)$$

Hence:

$$\hat{u} = K\hat{x} + K_5\hat{x}_5$$

$$\begin{aligned}
&= K_1 \hat{x}_1 + K_2 \hat{x}_2 + K_3 \hat{x}_3 + K_4 \hat{x}_4 + K_5 \int \hat{x}_5 dt, \text{ and so:} \\
u &= K_1(x_1-x_0) + K_2(x_2-x_0) + K_3x_3 + K_4x_4 + K_5 \int x_5 dt \\
&= (K_1+K_2)(x_1-x_0) + K_2(x_2-x_1) + (K_3+K_4)x_3 + K_4(x_4-x_3) + K_5 \int (x_2-x_1) dt
\end{aligned} \tag{2.35}$$

From equation (2.26):

$$x_1-x_0 = -(u+M_1 \dot{x}_3)/\lambda \tag{2.36}$$

Substitution into (2.34) gives:

$$\begin{aligned}
u &= -(K_1+K_2)(u+M_1 \dot{x}_3)/\lambda + K_2(x_2-x_1) + (K_3+K_4)x_3 + K_4(x_4-x_3) + K_5 \int (x_2-x_1) dt \\
&= C_1 \ddot{x}_1 + C_2(x_2-x_1) + C_3 \dot{x}_1 + C_4(\dot{x}_2-\dot{x}_1) + C_5 \int (x_2-x_1) dt
\end{aligned} \tag{2.37}$$

where:

$$C_1 = -(K_1+K_2)M_1/(\lambda+K_1+K_2)$$

$$C_2 = \lambda K_2/(\lambda+K_1+K_2)$$

$$C_3 = \lambda(K_3+K_4)/(\lambda+K_1+K_2)$$

$$C_4 = \lambda K_4/(\lambda+K_1+K_2)$$

$$C_5 = \lambda K_5/(\lambda+K_1+K_2)$$

A Proportional-Integral-Derivative (PID) filter is then defined with output y_2 :

$$y_2 = K_p y_1 + K_i \int y_1 dt + K_d y_1 \tag{2.38}$$

The performance integral is defined as:

$$J = \int_0^{\infty} (Ru^2 + q_1 x_1^2 + q_2 (x_2-x_1)^2 + q_3 y_2^2) dt \tag{2.39}$$

which includes a penalty on the output of the filter and thereby influences the optimum gains, $K_a = [K_1 \ K_2 \ K_3 \ K_4 \ K_5]$ such that they are 'frequency shaped'. The transfer

function of the filter is:

$$\frac{Y_2(s)}{Y_1(s)} = K_d s + K_p + \frac{K_i}{s}$$

$$= K_d \left(s^2 + \frac{K_p s}{K_d} + \frac{K_i}{K_d} \right) / s \quad (2.40)$$

where $Y(s)$ denotes the Laplace transform of $y(t)$.

The optimum gains K'_a are determined:

$$\begin{aligned} u_{\text{opt}} &= K'_a x_a \\ &= -G'_a P x_a / R \end{aligned} \quad (2.41)$$

where: $x_a = [x_1 \ x_2 \ x_3 \ x_4 \ x_5]'$, $K'_a = [K_1, K_2, K_3, K_4, K_5]'$ and P is the positive definite

symmetric solution to the matrix Riccati equation:

$$P F'_a + F'_a P - P G'_a G'_a P / R + Q = 0 \quad (2.42)$$

where:

$$F'_a = \begin{bmatrix} 0 & 0 & 1 & 0 & 0 \\ 0 & 0 & 0 & 1 & 0 \\ -\lambda/M_1 & 0 & 0 & 0 & 0 \\ 0 & 0 & 0 & 0 & 0 \\ -1 & 1 & 0 & 0 & 0 \end{bmatrix} \quad G'_a = \begin{bmatrix} 0 \\ 0 \\ -1/M_1 \\ 1/M_2 \\ 0 \end{bmatrix}$$

The reference (Thompson & Davis, 1992) shows that choosing $q_3 = 1$, Q becomes:

$$Q = \begin{bmatrix} q_1 + q_2 + K_p^2 & -q_2 - K_p^2 & K_p K_d & -K_p K_d & -K_p K_i \\ -q_2 - K_p^2 & q_2 + K_p^2 & -K_p K_d & K_p K_d & K_p K_i \\ K_p K_d & -K_p K_d & K_d^2 & -K_d^2 & -K_d K_i \\ -K_p K_d & K_p K_d & -K_d^2 & K_d^2 & K_d K_i \\ -K_p K_i & K_p K_i & -K_d K_i & K_d K_i & K_i^2 \end{bmatrix} \quad (2.43)$$

Thus it can be seen that the system itself does not implement a filter but instead the desired characteristics are introduced via the weighting factors which influence the calculated optimum feedback gains.

Implementation is as for the Standard Form LQR controller, with the difference between the actual and desired forces being used as the error signal to control the actuator. It should be noted that the system will have zero steady state error in the output ($x_2 - x_1$) due to the integration introduced in (2.32) and thus has infinite static stiffness. By careful choice of the

filter characteristics it is possible to influence the natural frequency and damping of system modes. One example of the use of such a scheme is by Lee and Salman (1989) where weighting factors were used which attempt to reduce vehicle body motions in the frequency range to which humans are most sensitive, as determined by International Standard ISO 2631.

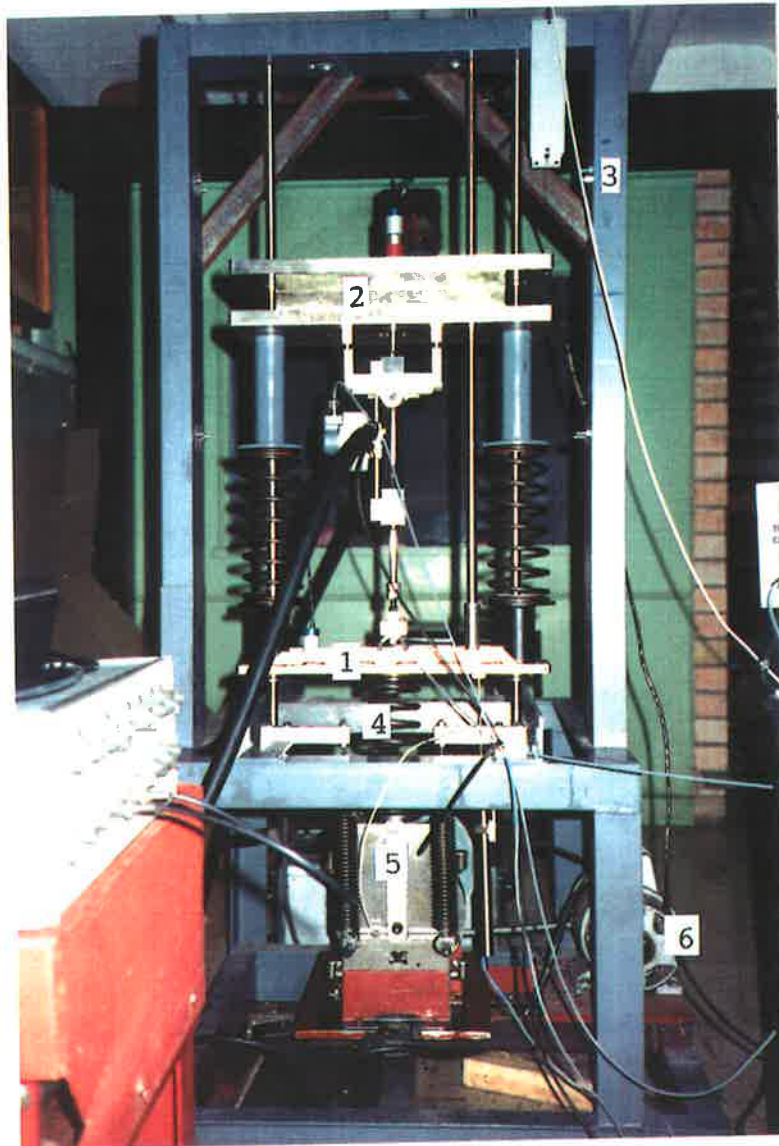
CHAPTER 3

CONSTRUCTION OF THE EXPERIMENTAL SUSPENSION

3.1 General Layout of the Experimental Suspension

The experimental test rig was designed to be as close as possible to the ideal quarter car model in Figure 1.2, to ensure close correlation of the actual performance to that predicted by the digital simulation model. The general design of the suspension was heavily influenced by the choice of active force generation. Two possible means for actuation of the suspension were available, an hydraulic actuator with servo valve control or a Samarium-Cobalt, permanent magnet direct current motor with a high precision linear ball screw. The direct current motor produced a maximum of 300 Watts and had sufficient bandwidth for the application. The linear ball screw had a total stroke of 50 millimetres. The limited power would require a small scale model. The hydraulic servo valve available was a Moog series 077-101 flow control type and had sufficient bandwidth for the application and was limited to a maximum flow rate of a nominal 3.8 litres per minute, equating to an available power of 950 Watts at the maximum system operating pressure of 15MPa. This was clearly superior to the electric motor and since an actuator could be purpose built for this test rig, it allowed far more flexibility in choice of the actuator details. The power limitation still required that the experimental test rig be scaled down from a full size vehicle in order to maintain acceptable suspension performance. The course of hydraulic actuation also is perhaps the method most likely to be used for any vehicle fitted application of an active suspension. Thus hydraulic power was chosen for the experimental suspension.

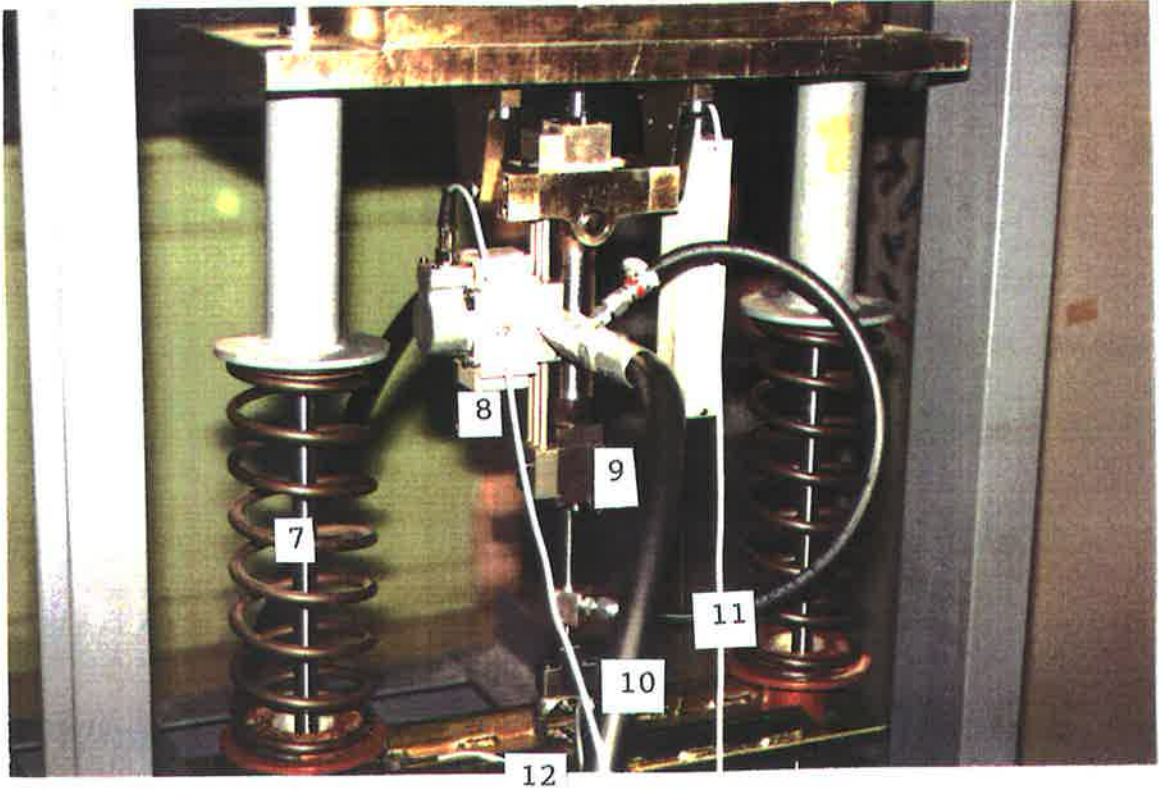
Thus the basic layout of the suspension was chosen to be as close as possible to the quarter car theoretical model, with lumped masses representing the axle and body. Figures 3.1 a. to c. show photographs of the completed rig. Figure 3.6 d records key measured parameters.



Legend:

1. Mass representing axle and wheel.
2. Mass representing vehicle body.
3. Support frame, including vertical guide shafts.
4. Tyre spring.
5. Belt driven sinusoidal cam providing roadway input displacement.
The cam can be adjusted to provide a fixed displacement from 8mm to 25mm.
6. Variable speed DC motor to control frequency of roadway input over the range 0.5 Hertz to 15 Hertz.

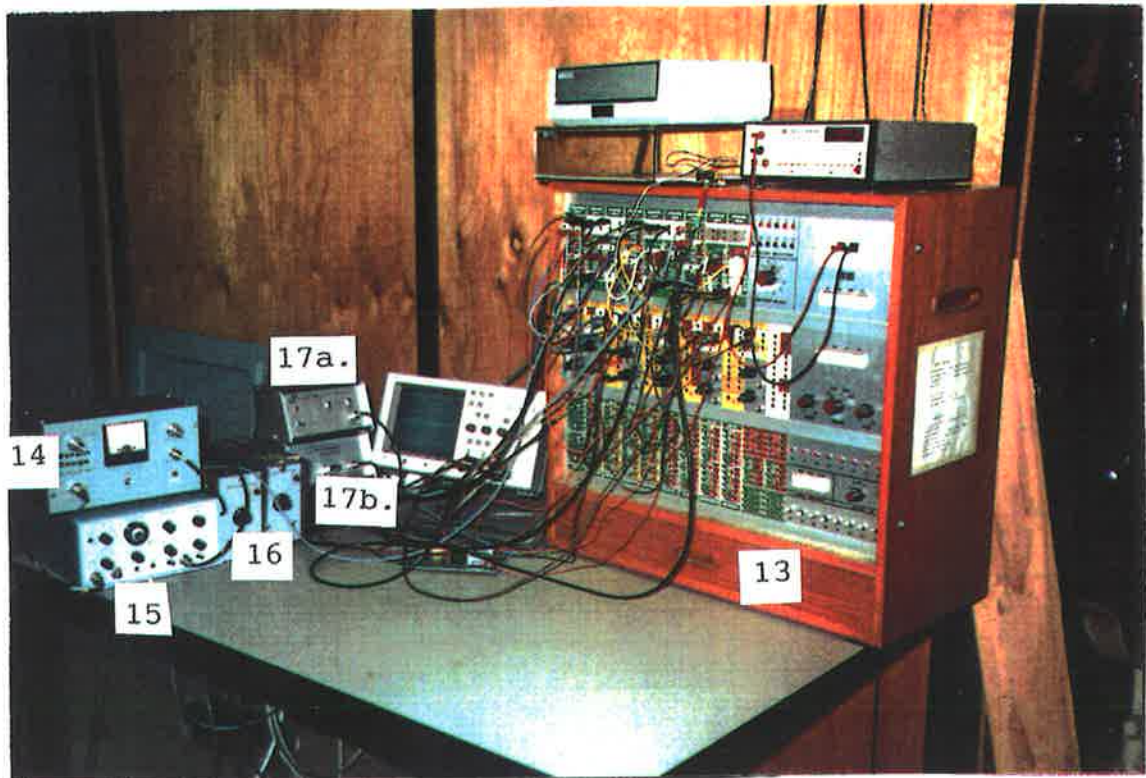
Figure 3.1 a. Experimental 1/4 car active suspension test rig.



Legend:

7. Springs in parallel with actuator (see Figure 2.1) and mounting spacers. NOTE: the vertical guide rods can be seen passing through the centre of the springs.
8. Servo valve.
9. Hydraulic actuator. The actuator is mounted on a gimbal assembly to allow free rotation while maintaining high structural stiffness.
10. Hydraulic fluid return hose. The hose supplying pressurised fluid can be seen on the far side of the servo valve.
11. Drain hose from piston tapered bearing (see Figure 3.1).
12. Load cell. Ring type cell has a strain gauge Wheatstone bridge sensing element.

Figure 3.1 b. Experimental 1/4 car active suspension test rig. Close up showing hydraulic actuator and servo valve assembly.



Legend:

- 13. Analogue computer. This was used to perform integrations, amplifications and summing to generate the electrical signal to the servo valve which represented the "desired" force.
- 14. Load cell amplifier.
- 15. "DISA" Butterworth filter, with adjustable characteristics.
- 16. Servo-accelerometer amplifiers.
- 17a. (top) Accelerometer amplifier for piezo accelerometer used for monitoring of the sinusoidal input.
- 17b. (bottom) String potentiometer amplifier. The string pot was used for providing the body displacement signal.
- 18. CRO.

Figure 3.1 c. Experimental 1/4 car active suspension test rig. Analogue computer and instrumentation amplifiers.

axle mass:	11.9 kilograms
body mass	72.3 kilograms
body spring rate :	17.5 kiloNewtons/metre
tyre spring rate(λ):	31.5 kiloNewtons/metre
road input displacement:	8.2 millimetres
step input displacement:	10.6 millimetres

Figure 3.1 d. Experimental 1/4 car active suspension test rig. Summary of physical data.

The spring rates and masses have values approximately one quarter of those corresponding to a typical medium sized passenger vehicle. The effective masses including all fittings and attachments are shown in Figure 3.1 d.

The body mass is made up from a number of 20 millimetres thick steel plates which could be added or removed as desired to obtain a suitable mass ratio between the axle and body.

The masses are guided to vertical motion only by two hardened steel shafts and linear recirculating ball bearings fitted to each of the masses. The axle mass also has an additional guide shaft running through a clearance hole in the body mass and through a linear ball bearing in the top beam of the test rig frame. This was not initially fitted but was needed to ensure that the axle moved only vertically and did not rotate. The forces applied to the axle by the tyre spring, body springs and actuator are nominally aligned with the centre of gravity. However small errors in this alignment caused significant moments in the axle mass which produced easily visible angular movements when transitioning between up and down motions. This had led to rapid damage of the guide

shafts by the linear bearings. There was a small amount of friction created by the bearings, requiring less than 5 Newtons applied body force to be applied to overcome it.

Figure 3.2 shows the schematic layout of the actuator and the hydraulic system. The barrel of the hydraulic actuator is mounted to the body mass via a gimbal assembly and to the axle in series with a load cell. The actuator is positioned in the centre of the rig to apply force through the centre of gravity of each mass. Drawings of key items of the rig are included in Appendix 2. The gimbals were included to prevent any moments on the actuator and load cell as a result of minor misalignments. The load cell is of ring type with four strain gauges fitted in a Wheatstone bridge. Two body springs were used. The stiffness of these in parallel is 17.5 kilo-Newtons/metre. This produced a body resonant frequency of 2.47 Hertz, rather than the intended frequency of approximately 1 Hertz which is typical of actual passenger vehicle suspensions. This difference is of no significance to the outcome of the experimental work. A major complication with these springs was the existence of a resonant mode near 50 Hertz. This resulted in any 50 Hertz interference in the servo valve drive signal from AC mains supplies exciting this mode, causing severe vibration.

A single spring representing the tyre connects the moving components to a sinusoidal shaker which is used to provide simulated roadway input deflections. The spring stiffness is 31.5 kilo-Newtons/metre and is also approximately one quarter of the stiffness of the nominal full scale tyre.

The shaker is an adjustable eccentric cam with a slider arrangement to provide vertical sinusoidal motion to the tyre spring. A direct current motor with infinitely variable speed drives the cam via speed reduction pulleys and a single shaft supported by two roller bearings. The maximum cam speed provides 13.5 Hertz roadway input. The cam shaft is fitted with a flywheel to maintain a constant speed. The entire assembly is supported by a steel channel frame which is bolted to the concrete laboratory floor.

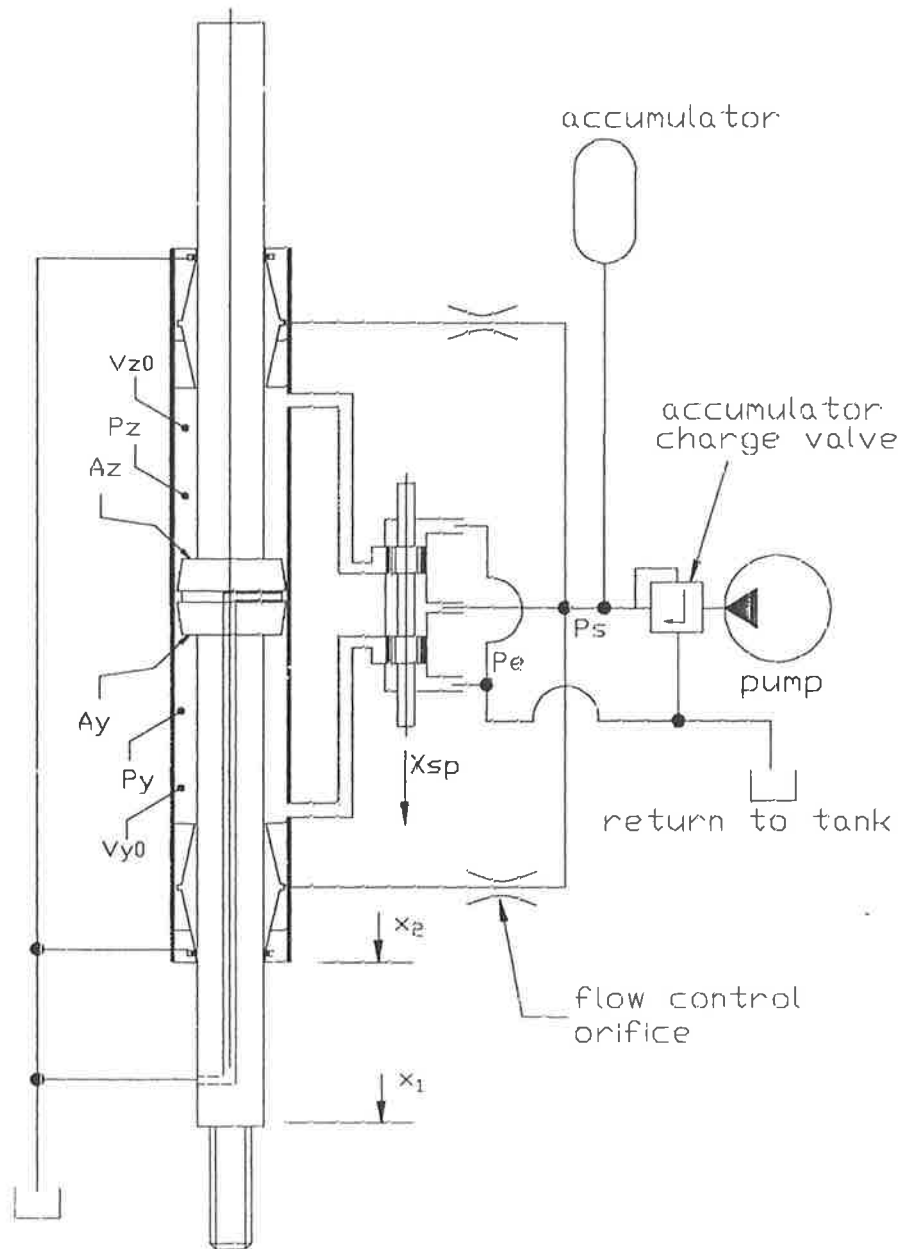


Figure 3.2 Hydraulic system and actuator arrangement.

3.2 Design of Hydraulic Servo and Actuator

The Moog 077-101 two stage servo valve was used because it was available and provided a bandwidth well in excess of that required for the suspension design. The frequency and phase response of this valve are shown in Figure 3.3, noting that this performance test is made by the manufacturer with a load of negligible inertia. The actual flow past the spool is strongly dependent upon the load pressure as shown in Figure 3.4. The curves represent a relationship:

$$Q = K_v i (\Delta P)^{0.5} \quad (3.1)$$

where:

K_v is a constant for the valve,

i is the drive current

ΔP is the pressure difference across the load (actuator).

The demand input current to the valve is $\pm 40\text{mA}$ (maximum) with a proportional output flow rate. A servo controlled current amplifier with high output impedance is normally used to drive the valve since the back-emf created by the valve's torque motor coils may have a significant influence on the system performance. Such an amplifier was not deemed mandatory for this application however since the valve was operating at relatively low frequencies. The valve was mounted on the actuator to minimise fluid volumes in the connecting pipework in order to keep any resonances caused by the hydraulic fluid compressibility well above any range of interest. Since the fluid volumes change with actuator position, this resonant frequency is dependant upon the piston position in the actuator; the centre position creating the lowest frequency. This is estimated from experimental results to be around 80 Hertz, well in excess of the field of interest for this study.

The servo valve null position can be adjusted by means of a mechanical screw on the side of the valve. The servo valve in initial operation required constant null adjustment to maintain a steady mean position of the axle and body masses. The null position

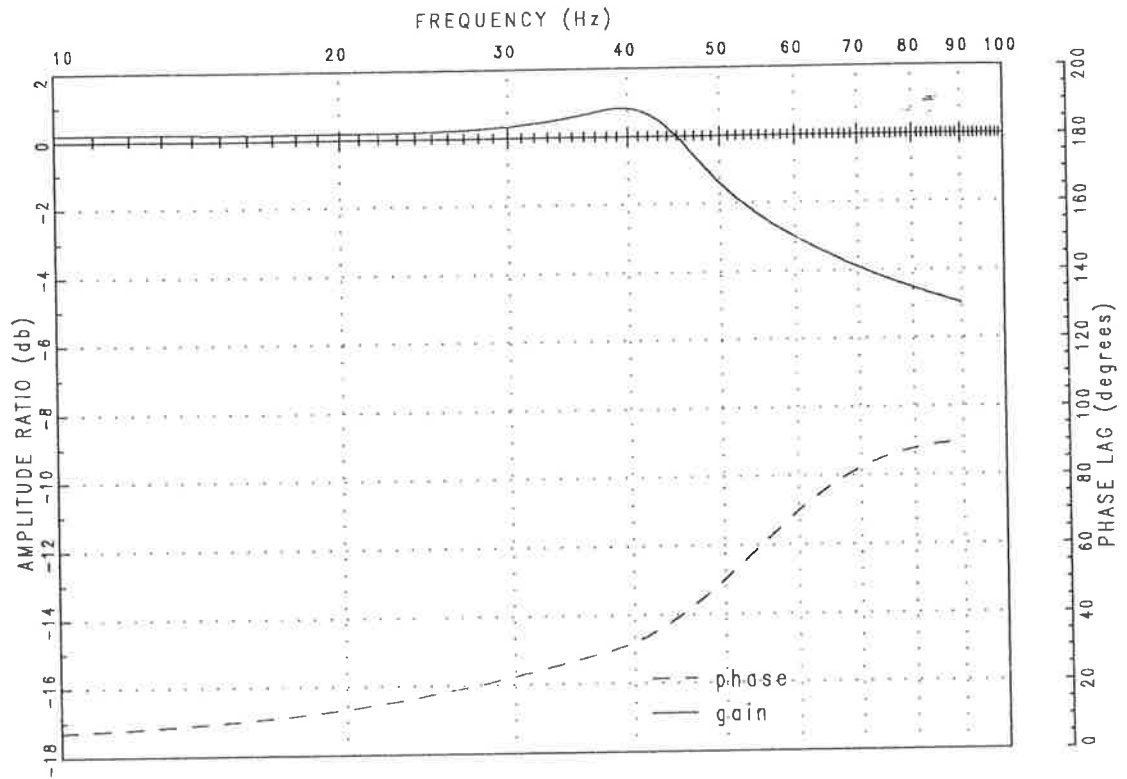


Figure 3.3 Servo valve frequency response; operating at 100% design current. Curves are taken from valve manufacturer's data and are adjusted for the actual mean operating pressure of 9.93MPa.

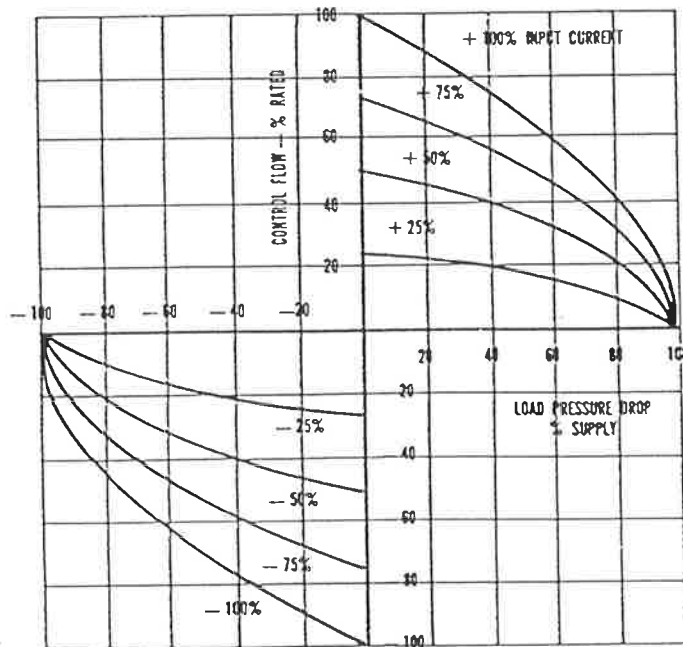


Figure 3.4 Servo valve load pressure versus output flow performance; curves are from Moog 770 series catalogue.

adjustment actually provides a relatively coarse control of the spool mid position. This offsets the spool position to apply a hydraulic bias to one side of the actuator to balance the forces acting on it to obtain a steady state. This steady state position however is highly sensitive to temperature fluctuations of the hydraulic fluid and also to changes in the hydraulic supply pressure. Since the supply used in this case fluctuated as the accumulator was discharged and refilled, the mean position also moved by several millimetres. The implementation of the 'frequency shaped' control law, which was initially attempted, used the integral of the body to axle relative displacement (ie: the position of the actuator) to maintain a constant body to axle displacement. This should have solved the valve drift problem however the gain required by the control law was large and even very small displacements at system start up made it extremely difficult to include this feedback without exceeding the servo valve maximum drive current. Implementing this control law was eventually abandoned for this reason. A solution to the valve drift problem was made by feeding back a low pass filtered signal from the body position transducer. The gain of this signal was set very low and the affect on system performance in the frequency range of interest between 1 and 15 Hertz was insignificant.

The hydraulic actuator is of double ended type. This provides identical system gains in each direction which simplifies the control law design and analysis of the performance results. The actuator was sized from some preliminary modelling of the theoretical suspension performance taking into account the maximum flow available from the servo valve. The upper bound for the required force was estimated to be approximately 250 Newtons. The actual values of course depend on which feedback control philosophy is implemented. A significant design margin needs to be allowed. The design case for the hydraulic cylinder force was chosen to be 2000 Newtons, which would consume less than 2.5 litres per minute of hydraulic fluid under the most severe operating conditions. Allowance for dynamic conditions must be made for the pressure losses through the

valve and pipes, noting that not less than 6.9MPa (1000psi) drop is required across the servo valve in order to maintain the manufacturer's stated frequency response. The actuator with bore diameter of 22millimetres and rod diameter of 11 millimetres meets the flow rate requirement and provides approximately 2000 Newtons of force at 7MPa. A stroke of 250 millimetres was chosen. The actuator incorporates conical hydrostatic bearings on the rods and piston. This is shown schematically in Figure 3.2. This design is based upon the method by Viersma (1980). Viersma reports that experience with this type of actuator has shown the Coulomb friction levels to be exceptionally low, less than one thousandth of one percent in one case. A similar result was confirmed in this actuator, where attempts to quantify the friction level failed because its virtual absence made detection unreliable with normal laboratory measuring equipment. The conical bearing design however is very expensive to produce, consumes high pressure oil to feed the bearings and has a high inherent leakage rate between the two sides of the cylinder compared to a conventional hydraulic actuator. Hydraulic cushioning is provided at the extremes of stroke to prevent excessive end cap loading if the piston is driven rapidly to full stroke.

The hydraulic fluid is supplied from a pump fitted with a one litre accumulator and charging valve, shown in Figure 3.2. This valve supplies the accumulator with fluid until the set operating pressure of 10.5MPa is reached. It then diverts the fluid back to the tank until the system pressure drops to 9.3MPa when it begins recharging of the accumulator. The pump is connected to the actuator by flexible hoses approximately four metres long.

3.3 Instrumentation

The state variables required to be measured were the body acceleration, the axle velocity and the body to axle relative velocity and displacement for generation of the desired actuator force. Control of the inner loop required the actual actuator force to be measured and additionally the body and axle absolute positions, relative to the fixed frame of the test rig were required for evaluation of the suspension performance.

A servo accelerometer and amplifier was used for the acceleration measurement of the body. The output from this was also integrated to provide a measurement of the body velocity. A similar servo accelerometer was fitted to the axle and the amplifier output integrated to obtain the axle velocity. The difference of these velocities was calculated in real time using an analogue computer. Initially the accelerometer outputs were integrated using standard analogue computer integrators. The output signals from the accelerometer amplifiers have a DC bias of approximately 0.5 volts which was trimmed out using adjustable DC inputs to summing junctions on the integrators. This adjustment was made with no roadway input to the suspension and proved to be very sensitive. With the suspension stationary the integrators would drift unacceptably after one or two minutes but when the body was cycled lightly up and down several times by hand the integrators drifted rapidly to the amplifier limits. This was understood to be because of non-linearities in the acceleration measurements. This problem meant that when running the shaker to provide an input, approximately 80% of the time was required to constantly adjust the integrator offsets to approximately zero volts, which was totally unacceptable.

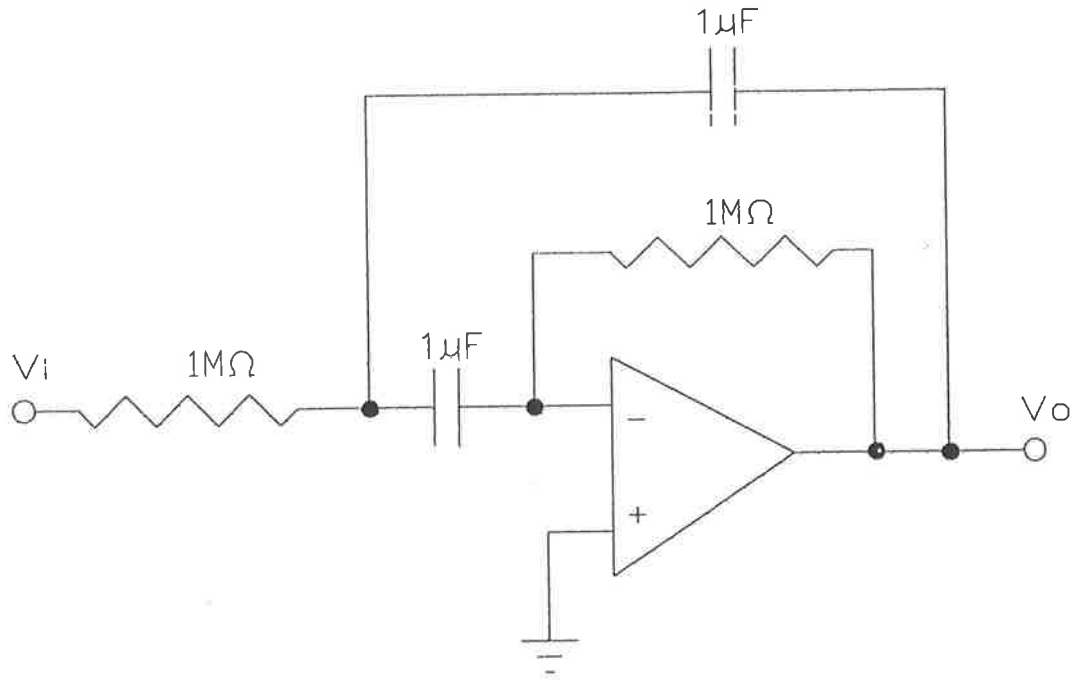
Two options were available to overcome the difficulties. The first was to use unity integral feedback around each integrator. This has an overall transfer function of:

$$H(s) = \frac{s}{s^2 + 1} \quad (3.2)$$

(where s is the Laplace Transform operator) which has identical phase response to a perfect integrator above 1 Hertz but produces a significant distortion in the amplitude response near 1 Hertz. It has however a large rejection of input drift and zero gain of DC input signals, which would eliminate drift problems. The second option was to use a second order bandpass filter, designed to behave as an integrator in the frequency range of interest. This is effectively a variant on the first option but can be tuned more readily to create desired behaviour. The design to implement this is shown in Figure 3.5 and has a transfer function of the form:

$$H(s) = \frac{-Ks}{s^2 + \alpha s + \beta} \quad (3.3)$$

where K , α and β can be designed by selection of resistors and capacitors. The break



$$H(s) = \frac{-C_1 K_2 s}{s^2 + G_2 (K_1 + K_2) s + C_1 K_1 C_2 K_2}$$

where: $G_i = 1/R_i = 1/2M\Omega$

$$K_i = 1/C_i = 1/2\mu F$$

The filter pass (break) frequency (ω_0) is calculated:

$$\omega_0^2 = C_1 K_1 C_2 K_2 = 0.0625,$$

hence: $\omega_0 = 0.25$ radians/second ≈ 0.04 Hertz.

Figure 3.5 Integrator design.

point was selected to be at 0.04 Hertz which produced the amplitude and phase plots shown in Figures 3.6 (a) and (b). This performance is quite close to that of a pure integrator above 1 Hertz and also has infinite rejection of DC inputs. This appeared to be the best approximation to the performance of an integrator in the frequency range of interest. Two such integrators were built to provide the velocity signals of the axle and body. The low break frequency in turn ensures a large time constant for the filter and approximately one minute was required for the steady state condition to approach zero volts DC offset in the output to be reached after an the integrators were first powered up. The only problem found with the integrators was a significant level of 50 Hertz electromagnetic interference from mains power. The integrators were a perfectly satisfactory method for performing the function intended however it would have been preferable to remove all 50 Hertz noise by additional screening. An alternative for future studies may be to use a dedicated velocity transducer for the differential velocity.

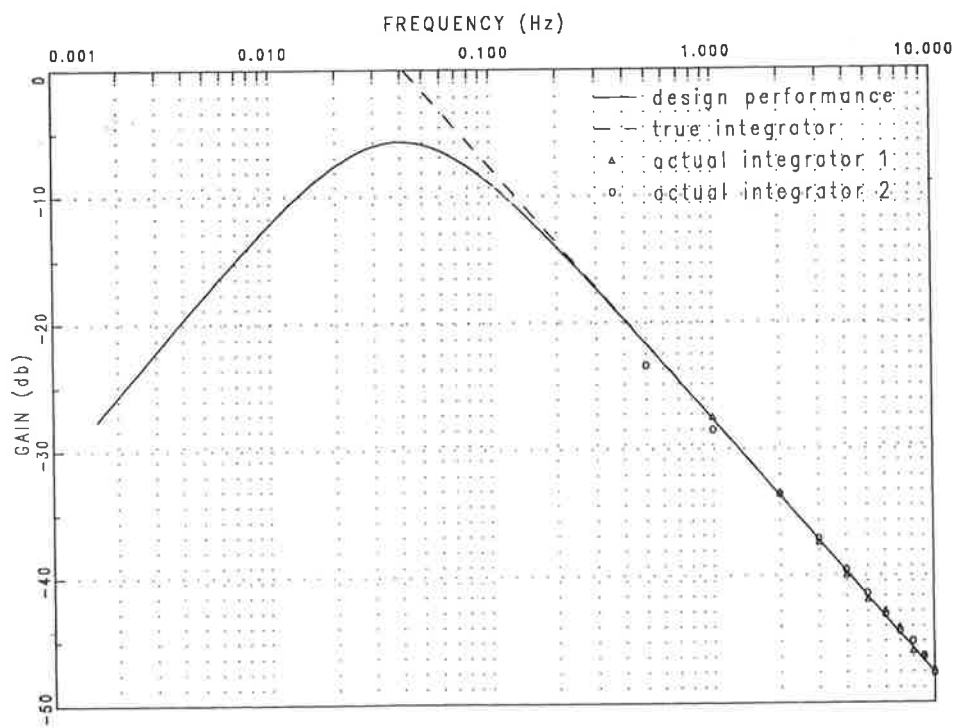


Figure 3.6 (a) Integrator gain characteristics.

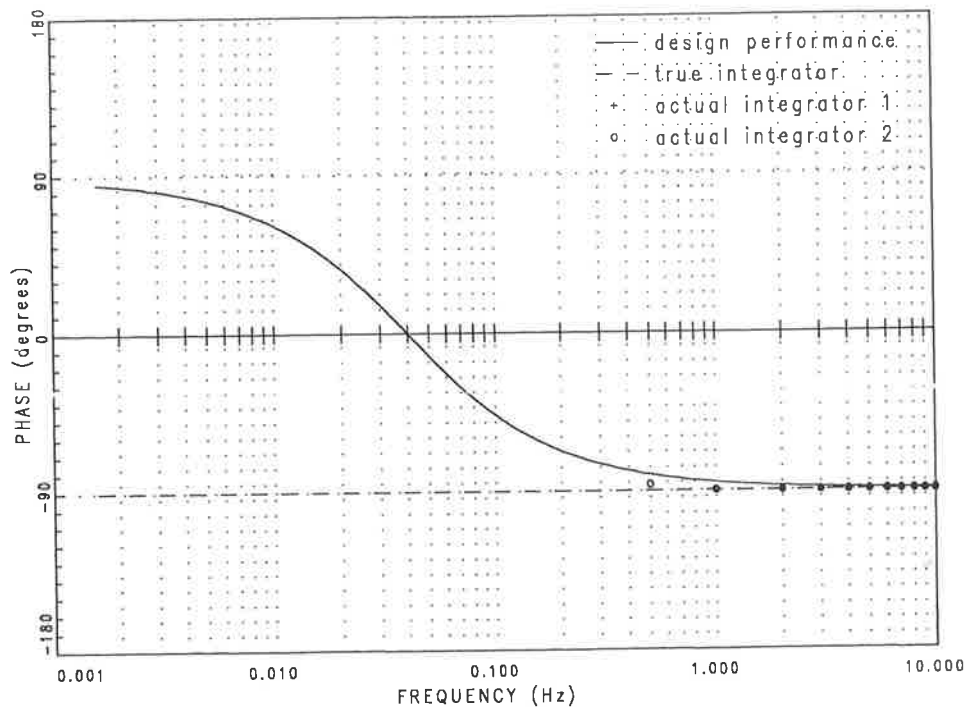


Figure 3.6 (b) Integrator phase characteristics.

A second order low pass filter to condition the body position feedback signal used an analogue computer amplifier as its active element and discrete resistors and capacitors assembled on a prototyping card. The cutoff frequency was set by component selection to be under 0.5 Hertz to ensure that the filter had negligible amplitude response in the range of interest above 1 Hertz but retained adequate gain under 0.5 Hertz to maintain a reasonably constant zero position for the axle and body. The design and performance of the filter is shown in Figure 3.7. Note that this filter introduces integration in the feedback path of the displacement transducer. Hence the steady state error of the feedback loop will be zero, albeit a slowly produced condition due to the low overall gain. This filter was built using an operational amplifier in the EA180 analogue computer. The theoretical performance is difficult to accurately predict since the transfer function is dependant on the unknown gain of the operational amplifier. This gain is assumed constant under all loading conditions, which may not be true. The modelled performance of the completed filter is shown in Figure 3.7. This assumes second order characteristics. The model shown is:

$$H(s) = \frac{-23s}{s^2 + 120s + 120} = \frac{V_o}{V_i} \quad (3.4)$$

where:

V_o is the output voltage,

V_i is the input voltage.

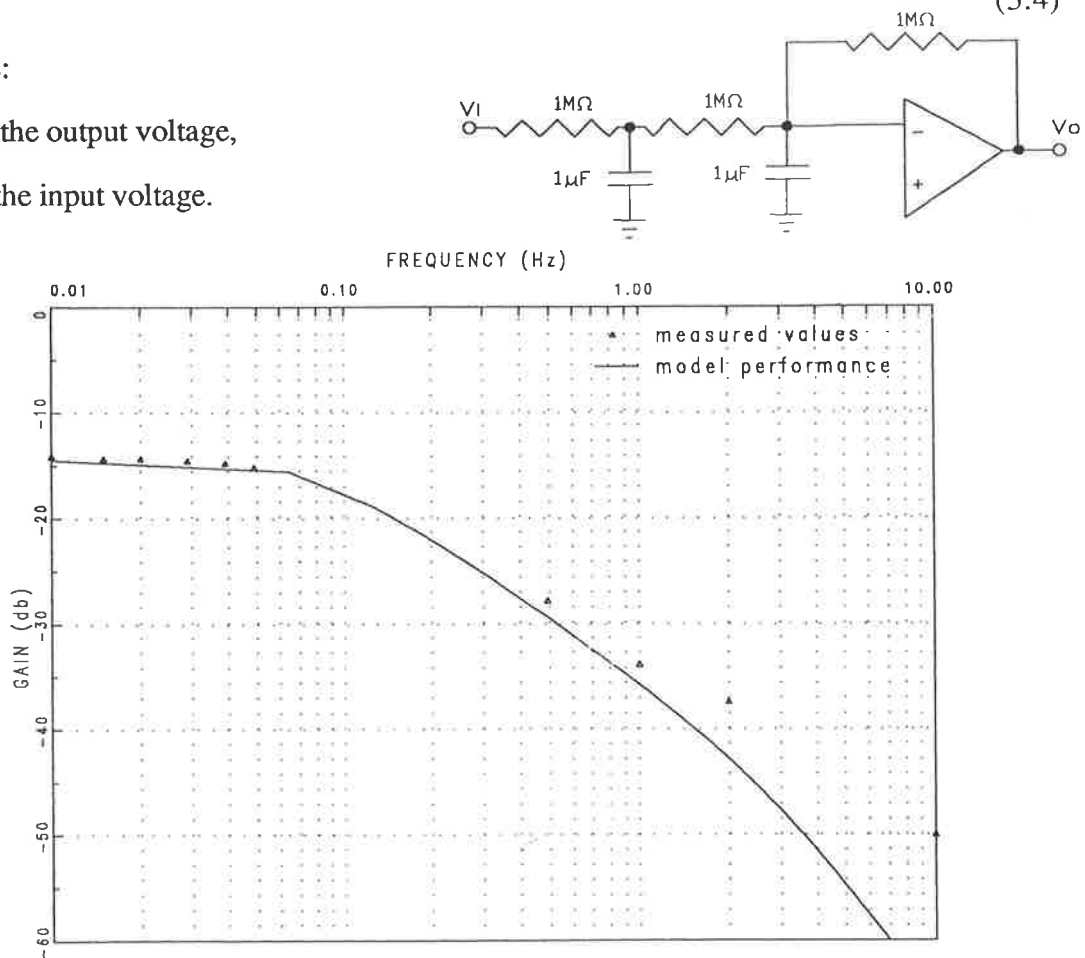


Figure 3.7 Low pass filter design and performance.

This was determined by trial and error to provide the best reasonable simulation of this filter. This is a reasonable model for low frequencies but increasingly poor as the frequency increases beyond 1.0 Hertz. It is evident that the response roll off does not match a second order response, presumably because of the unknown characteristics of the operational amplifier within the analogue computer. The only requirement for the filter is that the output response is insignificant over the range of system testing frequencies between 1 Hertz and 10 Hertz. This has been achieved hence accurate modelling was not necessary.



The load cell used was of ring type with strain gauges arranged as a Wheatstone bridge as the measuring elements. A dedicated load cell amplifier was used to power the Wheatstone bridge and produce an output. The ring was marginally sized for the task and had been yielded when the suspension was allowed to be operated at the body resonant frequency with no damping, although this condition was avoided during subsequent testing. The initial yield of the ring had produced a DC biased output which required trimming by using an adjustable DC offset added at the analogue computer amplifier summing junction.

The output of the amplifier has significant spurious noise at several distinct frequencies (50 Hertz and greater) superimposed on the measured signal. The cause of this is assumed to be from within the amplifier. The response of system components at these high frequencies is negligibly small.

Initially the axle to body relative displacement was measured directly by a string potentiometer and the body absolute displacement measured by a Linear Variable Differential Transformer (LVDT). Body and axle displacements were measured directly using a string pot and an LVDT respectively.

The LVDT has a centre position with zero volts output and positive and negative voltage output for corresponding position. The string potentiometer however has a zero output at one end of travel. The output signal was summed with a DC offset and amplified to produce a characteristic of zero output volts in the centre position with output sign corresponding to input displacement.

Measurement of the roadway input was made by using a piezoelectric accelerometer to provide an unscaled acceleration signal. This signal can be used to obtain a plot of the phase of the displacement. The actual displacement of 8.2 millimetres was measured by

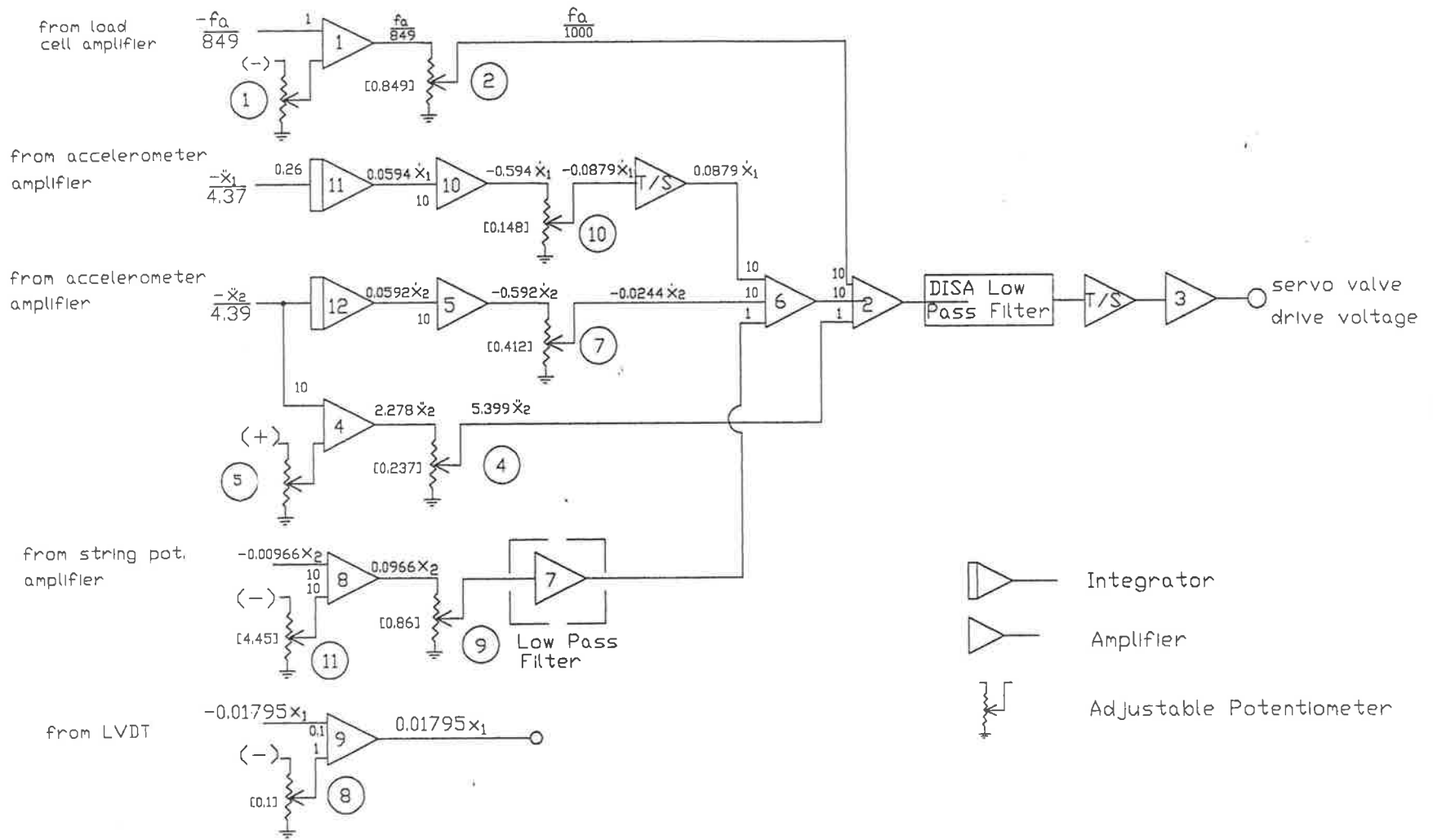
rotating the cam between highest and lowest positions and measuring the displacement of the slider with vernier calipers.

The EA-180 analogue computer, as shown in Figure 3.1 c, was used to calculate the electrical output signal to the servo valve. The circuit diagram for this is shown in Figure 3.8. The computer has a total of eight inverting amplifiers, four inverting integrators and four Track/Store inverting amplifiers which were used as unity gain inverters. The integrators were able to be alternatively configured as inverting amplifiers. Gains are chosen by suitable combination of feedback resistance via adjustable potentiometers. The set point of these potentiometers was found to be quite stable.

The servo valve drive signal is the difference between the voltages representing the desired force from the actuator and the actual force being produced. The valve was driven via two inverting amplifiers on the EA-180 after the filter to provide adequate amplification and retain the correct signal polarity because of current drive limitations of the commercial filter. The current drive limitations of the analogue computer amplifiers were evident when the system was driven with a roadway input at a frequency near resonance of the suspension system, when the shape of the valve current waveform was clearly distorted away from sinusoidal. Additional servo drive gain was available by amplifying via the EA-180.

Overcoming the problems of 50 Hertz noise and the related body spring resonance required the inclusion of a filter in the servo valve drive signal. This is not desirable as the introduction of any filters within the closed loop to attenuate signals above the range of interest will invariably introduce phase lags which may substantially affect the system performance. In spite of this, low pass filtering of the servo valve drive signal was mandatory to overcome the problem. The filter chosen was a 'DISA' brand, commercial third order Butterworth type, with the cutoff frequency adjustable on the front panel in

Figure 3.8 Analogue computer circuit design.



steps up from 10 Hertz. The actual effect of it on the system performance was found to be negligible; this is further discussed in Chapter 4. A better solution to this problem would be to redesign the springs to place any natural modes away from 50 Hertz and pay greater attention in the design of equipment to screening from electrical noise.

All signals were monitored and recorded using a Hewlett-Packard digital storage CRO and a digital volt meter.

3.4 Parameter Measurement and Calibration

The LVDT was calibrated off the test rig by setting the core position with a vernier caliper and reading the output voltage. A plot of the calibration curve is shown in Figure 3.9.

The results from the linear region shown on the figure were used to calculate a linear least squares best fit calibration figure of 52.5 mm/Volt.

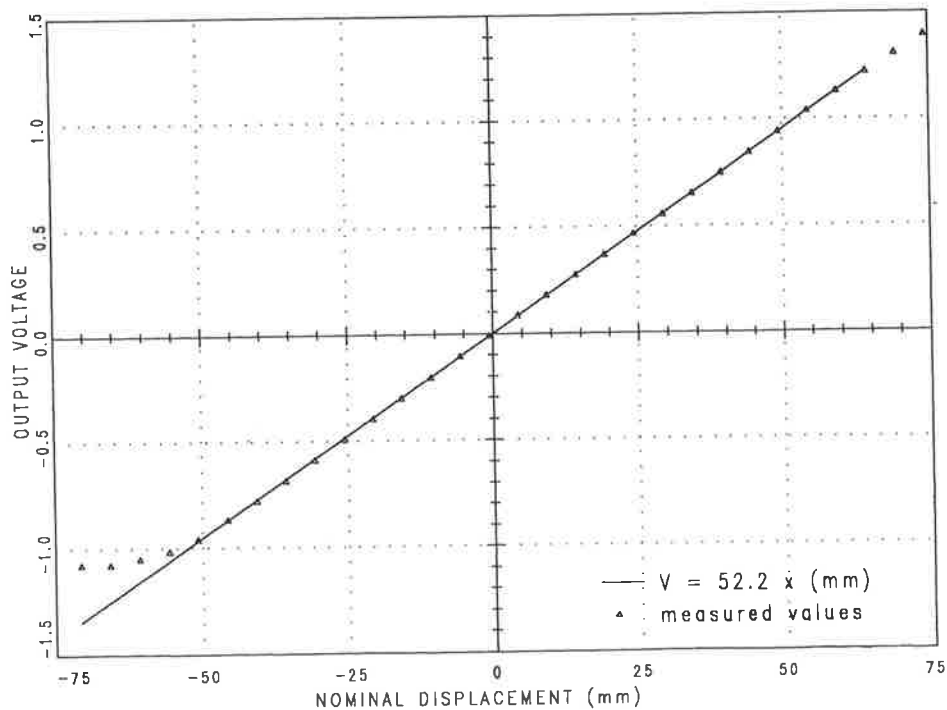


Figure 3.9 LVDT calibration curve.

Calibration of the string potentiometer was performed on the test rig by blocking the axle and body in a range of relative displacements and measuring the actual displacement with a vernier caliper. A plot of the calibration curve is shown in figure 3.10. The results appeared to be linear over the whole range shown and were used to calculate a linear least squares best fit calibration figure of 103.5mm/Volt.

Servo type accelerometer calibration is made by holding the accelerometer horizontally and measuring the amplifier output voltage. This must be measured on all four sides of the accelerometer and the results averaged as holding it truly horizontal is difficult to achieve. The accelerometer is then held vertically and the '1g' output measured. The vertical position is found when the output is maximum. Calibration constants were 4.37

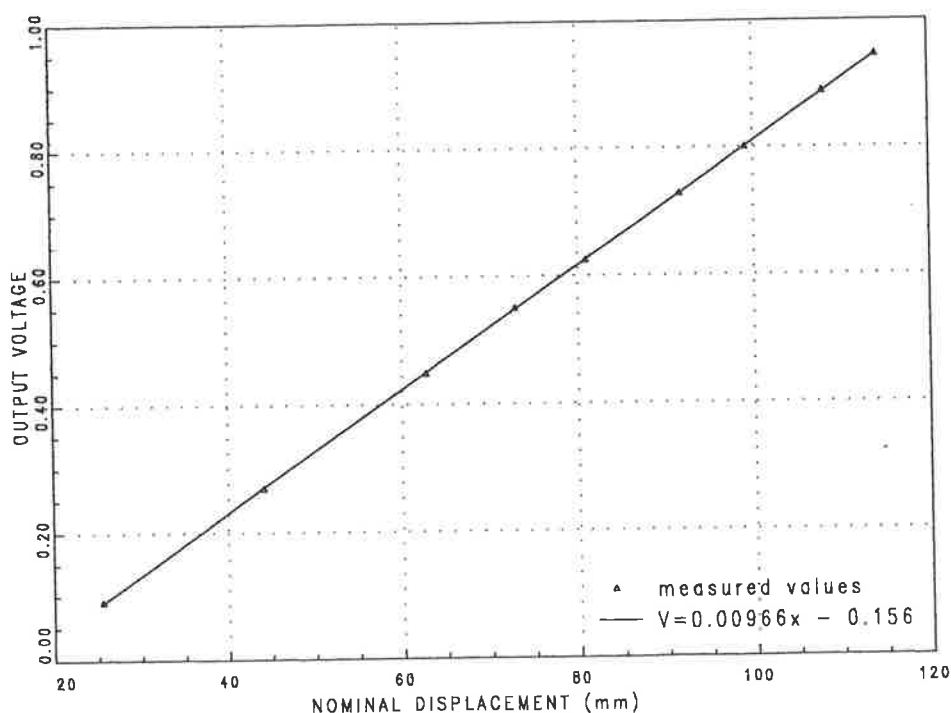


Figure 3.10 String potentiometer calibration curve.

Volts/(m/s²) and 4.39 Volts/(m/s²) for the axle and body accelerometer amplifier outputs respectively.

Measurement of the body spring stiffness was made by blocking the axle from moving and placing an accurately known mass on the body. The differential displacement was

measured using the string potentiometer. The effect of the small amount of linear bearing friction was noticeable while doing this so the average displacement of multiple measurements was used. The tyre spring stiffness was found using a similar method.

The gain constant of the integrators, K in equation (3.3), was measured by applying a 2.00 Volt sinusoidal signal at a number of frequencies and recording the output amplitude. Then the output is compared to the output of a pure integrator (which this is closely approximating). For an integrator:

$$\begin{aligned} V_{\text{output}} &= K \int V_{\text{input}} dt \\ &= K \int V_{\text{input}} \sin(2\pi f t) dt \end{aligned}$$

which assuming zero initial conditions:

$$= -KV_{\text{input}}/2\pi f \cos(2\pi f t) \quad (3.5)$$

therefore:

$$|V_{\text{output}}/V_{\text{input}}| = K/2\pi f \quad (3.6)$$

where:

V_{output} = integrator output voltage

V_{input} = integrator input voltage

K = actual gain constant of the integrator

f = input signal frequency.

The gain at each of ten frequency points up to 10 Hertz was calculated from this and averaged. Both integrators have an average gain constant of 0.26, very close to the theoretical value of 0.25.

The masses of the body and axle were measured by using a 100kg scale and making calculated allowance for a number of fittings and fixtures which could not easily be physically isolated for weighing. Springs were individually weighed and half the mass of each apportioned to the effective mass of the body and the axle. All measurements were made five times to account for minor variations due to guide rod friction.

The load cell was calibrated in situ by extending the actuator so that all forces applied to the body were via the load cell. Accurately known masses were then used to apply loads to the cell. A linear least squares best fit calibration of 849 N/Volt was made from the results. The results are shown in Figure 3.11.

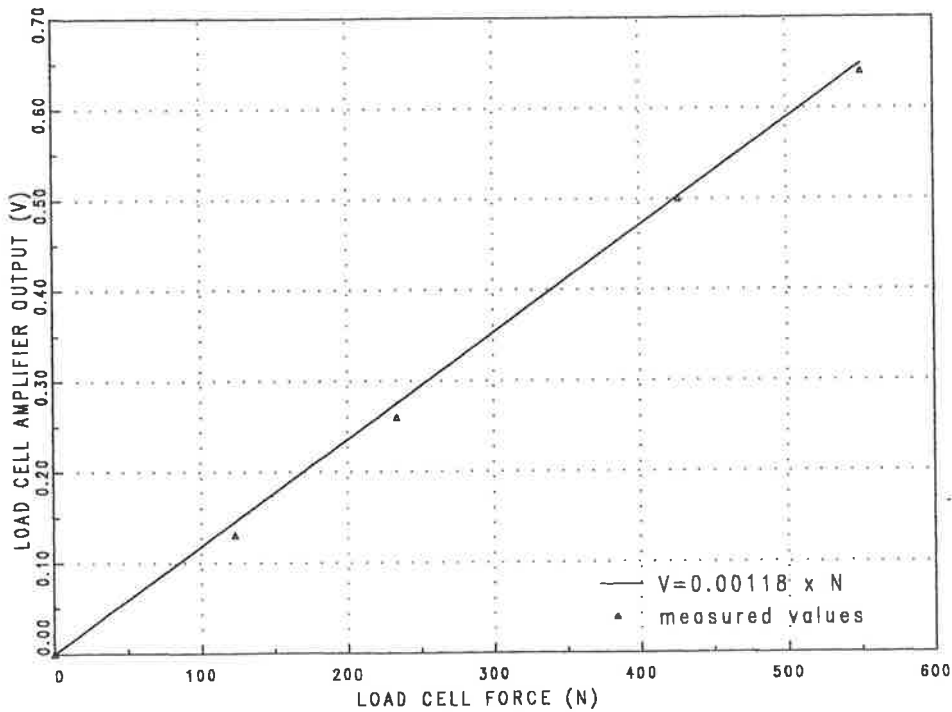


Figure 3.11 Load cell calibration curve.

CHAPTER 4

CALCULATIONS AND COMPUTER SIMULATION

4.1 Calculation of Optimum Feedback Gains

The feedback gains for the active suspension control laws to be studied are defined by equations (2.18) for the sub-optimal LQR, equation (2.22) for the optimal LQR and (2.37) for the frequency shaped types. The feedback gain calculations require solution of the Ricatti equation. The iterative method proposed by Davis and Thompson (1986) was used. The resulting Turbo-Pascal code is attached as Appendix 3. This method requires a starting vector from which to begin the search. The system must remain stable at all points through the search and hence several attempts at choosing starting vectors was necessary before finding a suitable one. The actual values in the vector are not of great importance but a solution could be achieved with fewer than thirty iterations if the search started with the sign of each element the same as the corresponding elements of the optimum solution. The system eigenvalues are calculated during the search and used to check stability.

4.1.1 Standard Form LQR Controller

The physical values for the masses and springs are stated in Chapter 3. Thompson (1976) gives some background into making an initial choice of weighting factors for the standard form LQR active suspension controller, applied in equation (2.6a). These are based on defined limits for the variables in the performance index which will not be exceeded for less than 99.7% of the time on a random road. The value of each limit would need to be adjusted on an operational suspension in accordance with the actual performance desired. For example the suspension travel limit will depend on the actual available travel between the static height of the suspension and the suspension bump stop. The available suspension travel is well in excess of the roadway input displacement hence the suspension will not bottom during operation and so there is no such limitation for the experimental suspension. Similarly, there are no defined limits for the body acceleration and dynamic tyre forces since the suspension is experimental only and on a real suspension the limitations would be

adjusted to suit a reasonable compromise in performance. The following values were assumed for this study, based on Thompson's (1976) suggested values as a start point to the suspension design:

$$q_1 = 10$$

$$q_2 = 1$$

$$\text{and } r \text{ is assumed as } 1 * 10^{-8}. \quad (4.1)$$

These values are aimed at producing similar magnitudes for each of the weighted terms in equation (2.6a).

Measured parameters were (from Figure 3.1 d.):

axle mass (M_1):	11.9 kilograms
body mass (M_2):	72.3 kilograms
body spring rate (k_s):	17.5 kiloNewtons/metre
tyre spring rate (λ):	31.5 kiloNewtons/metre

The system is described by equation (2.11). Substituting the values above:

$$A = \begin{bmatrix} 0 & 0 & 1 & 0 \\ 0 & 0 & 0 & 1 \\ -2.64 * 10^3 & 0 & 0 & 0 \\ 0 & 0 & 0 & 0 \end{bmatrix} \quad b_1 = \begin{bmatrix} 0 \\ 0 \\ -0.084 \\ 0.0138 \end{bmatrix}$$

$$Q = \begin{bmatrix} 11 & -1 & 0 & 0 \\ -1 & 1 & 0 & 0 \\ 0 & 0 & 0 & 0 \\ 0 & 0 & 0 & 0 \end{bmatrix} \quad R = 1 * 10^{-8}$$

(4.2)

The Kalman gains calculated from the Ricatti equation and equation (2.7) are:

$$K = [20825 \quad -10000 \quad 502.1 \quad -1396]^T \quad (4.3)$$

The desired control force is given by equation (2.15). Substituting the measured value for k_s and the values in equation (4.3) into equations (2.19) to (2.21) give:

$$k_s = 17480$$

$$k_a = -54.08$$

$$k_d = 877.7$$

$$k_v = -1562.5$$

Rearranging equation (2.18) for the desired control force:

$$\begin{aligned} u &= k_s(x_1 - x_2) + k_d(\dot{x}_1 - \dot{x}_2) + k_v \dot{x}_2 + k_a \ddot{x}_2 \\ &= k_s(x_1 - x_2) + \dot{x}_1(k_d) + \dot{x}_2(k_v - k_d) + k_a \ddot{x}_2 \end{aligned} \quad (4.4)$$

The body springs already provide the first term and hence this can be eliminated from the desired force to be produced by the actuator (u_{act}), leaving:

$$\begin{aligned} u_{act} &= \dot{x}_1(k_d) + \dot{x}_2(k_v - k_d) + k_a \ddot{x}_2 \\ &= \dot{x}_1(877.7) + \dot{x}_2(-2440) + \ddot{x}_2(-54.08) \end{aligned} \quad (4.5)$$

which may be directly implemented as amplified transducer output signals to produce an electrical signal representing the desired actuator force.

For the optimal LQR controller, the values in equation (4.3) are substituted into equations (2.25) and employing equation (2.22):

$$u_{act} = k_s(x_1 - x_2) + k_d(\dot{x}_1 - \dot{x}_2) + k_v \dot{x}_1 + k_a \ddot{x}_2 + k_b \ddot{x}_1 \quad (4.6)$$

Allowing for the body springs to produce the force associated with the k_s term:

$$\begin{aligned} u_{act} &= k_d(\dot{x}_1 - \dot{x}_2) + k_v \dot{x}_1 + k_a \ddot{x}_2 + k_b \ddot{x}_1 \\ &= 2440(\dot{x}_1 - \dot{x}_2) - 1563 \dot{x}_1 - 97.0 \ddot{x}_2 - 5.32 \ddot{x}_1 \end{aligned} \quad (4.7)$$

4.1.2 Frequency Shaped Controller

The desired control force is given by equation (2.37). Substituting the physical values into equations (2.43) gives:

$$F_a = \begin{bmatrix} 0 & 0 & 1 & 0 & 0 \\ 0 & 0 & 0 & 1 & 0 \\ -2.64 \times 10^3 & 0 & 0 & 0 & 0 \\ 0 & 0 & 0 & 0 & 0 \\ -1 & 1 & 0 & 0 & 0 \end{bmatrix} \quad G_a = \begin{bmatrix} 0 \\ 0 \\ -0.084 \\ 0.0138 \\ 0 \end{bmatrix} \quad (4.8)$$

Assume a PID filter characteristic of $(s^2 + 10s + 40)/s$, which gives:

$$Q = \begin{bmatrix} 111 & -101 & 10 & -10 & -400 \\ -101 & 101 & -10 & 10 & 400 \\ 10 & -10 & 1 & -1 & -40 \\ -10 & 10 & -1 & 1 & 40 \\ -400 & 400 & -40 & 40 & 1600 \end{bmatrix} \quad (4.9)$$

Arbitrarily assume a value for R of 1×10^{-7} . The optimum feedback gains (components of K_a) as determined from the solution of equations (2.41) and (2.42) are then given by:

$$\begin{aligned} K_1 &= -2.387 \times 10^4 \\ K_2 &= -2.939 \times 10^4 \\ K_3 &= 3.195 \times 10^3 \\ K_4 &= -2.585 \times 10^3 \\ K_5 &= -1.265 \times 10^5 \end{aligned}$$

The following coefficients may then be computed as required in equation (2.37):

$$\begin{aligned} C_1 &= 11.90 \\ C_2 &= -17350 \\ C_3 &= 360.2 \\ C_4 &= -1526 \\ C_5 &= -74700 \end{aligned}$$

Hence the desired control force (u_{act}) is:

$$u_{act} = (11.90)\ddot{x}_1 - (17350)(x_2 - x_1) + (360.2)\dot{x}_1 - (1526)(\dot{x}_2 - \dot{x}_1) - (74700)\int(x_2 - x_1)dt \quad (4.10)$$

This may be used as the basis for the design of appropriate sensor output amplification to generate an electrical signal representing the desired actuator force.

4.2 Computer Simulation of Suspension Performance

4.2.1 Simulation of Suspension Theoretical Performance

The theoretical performance of the LQR controller is described by equations (2.9). The term for the control force 'u', can be replaced with u_{act} from equation (4.4) for the sub-optimal controller and equation (4.6) for the optimal controller.

The time response performance of the suspension was modelled using a fourth order Runge-Kutta digital simulation on a personal computer. The simulation was written in Turbo Pascal (Version 5). The main program sets up initial conditions and controls a number of subroutines. The subroutine which defines the system by calculating the system derivatives at each time step is shown in Figure 4.1 a.. Figure 4.1 b. lists each variable and constant and states the values assumed for the modelling.

4.2.2 Simulation of Experimental Suspension Performance

Modelling of the experimental suspension is based upon the same derivatives subroutine as for the theoretical simulation. The calculation of actual force output from the inner loop is expanded to simulate the amplifier and hydraulic elements that actually produce the force on the experimental suspension. This is in contrast to the theoretical model, where the required force is produced without error.

The DISA third order Butterworth filter (discussed in Chapter 3) was initially included in the model but had a negligible effect on system performance. The practical testing had also showed that the filter performance had negligible affect on the suspension performance. Since this added a further three state variables which significantly increased the computer simulation run time, it was deleted from the final model. The filters used for integrating the acceleration signals to obtain body and axle velocities have phase characteristics which do not exactly conform to a desired 'pure' integrator. These characteristics were ignored as negligible also.

```

PROCEDURE derivs(t :extended; y:rarray; VAR dydt :rarray;
VAR Xsp,Fm,Fa,Qsy,Qsz,Qye,Qze,Ql,Qf,x3dot,x4dot :extended);

VAR Vdesire,Verr,Vlc,Vlpdd,Vposn,
    dPsy,dPsz,dPye,dPze,
    Qz,Qy,Qya,dQy,dQz,Qe,Qza,
    x0,dy,
    Vddd,
    u,
    Cy,Cz,
    Fy,Fz,Ff          :extended;

BEGIN (* derivs *)
x0      :=0.0041*sin(2*pi*9*t);
Fa      :=y[Py]*Ay-y[Pz]*Az;
Vlc     :=Klc*Fa;
Vposn   :=Klp*y[x2];      {now low pass filter it}
Vlpdd   :=Vposn-a1*y[Vlpd]-a2*y[Vlpout];
dydt[Vlpd] :=Vlpdd;
dydt[Vlpout]:=y[Vlpd];   { low passed }
Vdesire :=kd*y[x3]+(kv-kd)*y[x4]+ka*x4dot+Klpfilter*y[Vlpout];
Verr    :=Vdesire-Vlc;
Xsp     :=Kf*Verr;
IF ABS(Xsp)>1.0e-3 THEN Xsp:= sign(Xsp)*1.0e-3;
                                {defines spool limits of travel}

{valve}
{Qsy & Qze}
dPsy:=Ps-y[Py];
dPze:=y[Pz]-Pe;
IF Xsp<0 THEN
BEGIN
    Qsy:=0;
    Qze:=0;
END
ELSE
BEGIN
    Qsy:=sign(dPsy)*Xsp*Csp*Sqrt(ABS(dPsy));
    Qze:=sign(dPze)*Xsp*Csp*Sqrt(ABS(dPze));
END;

```

Figure 4.1a Pascal code for the derivatives subroutine used in computer simulation program.


```

{Qsz & Qye}
dPsz:=Ps-y[Pz];
dPye:=y[Py]-Pe;

IF Xsp>0 THEN
BEGIN
  Qsz:=0;
  Qye:=0;
END
ELSE
BEGIN
  Qsz:=sign(dPsz)*Xsp*Csp*Sqrt(ABS(dPsz));
  Qye:=sign(dPye)*Xsp*Csp*Sqrt(ABS(dPye));
END;

Qy:=Qsy+Qye; {get neg flow if rod retracting}
Qz:=Qsz+Qze; { " " " " }

{actuator}
Qya:=(y[x4]-y[x3])*Ay;
  {Qya +ve if rod is extending; ie: oil is added to side y}
dQy:=Qy-Qya; {+ve for rod extending}
Qza:=(y[x4]-y[x3])*Az;
  {Qza -ve if rod is retracting; oil is added to side z}
dQz:=Qza-Qz; {+ve for rod retracting}
dy :=y[x1]-y[x2];
Cy:=(Vy0-Ay*dy)/Bmod;
Cz:=(Vz0-Az*dy)/Bmod;
dydt[Py]:=dQy/Cy; { dydt(Py) }
dydt[Pz]:=dQz/Cz; { dydt(Pz) }

{load}
x4dot:=(Fa+ks*dy)/m2;
x3dot:=(1a*(x0-y[x1])-Fa-ks*dy)/m1;
dy :=y[x1]-y[x2];
u :=ks*dy+100*(kd*(y[x3]-y[x4])+kv*y[x4]+ka*x4dot);
  {x100 since constants are /100. This maps the analogue
  computer implementation}
dydt[x4]:=x4dot;
dydt[x3]:=x3dot;
dydt[x2]:=y[x4];
dydt[x1]:=y[x3];

END; (* derivs *)

```

Figure 4.1a (continued) Pascal code for the derivatives subroutine used in computer simulation program.

Variables of type EXTENDED:

Vdesire	Voltage representing desired force output.
Verr	Error between demand and actual servo voltage.
Vlc	Voltage output from load cell amplifier.
Vlpdd	Voltage internal to digital low pass filter, see Figure 4.2.
Vposn	Voltage at input to low pass filter, see Figure 4.2.
dP _{sy} , dP _{sz}	Incremental pressure differentials between hydraulic supply and y and z chambers.
dP _{ye} , dP _{ze}	Incremental pressure differentials between hydraulic return and y and z chambers.
Q _{sy} , Q _{sz}	Flowrate from supply to y and z chambers.
Q _z , Q _y	Net flowrate to y and z chambers through servo valve.
Q _{ya} , Q _{za}	Flowrate component due to velocity of piston.
dQ _y , dQ _z	Net flowrate to y and z chambers.
Q _{ye} , Q _{ze}	Flowrate from y and z chambers to return.
x0	Road input displacement.
dy	Difference in displacement between body and axle.
u	Force developed by actuator.
C _y , C _z	Hydraulic capacitance of y and z chambers.
F _y , F _z	Force developed by y and z chambers on piston.
F _a	Net force developed by actuator.
X _{sp}	Spool displacement.
x3dot, x4dot	Acceleration of axle and body.
end_time	Time limit for simulation.
t	Current value of time.
h	Time variable used in Runge-Kutta routine.

Array variables:

y	Contains current value of integrated variables at time 't'.
dydt	Contains current value of differential of integrated variables at time 't'.

Figure 4.1b Variables and constants used in computer simulation program.

```

CONST
Bmod  = 1500.0e6;
pi    = 3.141592654;

      {power supply}
Ps    = 9.93e6;   {the mean between 1530 and 1350 psi, which
                  is the operating range}
Pe    = 0.1e6;

{Pz0= 4.265e6;   Py0= 5.565e6;  these are settings for the
10.6mm 'step' input, since that simulation is dependant upon
the initial conditions, where the sinusoidal input assumes a
steady state}

Py0   = 4.915e6;
Pz0   = 4.915e6;
      {valve}
Csp   = 3.0e-5;
      { m^3/s/m/Pa^0.5 flow coefficient - estimated!}
Kf    = 1.0e-4;  {=spool displ/input voltage}

Ay    = 0.285e-3;
Az    = 0.285e-3;
m1    = 11.9;
m2    = 72.3;
Vy0   = 0.05e-3;
Vz0   = 0.05e-3;
Cp    = 0.0e-10;  { leakage factor past the piston }
Klc   = 0.01;    { V/N - load cell scale*0.849*10 }
Klp   = 0.1932;  { V/mm - string pot scale*0.2*10 }
la    = 31450.0;  {N/m}
ks    = 17480.0;  {N/m}
ka    = -0.5408;  {N/m/s/s, /100}
kd    = 8.79;    {N/m/s, /100}
kv    = -15.625; {N/m/s, /100}
Klpfilter = 2.1;
a1    = 20.0;
a2    = 10.0;    {2nd order low pass filter chars}

nvar=8;
{ The following are indeces within arrays y & dydt; eg: y[Py]
contains current value of Py. }
Py    = 1;
Pz    = 2;
x1    = 3;
x2    = 4;
x3    = 5;
x4    = 6;
Vlpd  = 7;
Vlpout = 8;

```

Figure 4.1b (continued) Variables and constants used in computer simulation program.

The roadway input is simulated by a sinusoidal displacement:

$$x_o = 0.0041 * \sin(2\pi ft) \quad (4.11)$$

where x_o represents the vertical motion at time t of the eccentric cam used to excite the test rig at frequency (f).

The valve and actuator model can be developed from that presented by Zeller (1969) and Dransfield (1981). For a reference to and description of symbols used in the following discussion, see Figure 4.1 b. The instantaneous actuator force (F_a) is given by:

$$F_a = P_y * A_y - P_z * A_z \quad (4.12)$$

where:

P_y and P_z are the instantaneous pressures applied to each side of the piston and A_y and A_z are the areas of each side of the piston; see Figure 3.2 (page 41).

The load cell has a linear output:

$$V_{lc} = K_{lc} * F_a \quad (4.13)$$

The output from the body position transducer is:

$$V_{posn} = K_{lp} * x_2 \quad (4.14)$$

where K_{lp} is the calibration constant of the transducer, and x_2 is the body displacement from the rest position. This signal is then passed through the body position feedback, low pass filter discussed on page 49. Constants $K_{lpfilter}$, a_1 and a_2 were determined by simulating the filter (using MATLAB mathematical package) and matching the modelled performance to the actual shown in Figure 3.7 (page 50). The constants were selected to have negligible effect on the model performance in the frequency range of interest.

The desired force output from the actuator for the sub-optimal LQR controller is given by equation (4.4) but modified by the addition of the position feedback signal and the deletion of the term associated with the body springs:

$$u_{act} = \dot{x}_1(k_d) + \dot{x}_2(k_v - k_d) + \ddot{x}_2 k_a + K_{lpfilter} * V_{lpout} \quad (4.15)$$

The voltage V_{desire} is a scaled representation of u_{act} in the simulation. The values for feedback constants k_d , k_v and k_a must be modified by the load cell constant as was done for the actuator force in equation (4.13). This has been done in the definition of the constants resulting in:

$$\begin{aligned} k_a &= -0.5408 \\ k_v &= 8.79 \\ k_d &= -15.625 \end{aligned} \tag{4.16}$$

The error between the desired and actual actuator forces is the difference between u_{act} and F_a , represented by:

$$V_{\text{err}} = V_{\text{desire}} - V_{\text{lc}} \tag{4.17}$$

where " V_{err} " is the error voltage.

The error voltage is amplified and converted into spool movement by the servo valve. The simulation ignores all servo valve and input amplifier dynamics in making the assumption that the spool displacement produced by the first stage of the valve is proportional to the applied voltage:

$$X_{\text{sp}} = K_f * V_{\text{err}} \tag{4.18}$$

This is justifiable since the bandwidth of the servo valve used was in excess of ten times the maximum frequency simulated and hence the servo transfer function had little affect. The servo valve manufacturer advises that servo valves are usually modelled by first or second order approximations to the actual relationship between input drive current and output flow rate. A first order approximation was initially included but the performance difference between this and the simple linear gain model in equation (4.18) was confirmed to be negligible and obtained at the expense of greater model complexity with a consequent increase in run time. Spool displacement limits are applied. These were found to have a significant effect on the modelled system performance near the resonance frequency of the suspension.

The flow rate of hydraulic fluid into the actuator is dependent on the flow rate delivered by the valve, the load pressure and the actuator velocity. The instantaneous pressure differential across the valve spool is given by:

$$dP_{sy} = P_s - P_y \quad (4.19)$$

where P_s is the hydraulic supply pressure and P_y is the pressure in the 'y' chamber of the actuator. Similarly the pressure differentials between the 'z' chamber and the supply and both chambers and the return port may be formulated.

The spool's flow characteristics are assumed to be:

- a. zero flow at the null position or at displacements where the spool land overlaps the port.
- b. Flow proportional to the square root of the pressure differential across the spool for spool displacements where the land opens a port, see Figure 3.4.

The actual flow will also be dependent on the overlap or underlap of the spool land on the valve ports. The servo valve's data sheet from the manufacturer does not state any specific details regarding the spool lap, however it is evident from the Null Flow Gain information provided that the production valves vary about the 'null lap' condition from overlapped to underlapped. The actual lap condition is complex to model as it is influenced by the lap of each spool land with each port and also by the radial clearance of the spool in the valve body. A simple model of valve underlap was initially included in the simulation, where it was assumed that all ports were overlapped or underlapped by the same amount. Whether the valve was overlapped or underlapped was found however, to have a negligible affect on performance. Viersma (1980) points out that it is normal practice to neglect the effects of valve lap. Consequently this complication was removed from the model.

The flow rate through the valve is then:

$$Q_y = \text{sign}(dP_{sy}) * X_{sp} * C_{sp} * \sqrt{|dP_{sy}|} \quad (4.20)$$

where C_{sp} is the constant spool flow coefficient relating flow rate to spool displacement. It is strictly correct to include the first term and to use the absolute value of dP_{sy} to ensure that correct flow directions are maintained. In actual practice the only conditions where the value of the differential pressure (dP_{sy} in this case) drops below zero is when the system operating conditions are either forcing fluid back into the supply port or the return line is supplying fluid into the actuator. Such conditions could only be achieved under severe resonance and hence equation (4.20) can be simplified to:

$$Q_y = X_{sp} * C_{sp} * \sqrt{dP_{sy}} \quad (4.21)$$

Four such flow equations need to be formulated to define the instantaneous flows to and from each actuator chamber from both the supply and return lines. Note that the constants representing the servo valve characteristics C_{sp} and K_f could have been reduced to a single constant since they are always multiplied together in the model. They were kept separate only to simplify discussion on the torque motor and spool valve characteristics the model.

The flow into or out of the actuator chamber can be calculated:

$$Q_{ya} = A_y * (x_4 - x_3) \quad (4.22)$$

where A_y is the effective piston area and $(x_4 - x_3)$ is the piston velocity in the actuator body representing the differential velocities of the vehicle body and axle. The difference between Q_y and Q_{ya} is due to the compressibility of the hydraulic fluid and the rate of change of chamber pressure can be determined from:

$$\frac{dy}{dt}(P_y) = \frac{dQ_y}{C_y} \quad (4.23)$$

$$\text{where } dQ_y = Q_y - Q_{ya} \quad (4.24)$$

and C_y is the compliance of the fluid in the actuator calculated:

$$C_y = (V_{y0} - A_y * dy) / B_{mod} \quad (4.25)$$

Thus the simulation has eight state variables; including the actuator chamber pressures, P_y and P_z ; the vehicle body and axle displacements and velocities x_1 to x_4 and the body displacement feedback filter variables V_{lpd} and V_{lpout} . The derivatives for each are

calculated by the fourth order Runge-Kutta method at each iteration. The state variables are stored in the array $y[]$ and the estimate of corresponding derivatives is stored in array $dydt[]$; for example, the array elements $y[x1]$ and $dydt[x1]$ hold the current values of the axle displacement and velocity.

The computer model could readily be used for simulation of the system step input response and the steady state response with sinusoidal input. The response to a step input was modelled to simulate the step input used on the physical test rig. The initial conditions were:

- a. The axle was given a fixed displacement upward of 10.6 millimetres. At time zero this displacement was released.
- b. The initial actuator pressures were adjusted to provide the correct values for the system to maintain all other initial conditions at zero; ie: the initial pressure differential balances the spring force due to the upward movement of the axle with zero displacement of the body.

For the steady state response each simulation run was made by using a sinusoidal input at the desired frequency, assuming zero values for initial conditions and continuing the simulation until transients had dissipated. The frequency response of the axle and body were determined by performing a number of such simulations across the range of frequencies from 1.0 to 15 Hertz.

During each simulation run values for each of the key variables at one thousand time steps were stored for later plotting.

The values for the assumed performance parameters used to model the servo valve C_{sp} and K_f , were estimated first from data supplied by the valve manufacturer and then adjusted until the modelled performance fitted as closely as possible to the measured performance. Such an adaptation of the model is justified since C_{sp} is dependent on many factors and will vary from valve to valve and with different operating conditions. In any case, it cannot be measured directly and must be inferred from the performance of a driven system. The

parameter K_f is an assumed value which could be accurately determined if desired.

However since only the product of C_{sp} and K_f controls the model output and the precise value of each is not so important.

the axle and body displacements. The result at each frequency R_f , is calculated from:

$$R_f = 20 \cdot \log \left(\frac{\text{peak-peak body/axle displacement}}{\text{peak-peak of input displacement}} \right) \quad (5.1)$$

Smooth curves were produced through these points with splines. It is evident from Figure 5.1 that the sub-optimal controller has only a small variation in performance from the optimal controller, the curves being within 2db over the range 1 Hertz to 10 Hertz. This has an interesting practical implication in that the sub-optimal type requires one less state variable measurement and hence needs less feedback signal processing, although still achieving near optimal performance.

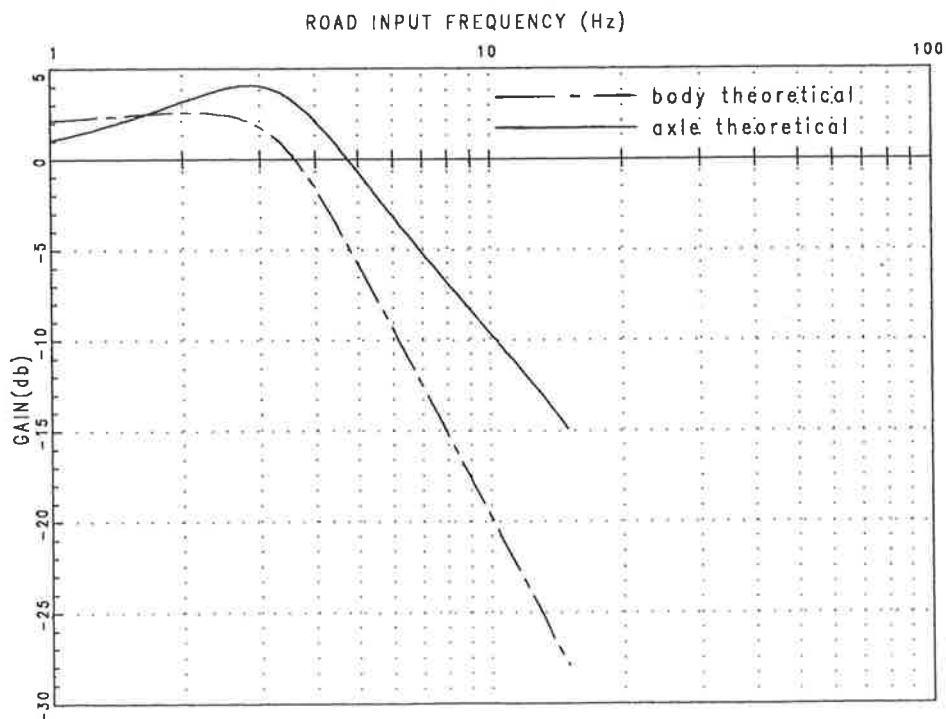


Figure 5.2 Theoretical suspension performance for the 'frequency shaped' controller.

The theoretical response of the frequency shaped controller can be modelled similarly for the LQR controllers. The results of simulation are shown in Figure 5.2. The theoretical performance calculation takes no account of the actuator dynamics. Simulating the laboratory suspension requires using the model developed in Chapter 4. The term for the control force 'u', is replaced with u_{act} from equations (4.5) for the sub-optimal controller and from equation (4.7) for the optimal controller. In the same way, equations (2.26) and (2.27) are applied for the simulation of the 'frequency shaped' suspension with the control force described by equation (4.10). The response of the suspension, including the actuator

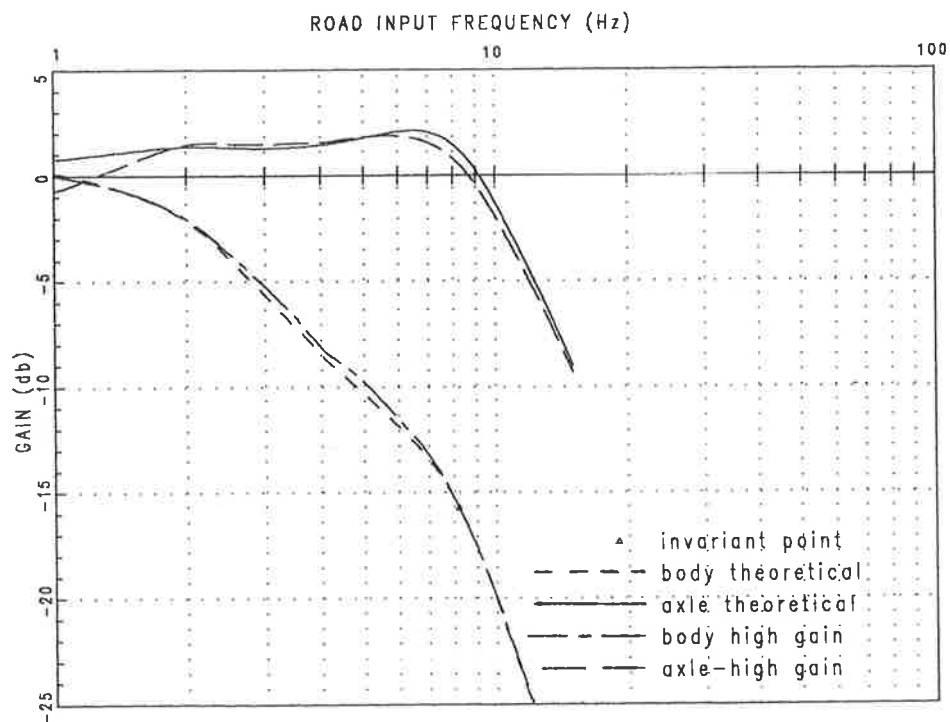


Figure 5.3 Comparison of frequency response of theoretical and modelled laboratory suspension with sub-optimal controller.

dynamics can be made to closely match the theoretical response. Increasing the product of the servo-valve gain constants, K_f and C_{sp} brings the modelled performance closer to the theoretical curve. Figures 5.3 and 5.4 compare the modelled performance of the

laboratory suspension with the theoretical suspension performance. These curves assume a servo-valve overall gain ($K_f \times C_{sp}$) of 150×10^{-9} . It is evident in both cases that a suspension with an hydraulic powered 'inner loop' is able to perform very similarly to the theoretical suspension. From these results it appears that for the laboratory suspension to be able to perform as desired, adjustment of the gain of the 'inner loop' servo-valve control is required.

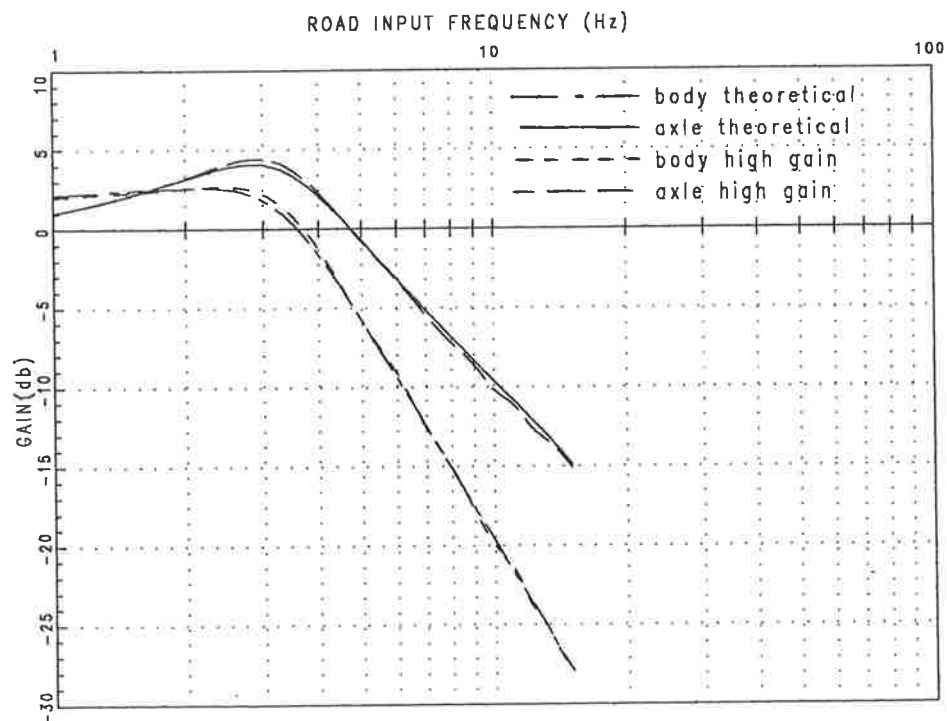


Figure 5.4 Comparison of frequency response of theoretical and modelled laboratory suspension with frequency shaped controller.

5.2 Experimental Results

The aim was to demonstrate an experimental controller for the frequency shaped and the LQR suspension designs. The frequency shaped feedback control was attempted first and several problems became immediately apparent. The problems found with the

instrumentation have been mentioned in Chapter 3. It is necessary to achieve simultaneous, near zero initial conditions for the suspension sensor outputs while connecting the servo-valve in order to prevent it being damaged by excessive feedback voltage; ie: ensure that each of the component terms on the right hand side in equation (4.10) is approximately zero to balance with the left hand side, since $u_{act}(t=0) = 0$. The difference between u_{act} and the sum of terms on the right hand side becomes the error signal for driving the servo valve. The high gain applied to the integral of the body to axle relative displacement made it very difficult to achieve approximately zero output from this component for any significant period of time. The situation was also exacerbated by the hydraulic supply pressure fluctuations as well as drift of the valve and integrator causing difficulty in trimming the integrator output voltage to zero. All attempts caused the integrator output to be well in excess of the maximum allowable servo valve drive voltage and so further efforts on the frequency shaped controller were abandoned. This problem could be solved by a controller design with a reduced gain on the integral of the relative displacement error, at least during system start up. Alternatively a drive current limiting device could be used to guarantee no damage to the servo-valve.

The sub-optimal LQR controller was then attempted. This was simpler to set up since it did not have the problems associated with the high gain integrator. When operating however the relative displacement between the body and axle was minimal, typically less than 1 millimetre for a sinusoidal input of 8.2 millimetres to the tyre. Such small relative motion gave the visual impression that the axle and body are locked together. Typical time traces are shown in Figures 5.5 and 5.6. Figure 5.5 shows a typical step input, where the axle and body moved with only a small relative displacement and phase difference. The step response is highly oscillatory compared to the theoretical (and the desired) response. The frequency response was determined by running the roadway input at fixed frequencies from 2 to 11.2 Hertz and recording the peak responses of the axle and body displacements.

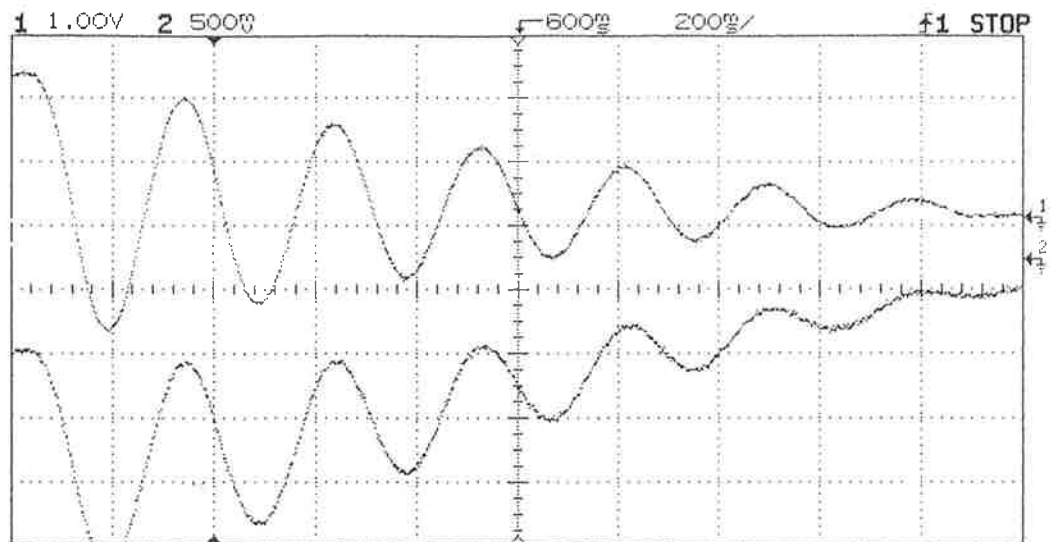


Figure 5.5 Typical recorded response with step input, sub-optimal LQR controller. (Note that the raw outputs from the transducers have different scales).

Trace 1 (upper) is the axle response.

Trace 2 (lower) is the body response.

The output signal from an accelerometer placed on the roadway input showed that the simple sinusoidal motion expected also included other influences. Figure 5.6 includes a typical trace of the raw recorded accelerometer output from the roadway input shaker. The accelerometer traces were recorded purely as an indication of the actual motions present and is much simpler to implement than fitting of a displacement transducer. The example presented was typical, with the disturbance at 50 Hertz constant both in frequency and displacement at all roadway input frequencies. As discussed in Chapter 3, it is strongly suspected to be electrical interference from an unidentified source. During some periods, recordings were made consistently free of the 50 Hertz component. The servo valve drive voltage also demonstrated an intermittent noise input, but clearly at 50 Hertz, indicating electrical interference from an unidentified item of equipment within the laboratory. The

noise in the accelerometer output is of no consequence to the results since the output is not used as part of the suspension system. The 50 Hertz noise in the servo-valve drive voltage was filtered before passing to the servo valve. The gain of this filter at 50 Hertz is -42db which ensures that the 50 Hertz component is of no significance.

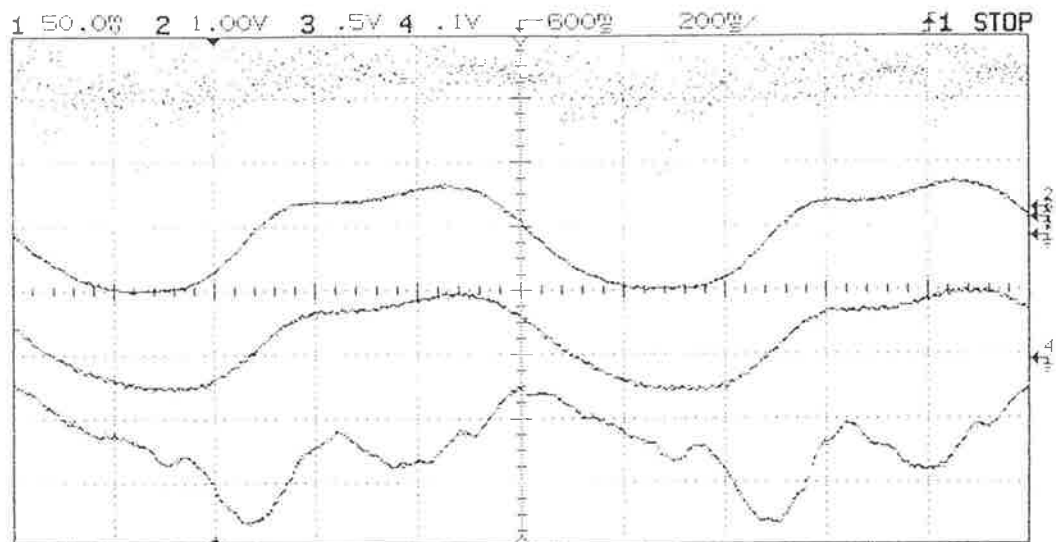


Figure 5.6 Typical recorded response with sinusoidal input, sub-optimal LQR controller.

Trace 1 (top) is the accelerometer response; placed on the roadway input shaker.

Trace 2 (second from top) is the axle response.

Trace 3 (third from top) is the body response.

Trace 4 (bottom) is the filtered accelerometer response; filter is third order Butterworth, 20 Hertz cutoff.

Step inputs were made by inserting a block between the axle and the test rig frame. This displaced the axle 10.6 millimetres upwards. The body position feedback causes the body position to drive to the original rest height, although this takes in excess of one minute because of the low feedback gain. Thus the step change in displacement was applied to the axle only and the hydraulic cylinder produced a force to exactly balance that caused by

compression of the body springs by 10.6 millimetres. To initiate the step, the block was removed rapidly.

Figure 5.7 shows a typical trace of body and axle step response with an expanded time axis. Note that before the step the axle displacement is constant and the body displacement is

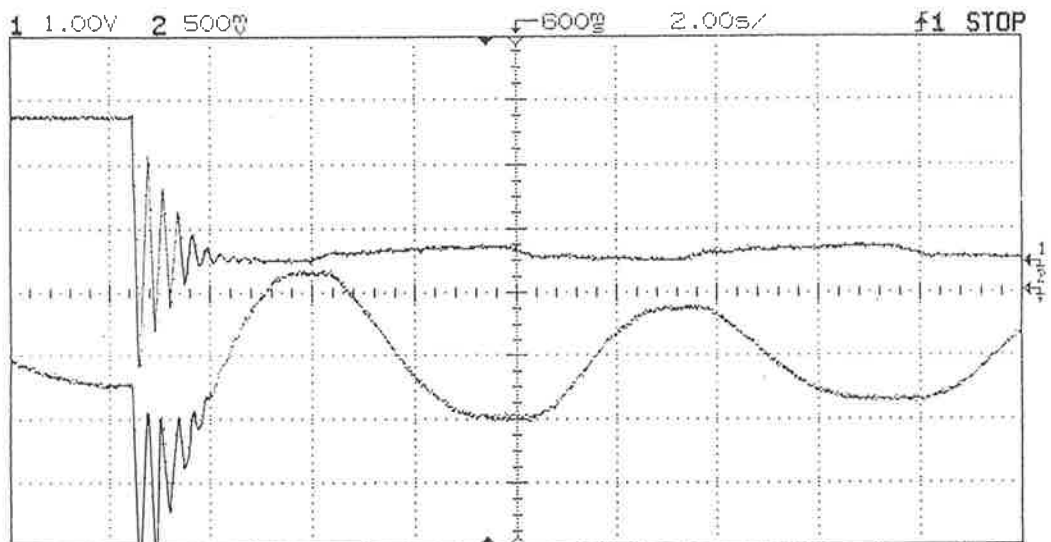


Figure 5.7 Typical recorded displacement for a step response, showing body and axle motion prior to and after the step input, sub-optimal LQR controller.

Trace 1 (upper) is the axle response.
Trace 2 (lower) is the body response.

fluctuating with the hydraulic pressure with a period of approximately 7.3 seconds. The overall feedback gain of the body displacement loop at this frequency is -59db. Hence the feedback loop had insignificant effect on maintaining a constant body position in response to the hydraulic fluctuations. After the step there are corresponding opposite motions of the body and axle with the same period as the hydraulic pressure changes, since the axle was

then free to move. The drift of the body upwards through the 'zero' displacement position can be seen in Figure 5.5 and Figure 5.7. This was consistent for all step response traces. The hydraulic accumulator holds only a very small volume of oil before the pressure has dropped sufficiently to initiate re-charging from the pump. This oil volume was consumed rapidly during the step input tests. Thus the hydraulic supply system was always charging the accumulator several seconds after the step input, as the transient response of the suspension was diminishing.

A smaller disturbance is also noticeable in the filtered trace of the roadway input. Figure 5.6 includes a trace of the roadway input, filtered to remove the 50 Hertz noise. The filter used (Kron-Hite model 3322) was set at 20 Hertz cutoff. Its frequency response appeared to be that of a third order Butterworth and the affect on the response up to 10 Hertz was negligible. The peaks in the trace were in identical angular positions irrespective of frequency. This disturbance is caused by the drive train characteristics, such as from the DC motor or from the roller bearing condition. The magnitude of this disturbance was greatest for rotating speeds in the region of 2.5 revolutions per second. The disturbing frequency is well above the axle resonant frequency and hence there is negligible transmission to the axle.

Figure 5.8 shows some measured amplitude frequency response points for the axle and body in the initial set-up condition. Also shown are curves indicating the computer modelled performance. These were produced as for the initial model of the laboratory suspension, except that the product $K_f \times C_{sp}$ was reduced to 3.0×10^{-9} and the spool travel was limited to 1.0 millimetres from the neutral position. These figures were chosen by trial and error to obtain a reasonable match between the actual and modelled performances.

Adjustment of the gain and spool travel to fit the measured data is justified since they could not be measured directly. Moog's published nominal data for the servo-valve indicates that $K_f \times C_{sp} \approx 8 \times 10^{-9}$. Moog's data applies to the valve only and makes no allowance for the pressure losses between the valve and the inside of the actuator. Making such an allowance

would effectively reduce C_{sp} . Since the fluid path involves a number of sharp corners and small supply channels, it is reasonable that the value of $K_f * C_{sp} = 8 \times 10^{-9}$ be reduced.

Thus it is concluded that adapting the constants to fit the measured results is valid.

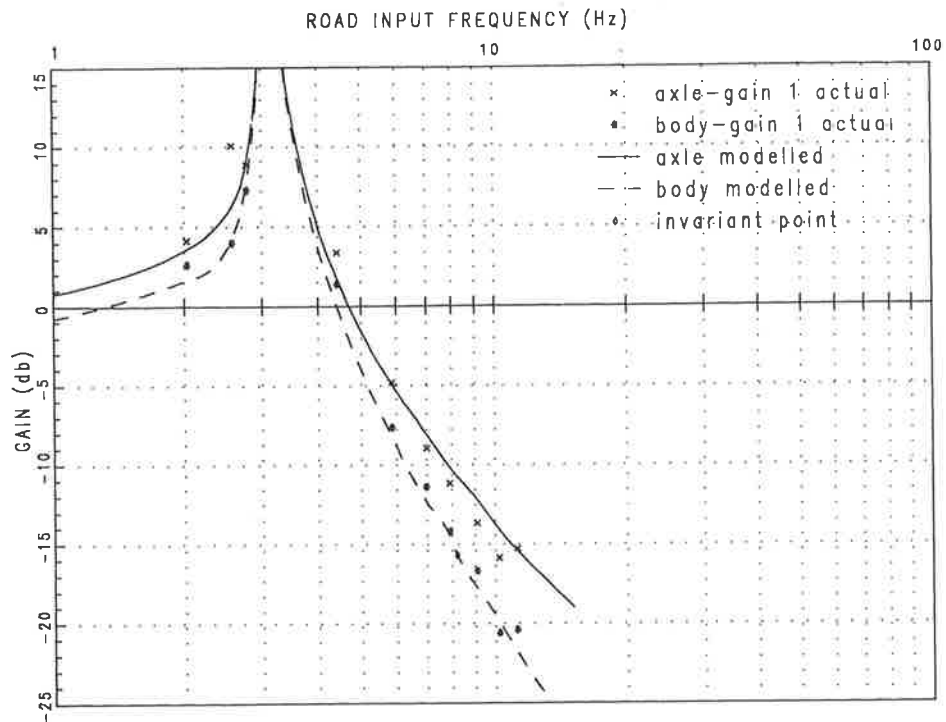


Figure 5.8 Body and axle frequency responses for the original set-up of the laboratory suspension; sub-optimal LQR controller.

The system demonstrated a sharp resonance at approximately 3.4 Hertz with overall response characteristics of a lightly damped single degree of freedom, mass/spring system. This is effectively the response for the single degree of freedom system of the combined body and axle mass on the tyre spring. The sharp response peak is due to the very light damping of the spring used to simulate the tyre. The limited travel of the spool is important in achieving the high resonant peak. This restricts the flow of fluid to the actuator and imposes a limit to the actuator response velocity. This can be easily demonstrated with the computer model by allowing unlimited spool travel, in which case the amplitude of the

resonant peak is significantly reduced. Spool displacement limiting occurs over the range of approximately 2.5 to 4.0 Hertz.

Recordings were also made with a roadway input at 1 Hertz. These results have not been presented as the speed of rotation of the roadway input cam drive shaft could clearly be seen to be non constant, slowing down as the cam lifted the vehicle masses to apply the vertical input and speeding up on the reverse side of the cam. The recorded body and axle positions clearly departed significantly from sinusoidal motion and have thus been ignored. This problem indicates that the motor power and flywheel mass were insufficient to maintain adequately constant rotational speed of the drive shaft at very low speeds.

The poor performance of the suspension was evidently due to insufficient gain within the inner, force control loop. This causes the actual force generated to differ significantly from the desired force produced by the actuator, thus violating a key assumption for satisfactory performance of the suspension controller. Improvements in the overall gain of this loop could potentially be made by either increasing the amplification of the servo drive voltage (K_{Ic}), or by changing the flow gain from the servo-valve. In practical terms this latter course is difficult as it requires a new servo-valve with modified first stage or larger diameter spool; possibly both. The servo-valve drive signal was amplified instead. The amount that the gain could be increased was limited since it could be observed that the servo valve drive voltage waveform became distorted from sinusoidal shape, indicating that the driving amplifiers in the analogue computer were becoming overloaded beyond an amplification of 2. This made a small improvement in the suspension isolation characteristics but did not bring satisfactory performance. That is, the frequency response showed characteristics slightly more toward those intended in Figure 5.1, with a slight change near the resonant peak and at higher frequencies. However, the changes were only very small. The body and axle remained almost exactly in phase and the resonant peak near 3.4 Hertz was unchanged. The results for this are shown in Figure 5.9.

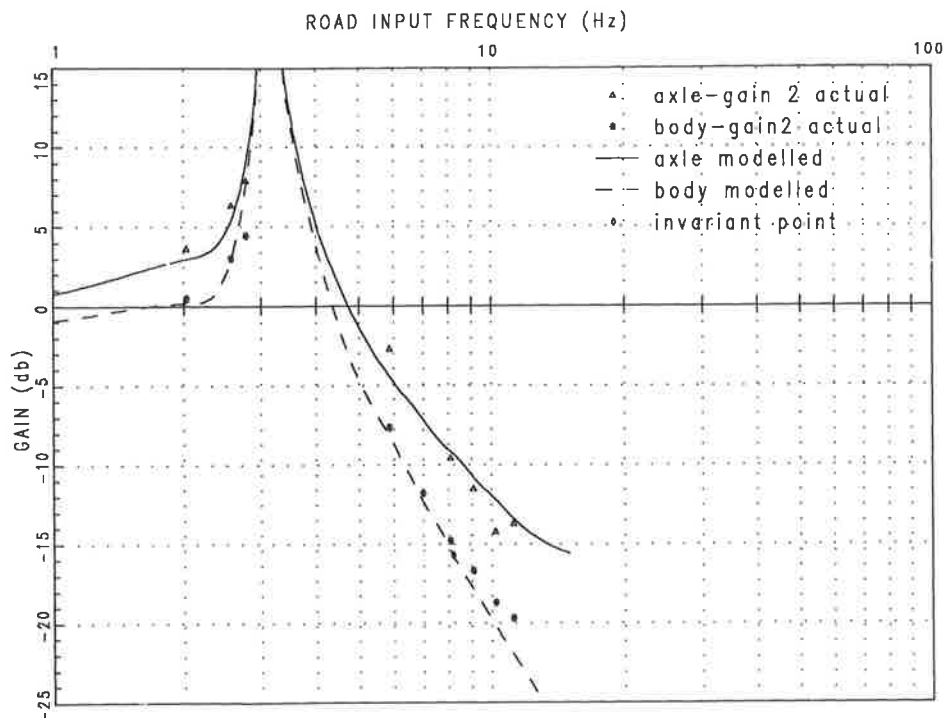


Figure 5.9 Body and axle frequency responses for the laboratory suspension with servo loop gain doubled; sub-optimal LQR controller.

The results in Figures 5.8 and 5.9 show reasonable correlation between the actual and modelled performances. The body response for both experimental and modelled results passes through the 'invariant point' as expected. Errors in estimation of the component masses and spring rates have caused the actual response to vary slightly from the theoretical curve, the error being not more than 1db for either body response and 2.5db for the axle response.

The flow rate demand from the servo-valve was well within the specifications and it was evident at this stage that lack of system gain was indeed likely to be the reason for the poor performance, despite the valve having been suitably sized using conventional design parameters.

5.3 Computed Results

The computer model was run with step inputs and sinusoidal roadway inputs at the same frequencies that the practical results were recorded. The modelled step responses showed the damping on the test rig to be somewhat less than predicted, as can be seen in Figure 5.10. The reasons for this difference are suspected to be due to the effect of the actuator

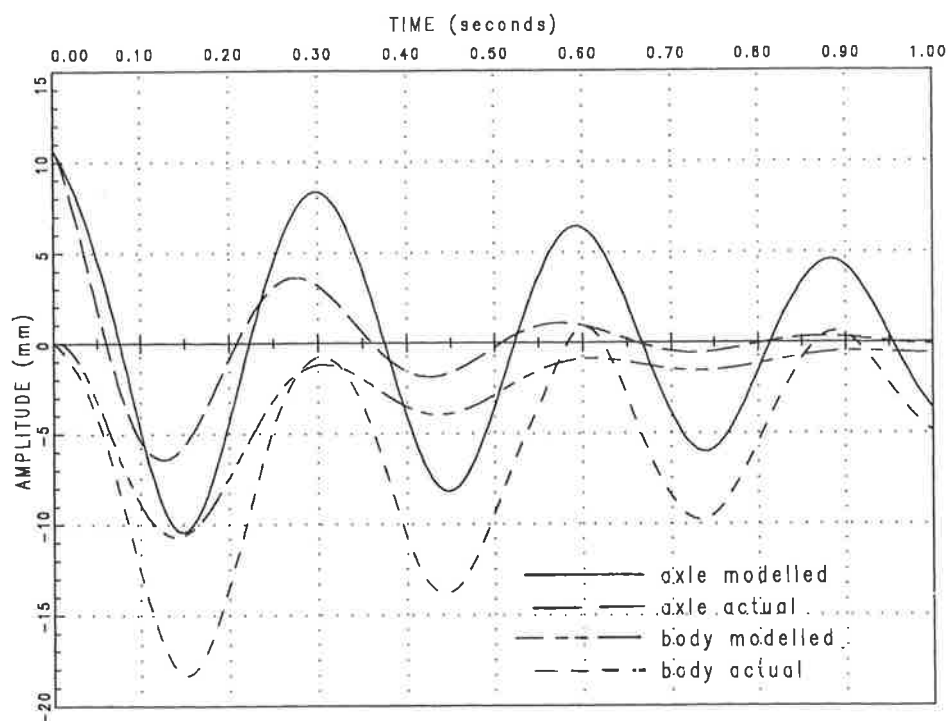


Figure 5.10 Comparison of typical simulated and recorded step responses, LQR controller.

leakage, since the actuator design has an inherently high leakage rate across the piston and of high pressure oil into each chamber. The leakage across the piston can be allowed for in the simulation by modifying the derivatives subroutine, as shown in Figure 5.11. The modelled suspension step response approaches that of the actual with increasing values of C_p . Inclusion of this term has no significant effect on the steady state

```

{actuator}
Ql:=Cp*(y[Py]-y[Pz]);          (* ADDED *)
Qya:=(y[x4]-y[x3])*Ay-Ql;      (* MODIFIED *)
      {Qya +ve if rod is extending; ie: oil is added to side y}
dQy:=Qy-Qya;                   {+ve for rod extending}
Qza:=(y[x4]-y[x3])*Az+Ql;      (* MODIFIED *)
      {Qza -ve if rod is retracting; oil is added to side z}
dQz:=Qza-Qz;                   {+ve for rod retracting}
dy :=y[x1]-y[x2];
Cy:=(Vy0-Ay*dy)/Bmod;
Cz:=(Vz0+Az*dy)/Bmod;
dydt[Py]:=dQy/Cy;              { dydt(Py) }
dydt[Pz]:=dQz/Cz;              { dydt(Pz) }

```

Figure 5.11 Modified section of the derivatives subroutine to include internal actuator leakage.

response, for values of C_p up to 1.0×10^{-10} , which represents a leakage rate well in excess of that designed. The effect of leakage of high pressure fluid from the cylinder end cap bearings into the cylinder chambers is unknown but could also contribute to the damping. Additional testing would be required to confirm the actual leakage rates and the effect of actuator leakage on system performance.

The system gain could not be further increased on the test rig, however this is simple to achieve in the computer model by adjusting the value of $C_{sp} * K_f$ as desired. As the value of C_{sp} was increased the response of the modelled LQR system improved. With $C_{sp} = 150 \times 10^{-5}$ the system response is close to the ideal response of the system; ie: the actuator force tracks the desired force with negligible errors, as was seen in Figures 5.3 and 5.4.

Figures 5.12 and 5.13 show the sub-optimal LQR system step performance with increasing values of C_{sp} . Low values produce lightly damped oscillatory responses while

increasing the value of C_{Sp} clearly moves the performance closer to the ideal. As for the frequency responses, setting $C_{Sp} = 150 \times 10^{-5}$ the step responses of the axle and body

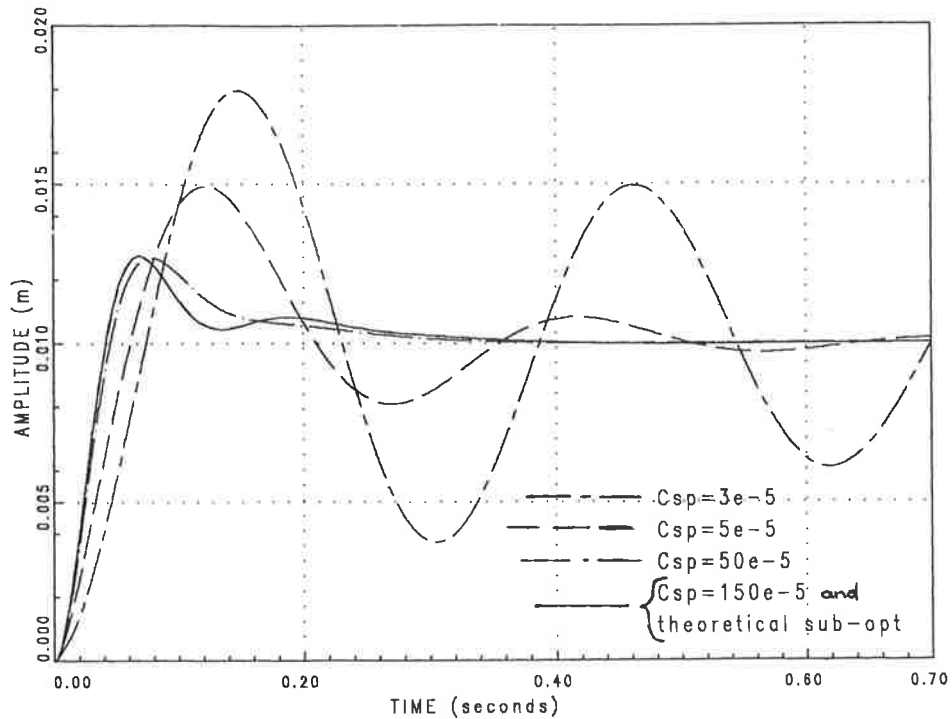


Figure 5.12 Simulated axle step responses with increasing C_{Sp} .

are very close to ideal. The value of C_{Sp} can be increased further to obtain even closer conformity. Similar results were found for the frequency shaped system but are not presented. Chapter 2 discussed the existence of an invariant point in the frequency response of the body. This point is indicated on a number of the frequency response plots. Each of the modelled curves pass through this point as expected. The recorded responses also approximately pass through this point. The invariant point does not lie exactly on the response curve due to measurement errors. Calculation of the position of the invariant point is subject to measurement errors in the actual spring rate and body mass body and errors will be present in the measurement of the body response.

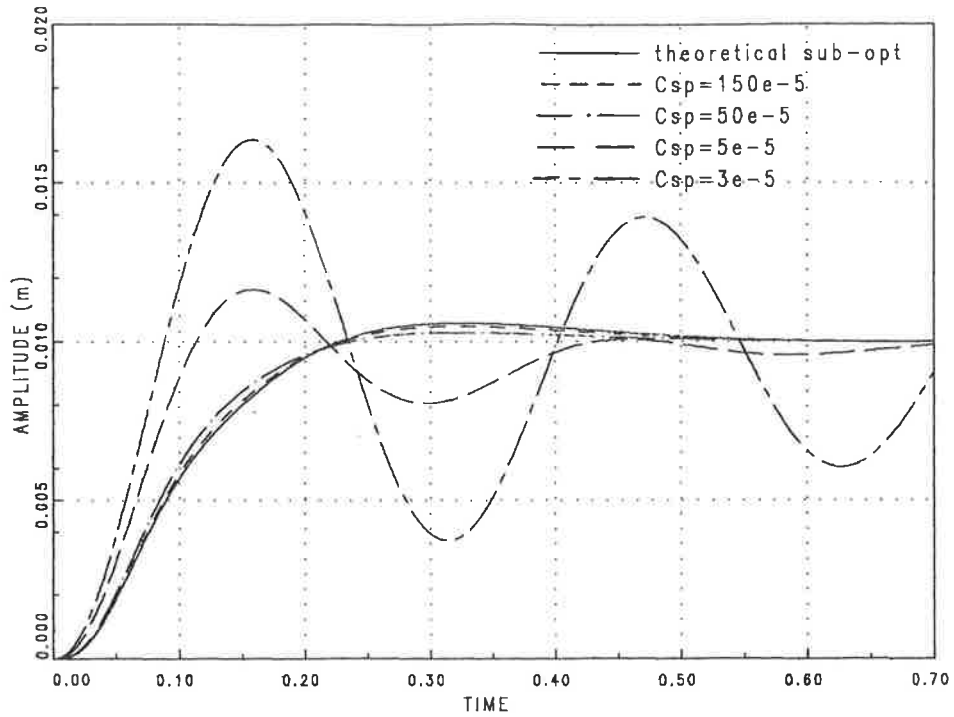


Figure 5.13 Simulated body step responses with increasing C_{sp} .

5.4 Discussion

The reason for the apparent lockup of the axle and body can be studied from the block diagram of the force control loop, Figure 5.14. Some simplifications should be first made for clarity. This represents the system as described by equations (4.11) to (4.23). Although not modelled, leakage past the spool does occur and creates an initial steady state pressure in each chamber of the actuator. The pressure during operation fluctuates about this steady state condition. In the simulation the pressure is initially set in each chamber to the mean of the supply and the return line pressures. This assumes identical spool-land matching at each of the four spool edges within the valve, ie:

$$dP_{Sy} = dP_{Ye} = dP_{Sz} = dP_{Ze} = (P_s - P_e)/2 \quad (5.2)$$

and
$$\partial = \sqrt{((P_s - P_e)/2)} \quad (5.3)$$

This assumption is reasonable since the pressure fluctuations with a sinusoidal input are typically about 4% of the mean and so the square roots are within 2% of ∂ . Making this

assumption allows the servo valve to be treated as a simple gain and greatly simplifies the block diagram. A further simplification is to assume that the actuator fluid compliances (C_y and C_z) are constant, ie: the movement of the actuator piston creates a negligibly small change to the fluid volume in each chamber of the actuator which causes a negligible change in the fluid compliance. The sinusoidal road input amplitude could be taken as an upper bound to the required actuator stroke as this would represent a zero absolute body deflection in a properly functioning system. The change in compliance due to displacement of the actuator is then approximately 1% which is indeed negligible. Thus let

$$V_{y0} = V_{z0} = V_0 \quad (5.4)$$

and since the piston areas are the same:

$$\dot{P}_y - \dot{P}_z = B_{\text{mod}}*(dQ_y - dQ_z)/V_0 \quad (5.5)$$

The flow rates from the servo valve into each actuator chamber are:

$$Q_y = Q_{sy} - Q_{ye} = \partial * C_{sp} * X_{sp} \quad (5.6)$$

$$Q_z = Q_{sz} - Q_{ze} = -\partial * C_{sp} * X_{sp} \quad (5.7)$$

The net flow rate into each actuator chamber is the sum of fluid supplied by the valve added to the rate of change of volume of the chamber due to actuator movement:

$$dQ_y = \partial * C_{sp} * X_{sp} + A_y * (x_4 - x_3) \quad (5.8)$$

$$dQ_z = -\partial * C_{sp} * X_{sp} - A_z * (x_4 - x_3) \quad (5.9)$$

The parallel integrations corresponding to equation (4.20) can be combined into a single integration and the resulting simplified block diagram is shown in Figure 5.15. From this it can be seen that there are two loops which affect the production of the actuator output force, F_a . One loop feeds back F_a to a summing junction to sum with F_d and attempts to cause F_a to track F_d . The other 'disturbance' input is feedback from the actuator piston relative velocity. This loop will have the effect of causing F_a to drive the actuator velocity to zero. The gain for the desired force must be sufficiently high to render the disturbance input negligible otherwise the overall effect of the system will be to attempt to drive the actuator relative velocity to zero which is the lock-up effect found in the laboratory testing.

To avoid lock-up in the laboratory suspension then, the product of K_f , K_{Ic} , C_{sp} and ∂ must be increased approximately 50 fold. Only a small increase in ∂ , maybe doubling, can be practically achieved and increasing K_{Ic} by any significant amount was found, as stated in section 5.1, to exceed the servo valve first stage current limitations. K_f and C_{sp} are inherent factors within the servo valve and increasing these represents the only practical method of achieving the desired gain increase. In other words, a substantially larger servo valve must be fitted to the laboratory system in order to approach the desired performance.

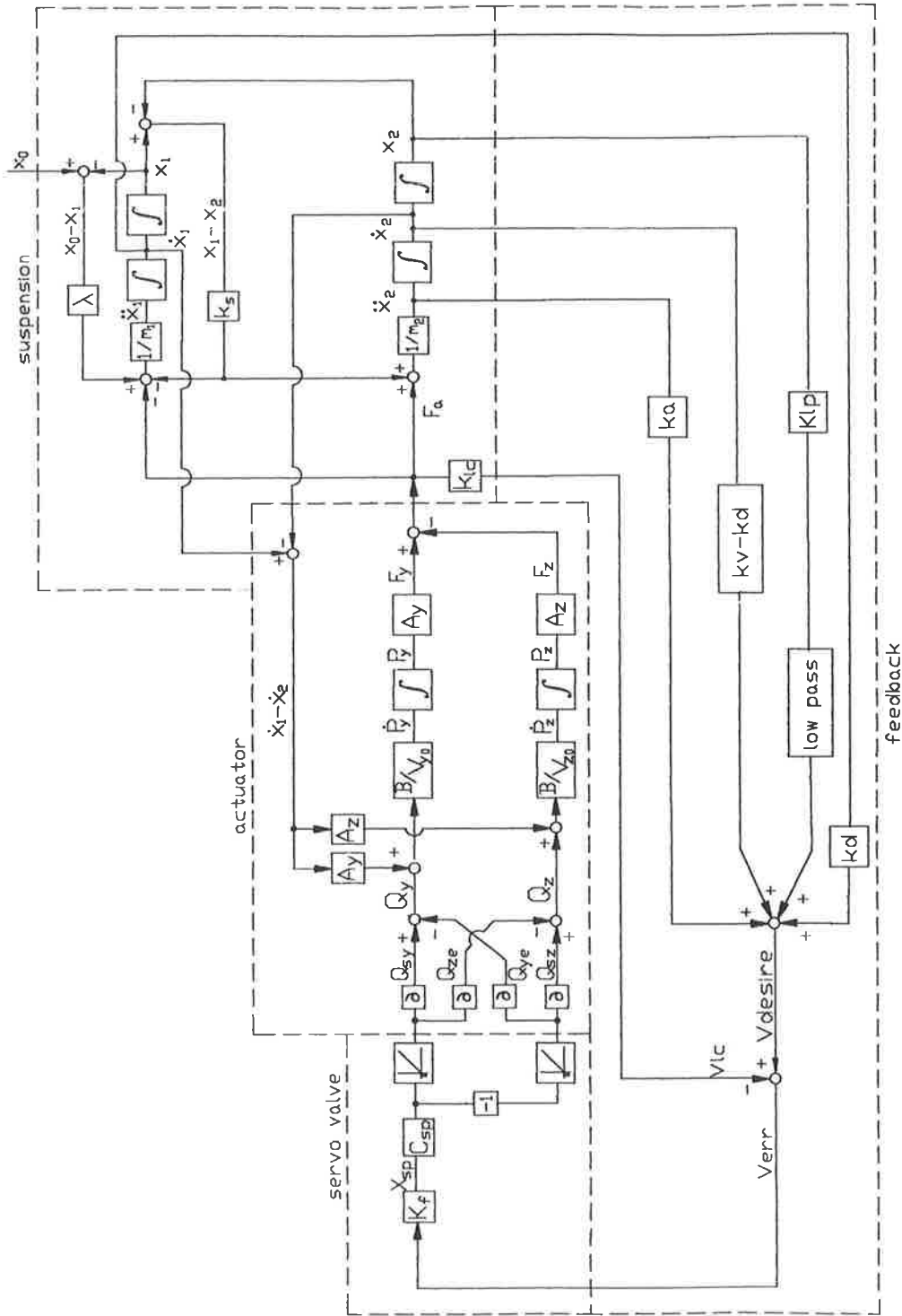


Figure 5.14 Active suspension block diagram.

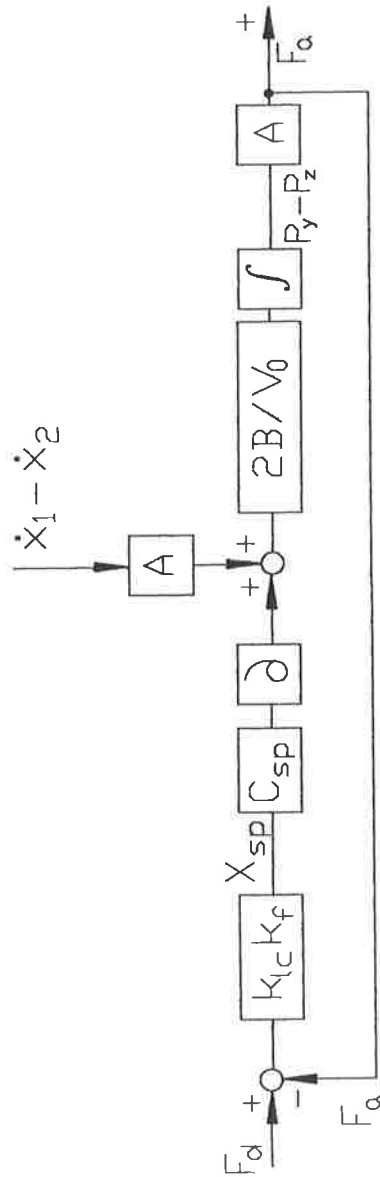


Figure 5.15 Simplified active suspension block diagram.

5.5 Summary & Conclusions

Modelling of the performance of two control algorithms for active vehicle suspension systems have been performed. An experimental suspension was built and each of the controllers tested. The model has been used to demonstrate why the laboratory suspension failed to perform as had been intended. Conclusions are:

1. The model developed predicts the performance of the experimental suspension quite closely.
2. The experimental suspension was constructed and is suitable for analysis of active suspension controller design. It however did not perform as expected because of the low system gain able to be achieved by the servo valve in the "inner" force control loop. Correction of this requires a larger servo-valve to be fitted. Using the model developed, it is evident that the control laws proposed for the active suspension would function as intended.
3. The frequency shaped controller was not able to be operated correctly due to problems with over loading of the servo-valve. An improved amplifier and current limiter would solve this problem.
4. The experimental instrumentation was fundamentally adequate but requires refinement to remove stray 50 Hertz electromagnetic interference from measured signals.

5.6 Recommendations for Future Study.

1. Confirm satisfactory operation of the laboratory suspension, once the servo-valve has been improved.
2. Study methods to allow quantitative comparison of performance between suspension controller types. This may involve definition of a performance indicator based on suitably weighted state variable outputs. There are numerous possible controllers which may be used as the basis for an active suspension. Each claims some advantage of performance, mathematical simplicity, robustness or minimum instrumentation.
3. Evaluate the effects of actuator friction and leakage on suspension performance.

REFERENCES

- K. N. Morman Jr & F. Giannopolous, RECENT ADVANCES IN THE ANALYTICAL AND COMPUTATIONAL ASPECTS OF MODELLING ACTIVE AND PASSIVE VEHICLE SUSPENSIONS, Computational Methods in Ground Transport Vehicles, American Society of Mechanical Engineers, AMD-Vol 50 (1982).
- R. S. Sharp and D. A. Crolla, ROAD VEHICLE SUSPENSION SYSTEM DESIGN-A REVIEW, Vehicle System Dynamics 16(1987) 167-192.
- A. G. Thompson, OPTIMUM DAMPING IN A RANDOMLY EXCITED NON-LINEAR SUSPENSION, Proc. Instn Mech. Engrs, 184(2A) 1969-70, 169-178.
- D. L. Margolis, THE RESPONSE OF ACTIVE AND SEMI-ACTIVE SUSPENSIONS TO REALISTIC FEEDBACK SIGNALS, Vehicle System Dynamics 11(1982) 267-282.
- T.J. Gordon, C. Marsh and M.G. Milstead; A COMPARISON OF ADAPTIVE LOG AND NON-LINEAR CONTROLLERS FOR VEHICLE SUSPENSION SYSTEMS; Vehicle System Dynamics 20(1991).
- M. Mitschke; POSSIBLE IMPROVEMENTS OF VEHICLE VIBRATION SYSTEMS; ASME Symposium on Simulation and Control of Ground Vehicles and Transportation Systems (1986) AMD-Vol. 80 DSC-Vol. 2 pp95-111.
- A.G. Thompson and B.R. Davis; OPTIMAL LINEAR ACTIVE SUSPENSIONS WITH DERIVATIVE CONSTRAINTS AND OUTPUT FEEDBACK CONTROL; Vehicle Systems Dynamics 17(1988).
- D. Karnopp, THEORETICAL LIMITATIONS IN ACTIVE VEHICLE SUSPENSIONS, Vehicle System Dynamics (1986) 55-59.
- M.M. ElMadany; OPTIMAL LINEAR ACTIVE SUSPENSIONS WITH MULTIVARIABLE INTEGRAL CONTROL; Vehicle Systems Dynamics 19(1990).
- F. Fruehauf, R. Kasper and J. Luckel; DESIGN OF AN ACTIVE SUSPENSION FOR A PASSENGER VEHICLE MODEL USING INPUT PROCESSES WITH TIME DELAYS; Vehicle System Dynamics 14(1985).
- A.G. Thompson and B.R. Davis; A TECHNICAL NOTE ON THE LOTUS SUSPENSION PATENTS; Vehicle System Dynamics 20(1991).
- H. Yamaguchi, S.-I. Doi, N. Iwama and Y. Hayashi; EXPERIMENTAL STUDY OF SYSTEM OPTIMIZATION FOR SUPPRESSION OF VEHICLE VIBRATION; Vehicle System Dynamics 22(1993).
- A. Alleyne, P.D. Neuhaus and J.K. Hedrick; APPLICATION OF NON-LINEAR CONTROL THEORY TO ELECTRONICALLY CONTROLLED SUSPENSIONS; Vehicles System Dynamics 22(1993).
- M. Yamashita, K. Fujimori, K. Hayakawa and H. Kimura; APPLICATION OF H_{∞} CONTROL SYSTEMS TO ACTIVE SUSPENSION SYSTEMS; Toyota Motor Corporation/Osaka Universty (1993).
- B. Acker, W. Darenberg and H. Gall, ACTIVE SUSPENSIONS FOR PASSENGER CARS, Proceedings of 11th IAVSD Symposium (1989) Supplement to Vehicle System Dynamics Vol. 18.

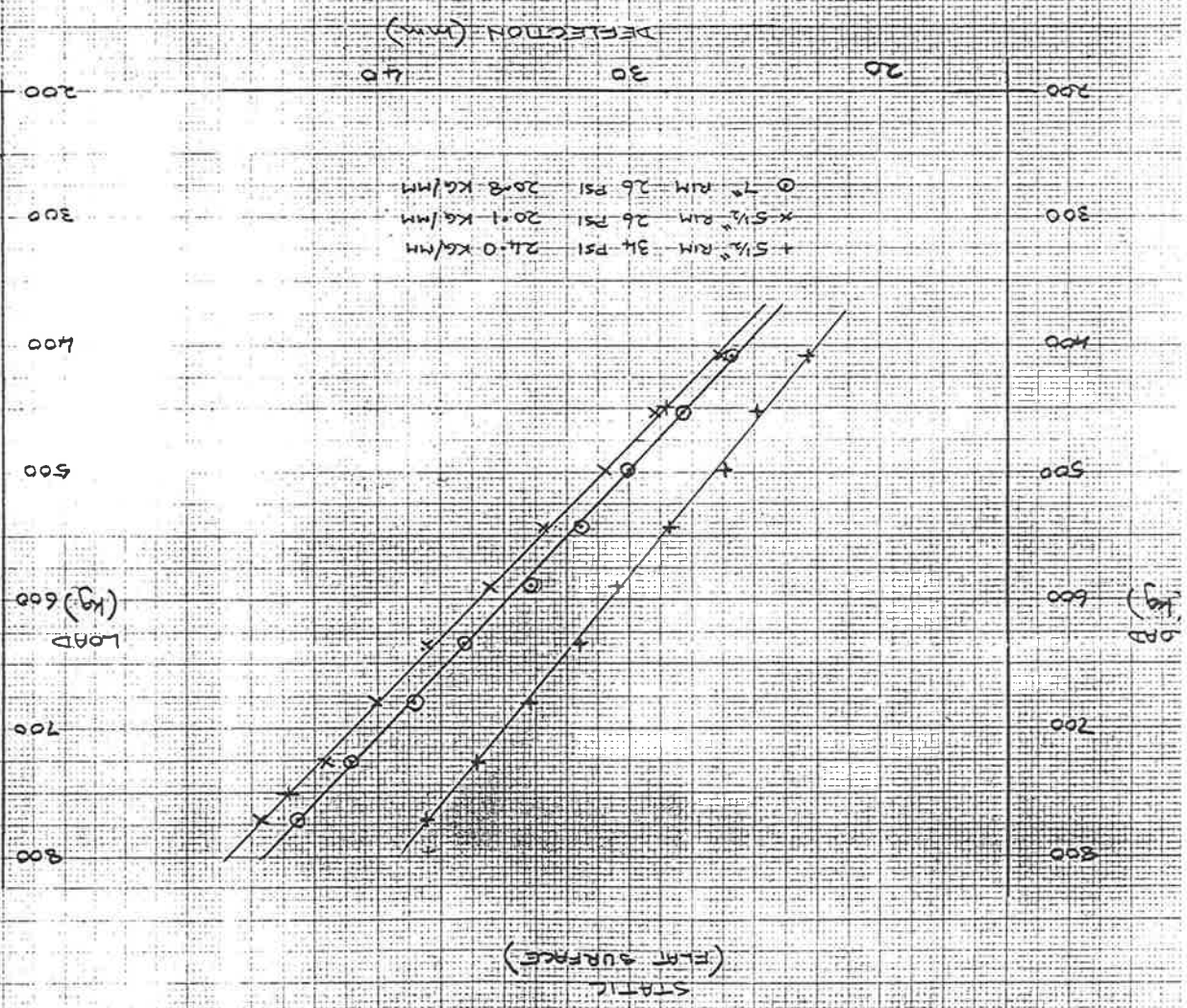
J.R. Zeller; ANALYSIS OF DYNAMIC PERFORMANCE LIMITATIONS OF FAST RESPONSE (150 TO 200 HZ) ELECTROHYDRAULIC SERVOS; NASA TN D-5388 (1969).

P. Dransfield; HYDRAULIC CONTROL SYSTEMS-DESIGN AND ANALYSIS OF THEIR DYNAMICS; Springer-Verlag 1981.

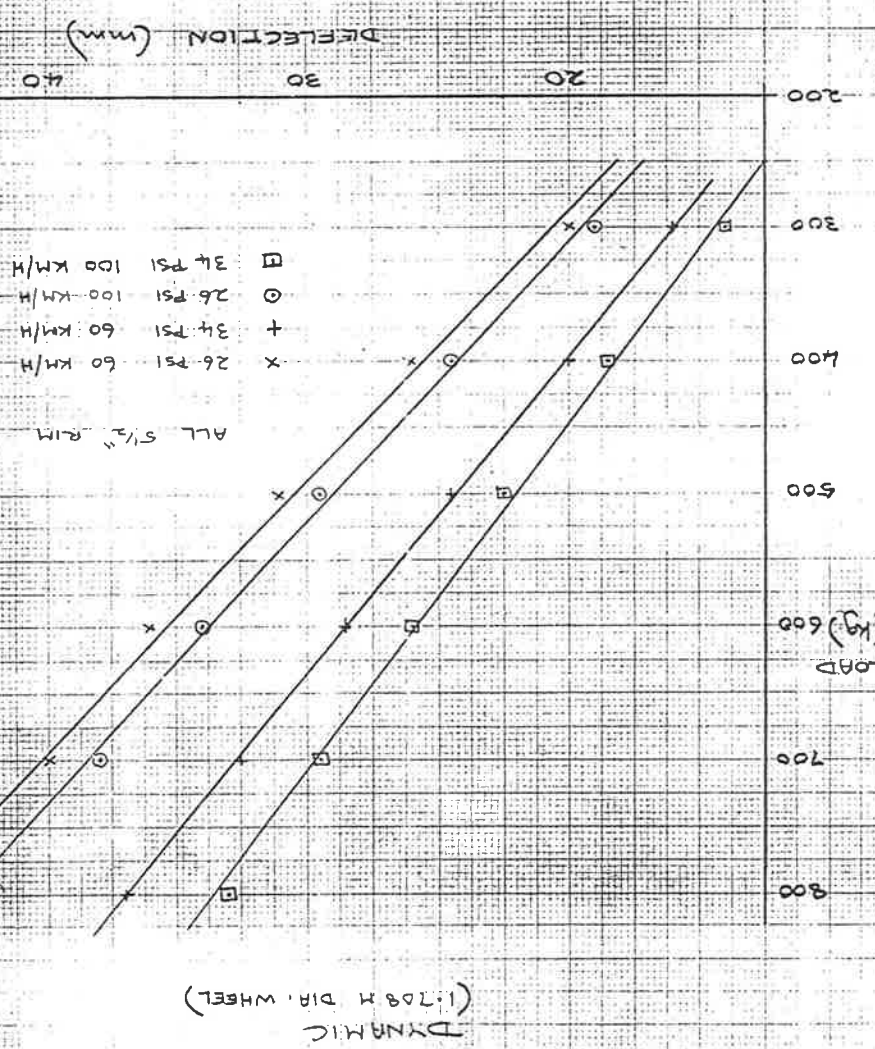
APPENDIX 1

MEASURED TYRE DATA FROM BRIDGESTONE AUSTRALIA LTD.

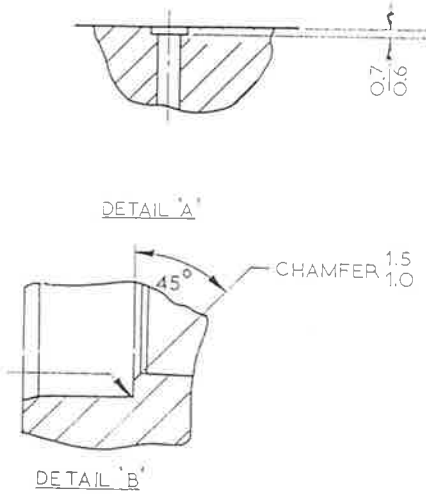
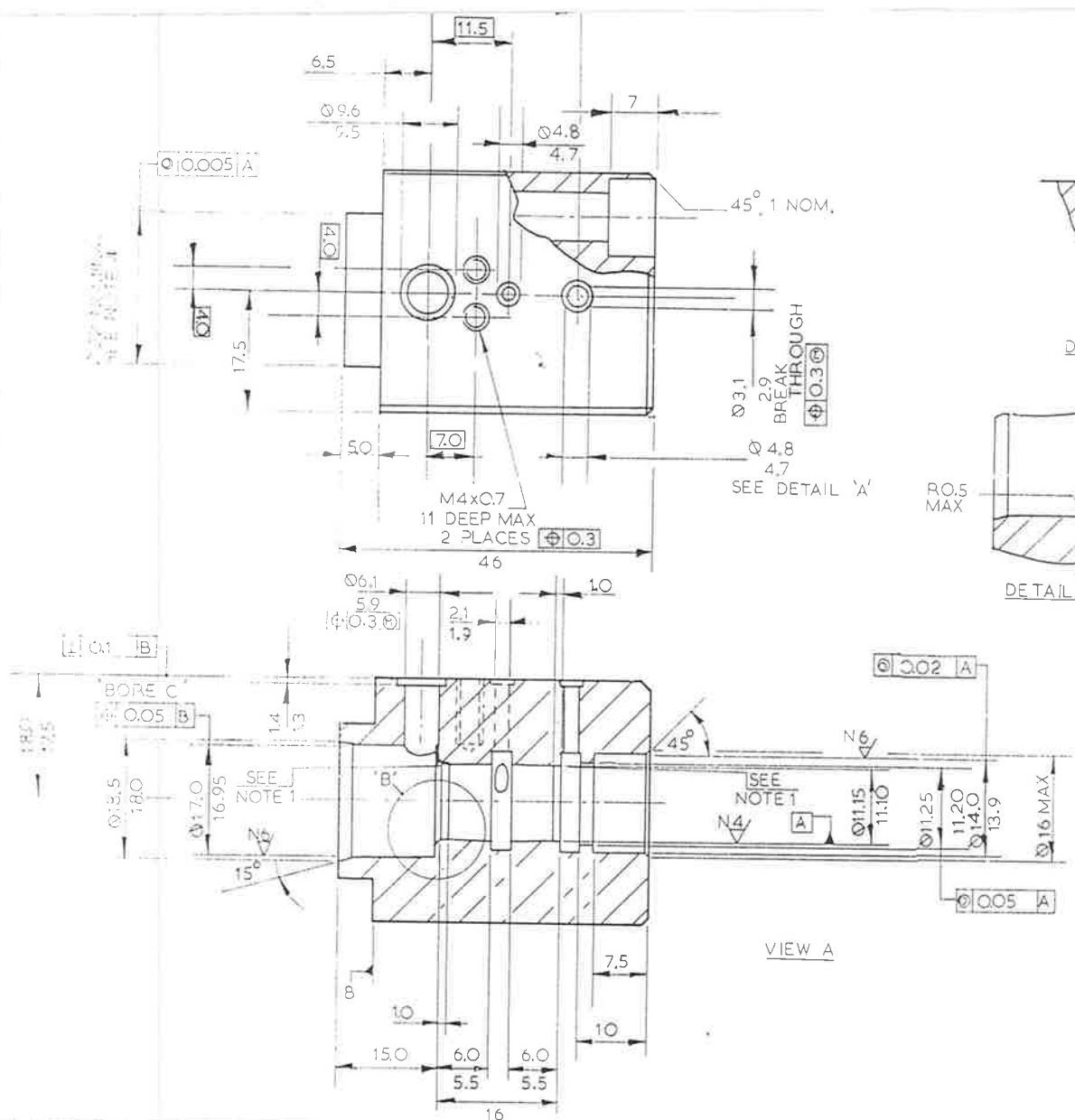
P205/75 R14 MICHELIN X



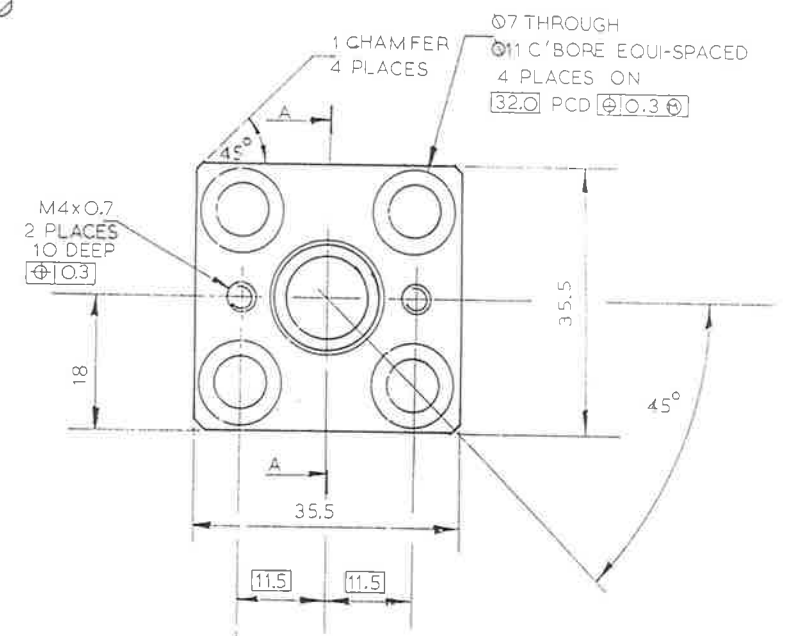
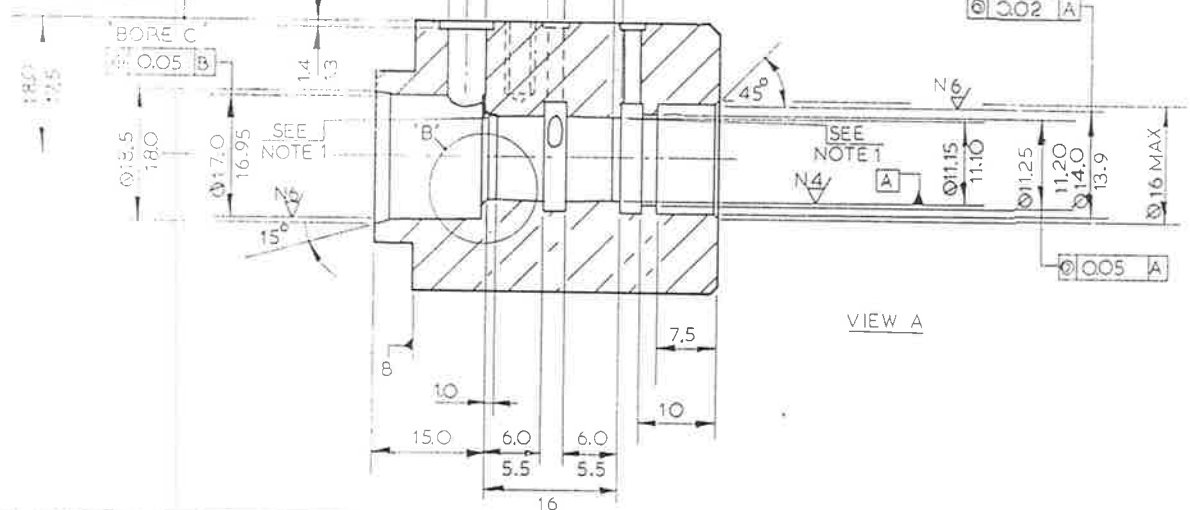
DYNAMIC (1:708 H DIA. WHEEL)



APPENDIX 2
DRAWINGS.



1. SEE GRINDING PROCEDURE, DRG 002.
2. SURFACE FINISH N8 ALL OVER.
3. REMOVE BURRS & SHARP EDGES.
4. LIGHT PRESS FIT IN BORE OF CYLINDER DRG 003.
5. MATL : STAINLESS STEEL TYPE 4
HEAT TREAT : 1 HR AT 980° C,
QUENCH, 1 HR AT 600° C
AIR COOL.

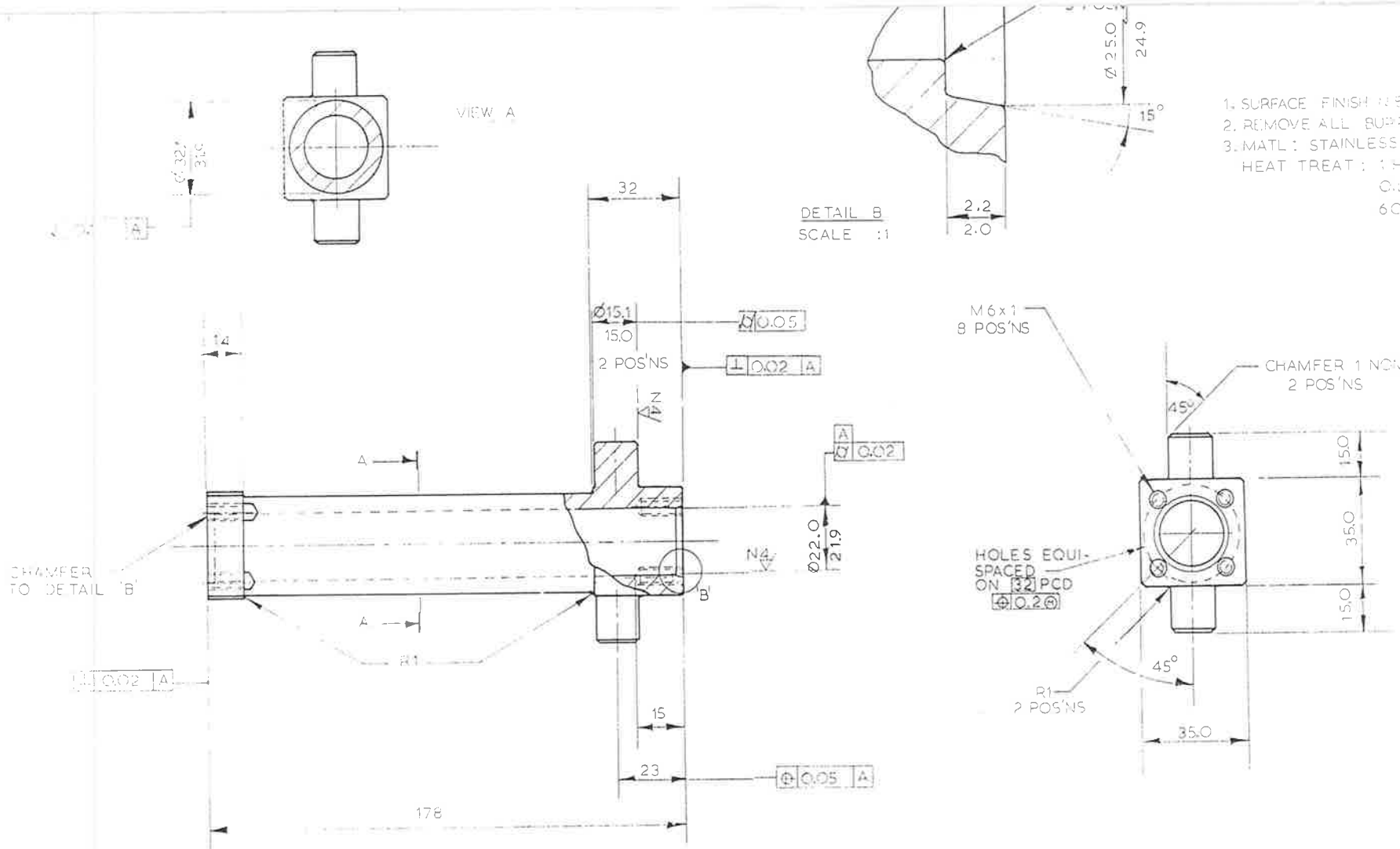


2-1

b2 b3: holes' dims ; d6 d7 : hole' dims note 5		DIMENSIONS IN mm TOLERANCES X.X ± 0.1 angles 1:3° X.X ± 0.5 DRAWING STANDARD			DEFENCE RESEARCH CENTRE SALISBURY		CONTRACTOR		TITLE CYLINDER END CAP		
DESCRIPTION		AUTH NO	DRN	CHKD	APPD/DATE	PB NO	MATERIAL REFER NOTE 5	DRN P. CHAPLIN	CONTRACTORS' REF	CODE IDENT NO Z0004	DRG NO
							FINISH NATURAL			SCALE 2:1	1ST MASS

1. SURFACE FINISH #8
 2. REMOVE ALL BURRS
 3. MATL: STAINLESS STEEL TYPE 416
- HEAT TREAT: 1 HR AT 980°C,
OIL QUENCH, 1 HR
600°C, AIR COOL

DETAIL B
SCALE: 1:1

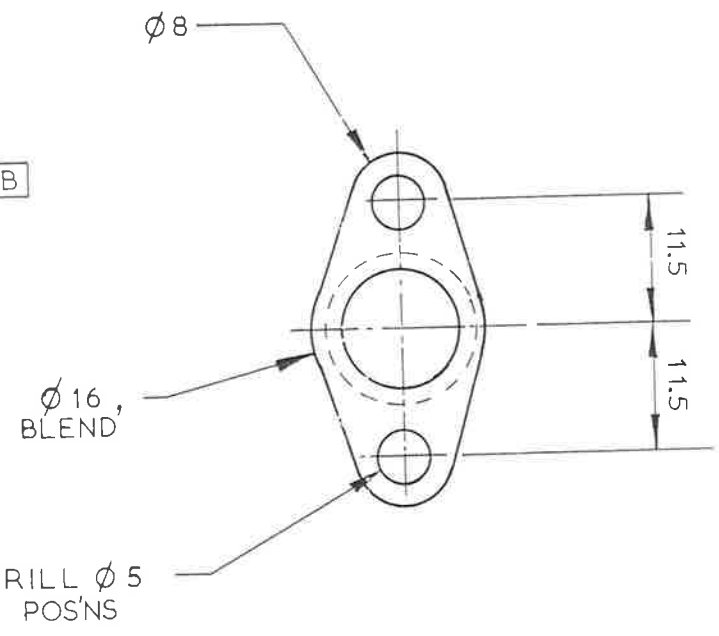
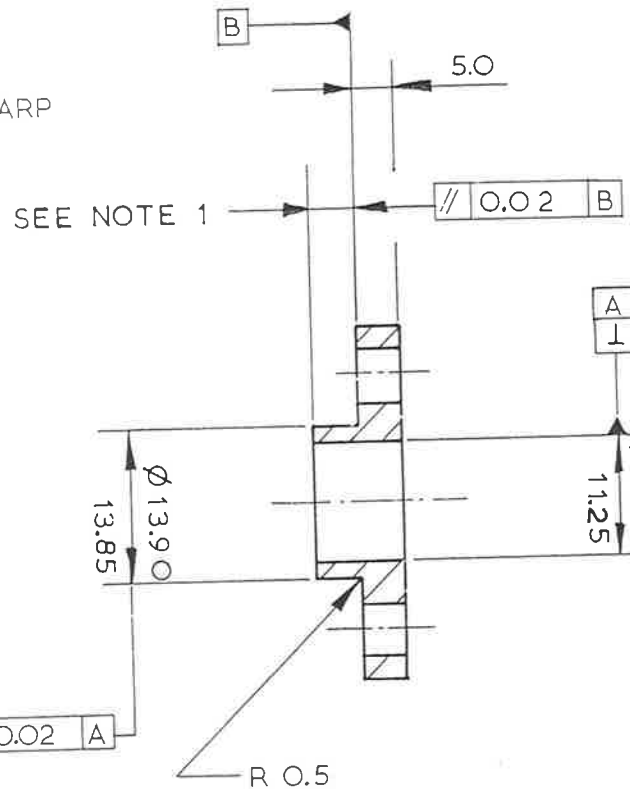


2-2


note 3: d6: M6x1 hole dims detail b added			DIMENSIONS IN mm		DEFENCE RESEARCH CENTRE SALISBURY		TITLE	
			TOLERANCES X: ±1 angles: ±1 XX: 0.5		MATERIAL REFER NOTE 3		CYLINDER	
DRAWING STANDARD			PB NO		DRN P. CHAPLIN		CODE INVENT NO	
					SPEC		Z0C04	
					FINISH		SCALE 1:1	
							DATE 3	

USED ON

1. REMOVE BURRS & SHARP EDGES.

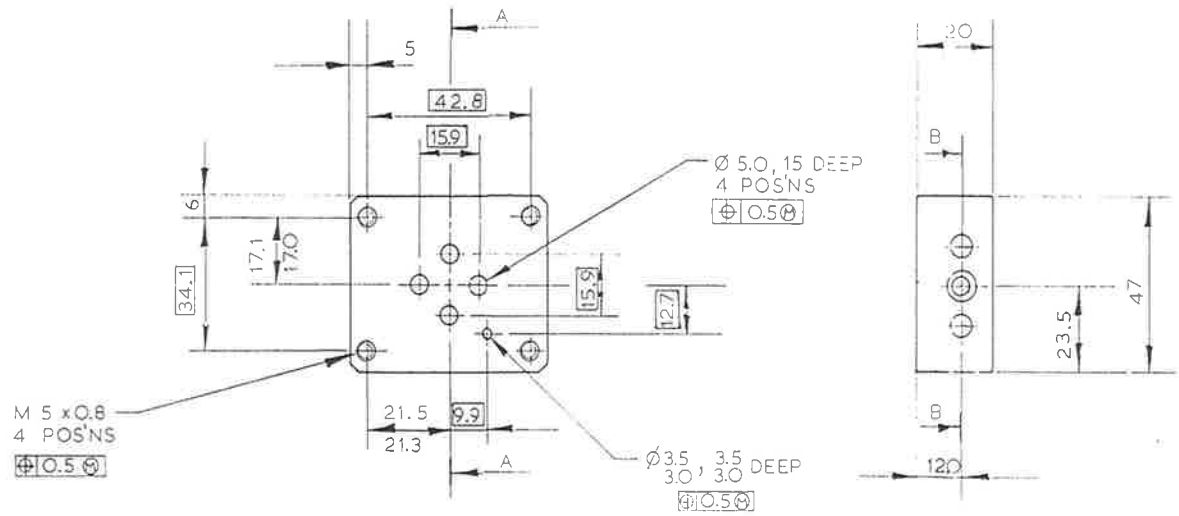
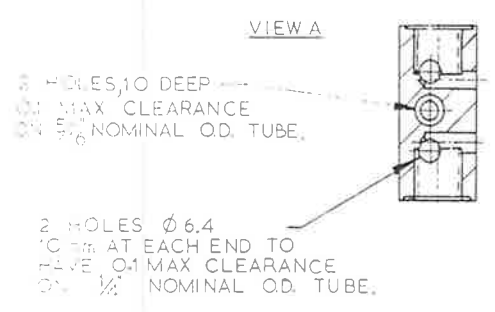
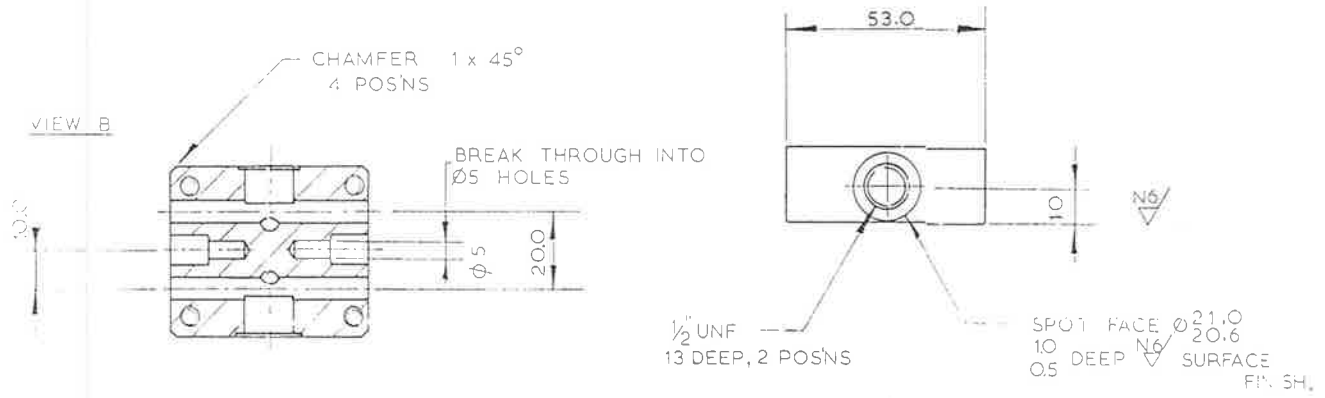


1. SPIGOT LENGTH = DEPTH OF CBR IN CYL
 END CAP - 4.2
 4.1

				DRN	P. CHAPLIN		 DEFENCE RESEARCH CENTRE SALISBURY		
				CHKD					
				APPD			TITLE SEAL RETAINER		
				CONTRACTOR			CODE IDENT NO		
				CONTRACTORS DRG REF			DRG NO	005	
				SECURITY CLASSIFICATION			Z0004		
				SCALE 2:1			EST MASS	SH NO	
DIMENSIONS IN mm TOLERANCES X: ±1 ; X.X: ±0.5				MATERIAL STAINLESS STEEL TYPE 316 SPECIFICATION AS RECEIVED				SHEET SIZE A3	

2-4

1. REMOVE SHARP EDGES & BURRS.
2. SURFACE FINISH $\nabla N6$ UNLESS SPECIFIED.

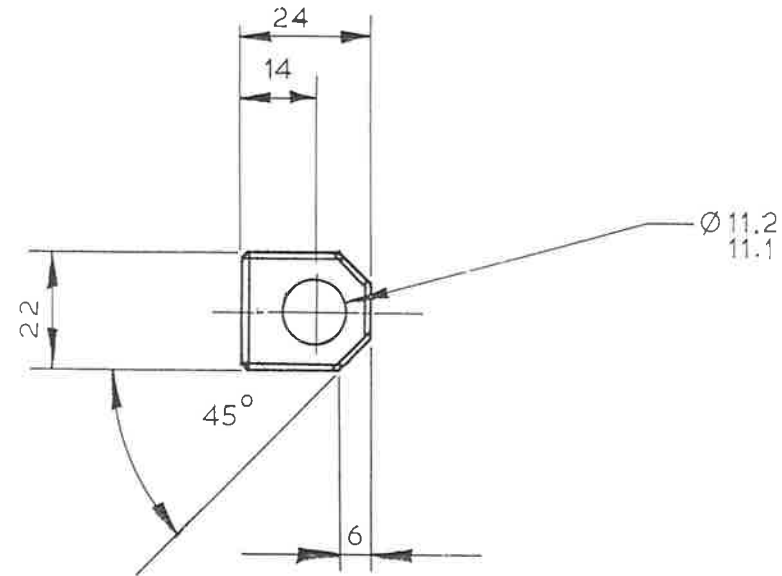
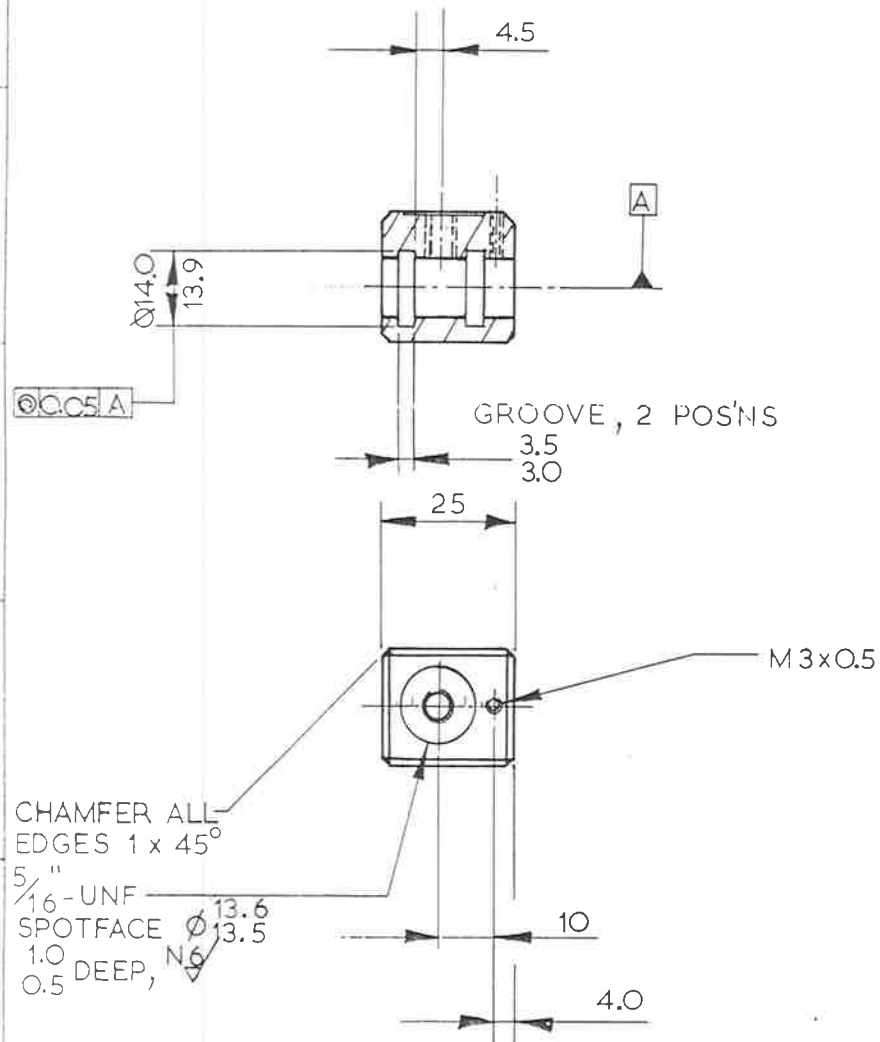


2-6

WGS 424 ; note added		DIMENSIONS in mm		DEFENCE RESEARCH CENTRE SALISBURY		SERVO VALVE MANIFOLD	
		TOLERANCES		MATERIAL MILD STEEL		CODE INDENT NO	
		XX: ± 0.5		DRN P. CHAPLIN		Z0004	
		DRAWING STANDARD		SPEC		DRG NO	
		DRN COND		FINISH		007	
2		3		4		7	
						SCALE 1:1	
						EST MAS	
						A2	

USED ON

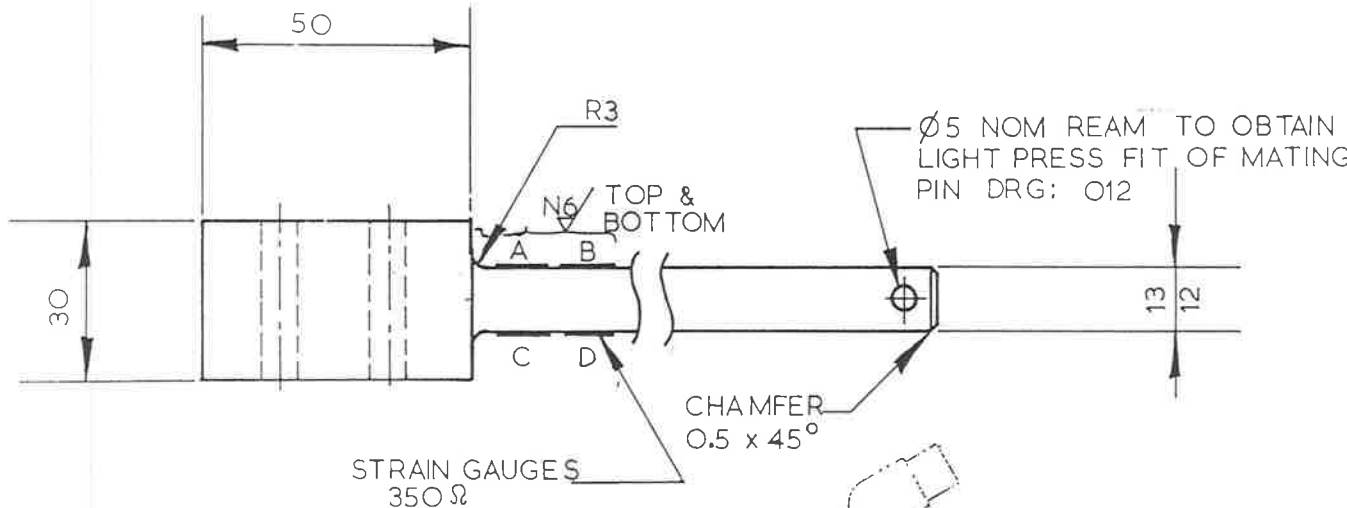
1. SURFACE FINISH : $\nabla N7$
2. REMOVE BURRS & SHARP EDGES.



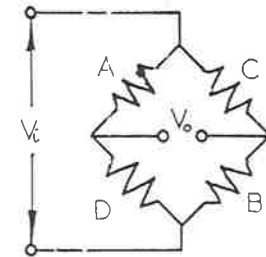
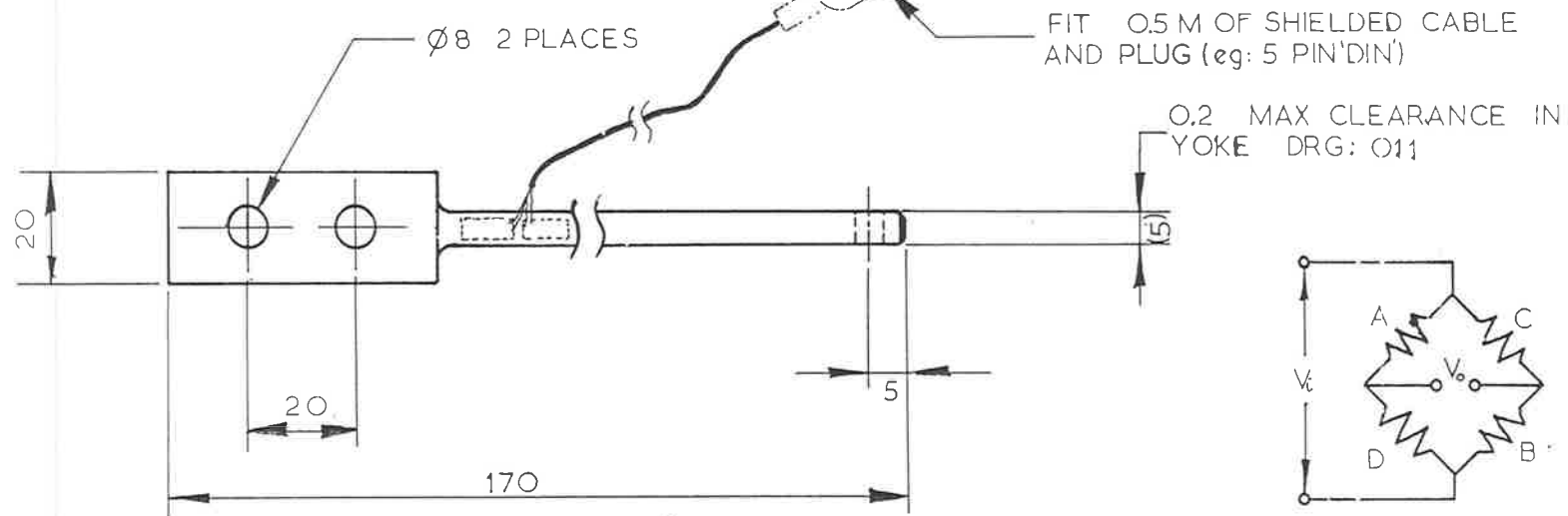
2-7

DRN P. CHAPLIN						DEFENCE RESEARCH CENTRE SALISBURY													
CHKD						CONTRACTOR													
APPD						TITLE SLEEVE													
A		ISS GRID				DESCRIPTION				AUTH NO		DRN		CHKD		APPD/DATE			
DIMENSIONS IN mm						MATERIAL MILD STEEL						CONTRACTORS DRG REF							
TOLERANCES X: ± 1						SPECIFICATION						CODE IDENT NO Z0004		DRG NO 008		SHEET SIZE A3			
DRAWING STANDARD						FINISH NICKEL PLATE						SECURITY CLASSIFICATION		SCALE 1:1		EST MASS		SH NO	


USED ON



NOTES:
 1. MAT'L: STAINLESS STEEL TYPE 410
 HEAT TREAT TO OBTAIN HARD-
 NESS OF 25-30 Rc.

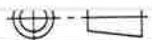


STRAIN GAUGE
 WIRING DIAGRAM

				DRN	P. CHAPLIN		 DEFENCE RESEARCH CENTRE SALISBURY		
				CHKD					
				APPD					
A				CONTRACTOR			TITLE		
ISS GRID	DESCRIPTION	AUTH NO	DRN	CHKD	APPD/DATE	LOAD CELL ASSEMBLY			
DIMENSIONS IN mm		MATERIAL SEE NOTE 1			CONTRACTORS DRG REF		CODE IDENT NO	DRG NO	SHEET SIZE
TOLERANCES ±1		SPECIFICATION			SECURITY CLASSIFICATION		Z0004	O10	
DRAWING STANDARD		FINISH N 8, NATURAL			SCALE 1:1		EST MASS	SH NO	
	2	3	4	5	6	7	8		

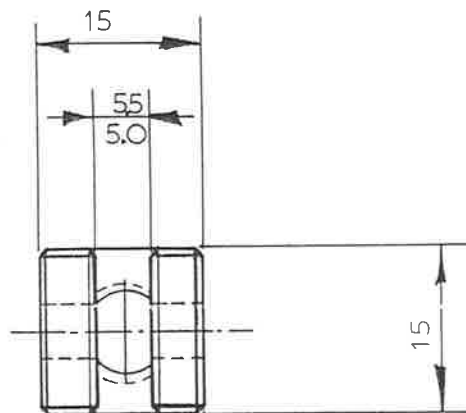
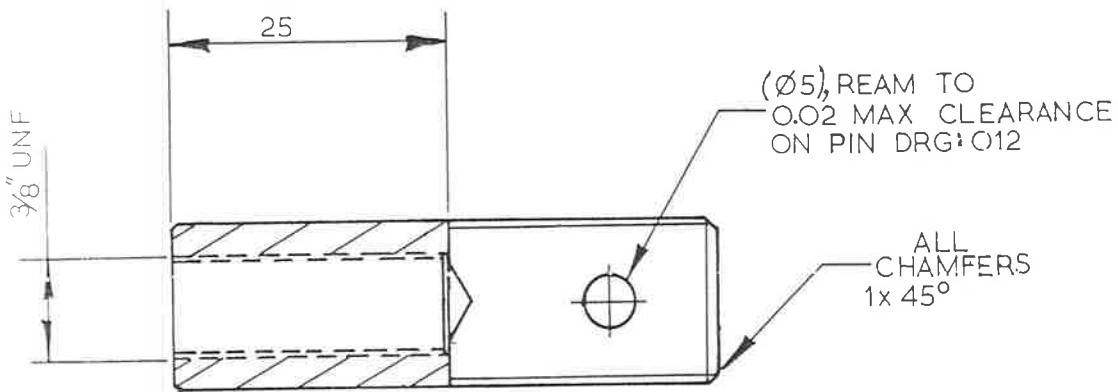
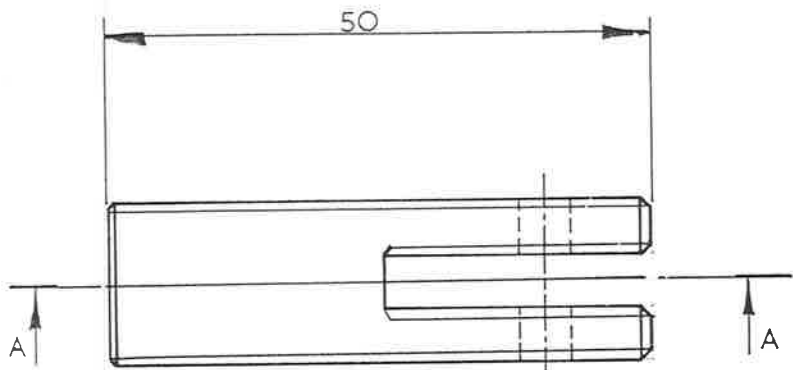
2-9

DRG NO. O11




DO NOT SCALE

USED ON

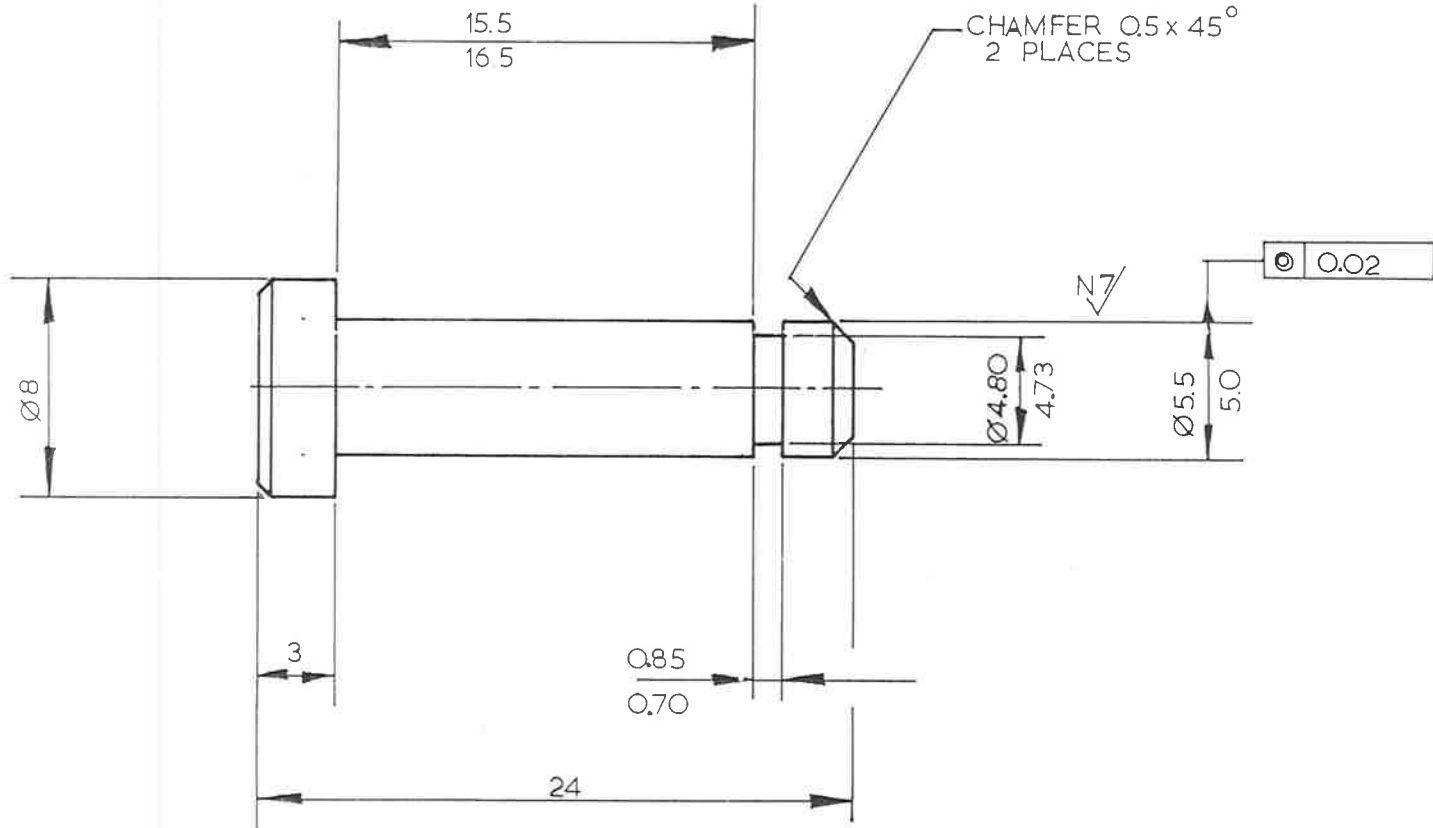


SECTION A

2-10

						DRN	P. CHAPLIN		 DEFENCE RESEARCH CENTRE SALISBURY			
						CHKD						
						APPD			TITLE ROD END YOKE			
						CONTRACTOR		CODE IDENT NO Z0004				
ISS GRID		DESCRIPTION		AUTH NO	DRN	CHKD	APPD/DATE				CONTRACTORS DRG REF	
		DIMENSIONS IN mm		MATERIAL PHOSPHOR BRONZE			SECURITY CLASSIFICATION		EST MASS		SH NO	
		TOLERANCES ± 1		SPECIFICATION			SCALE 2:1					
		DRAWING STANDARD		FINISH N 8								

USED ON



2-11

DRN P. CHAPLIN
 CHKD
 APPD



DEFENCE RESEARCH CENTRE SALISBURY

CONTRACTOR

TITLE

PIN

CONTRACTORS DRG REF

CODE IDENT NO
Z0004

DRG NO

013

SHEET
 SIZE

A3

SECURITY CLASSIFICATION

SCALE 5:1

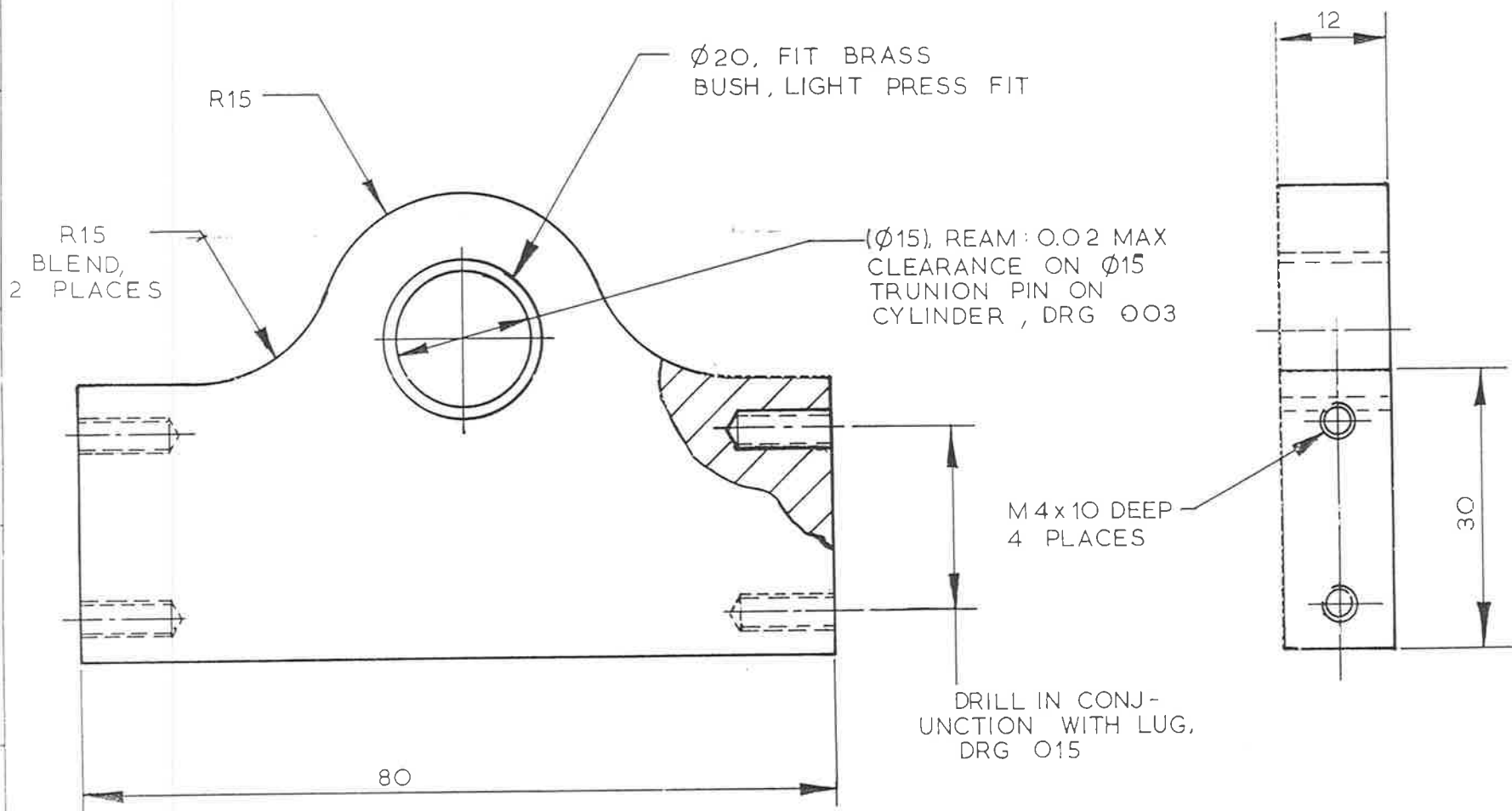
EST MASS

SH NO


ISS GRID	DESCRIPTION	AUTH NO	DRN	CHKD	APPD/DATE
A					
DIMENSIONS IN mm		MATERIAL STAINLESS STEEL TYPE420			
TOLERANCES ±1		SPECIFICATION			
DRAWING STANDARD		FINISH NATURAL			

1 2 3 4 5 6 7 8 R

USED ON

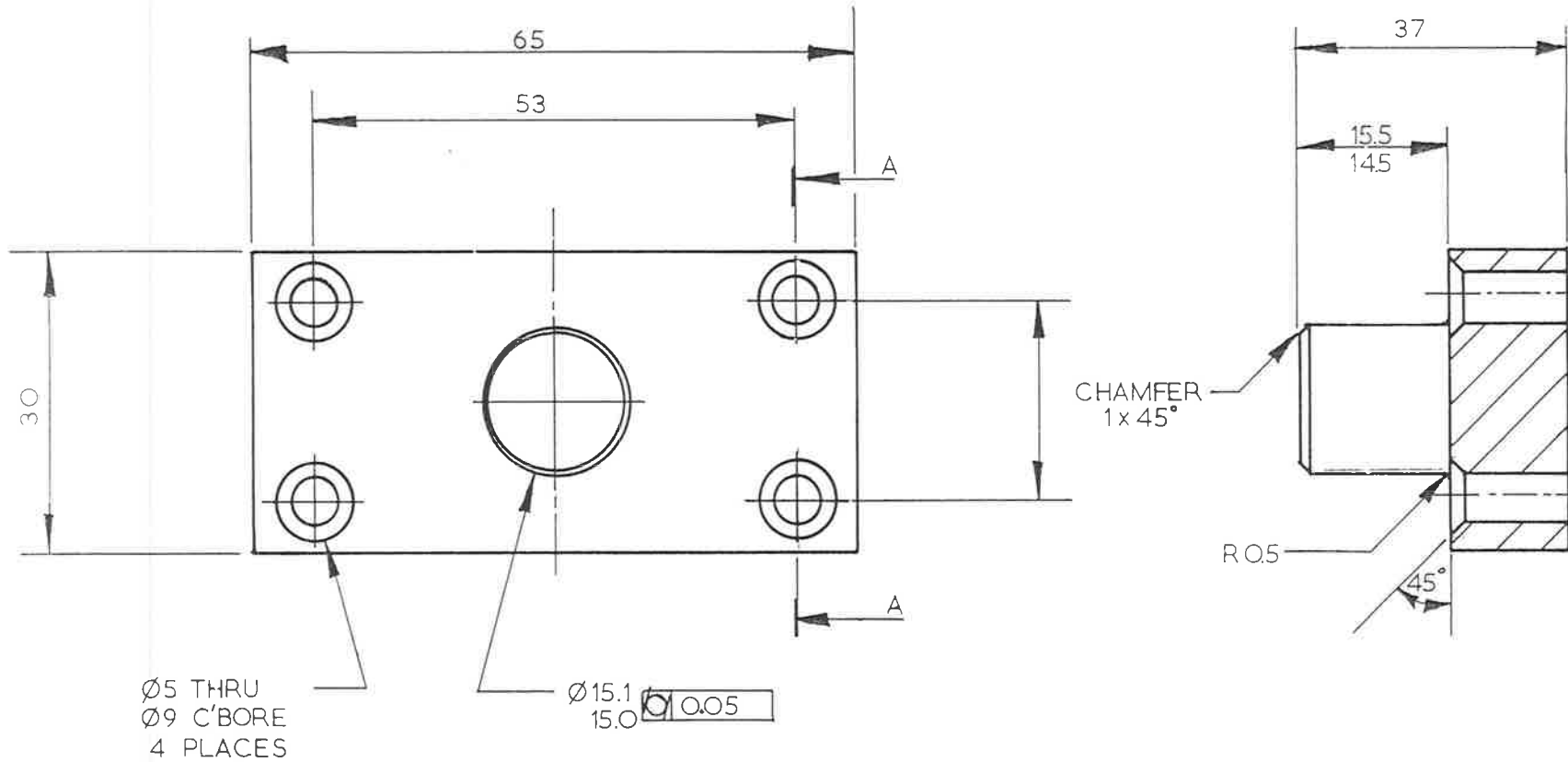


2-12


				DRN	P. CHAPLIN		 DEFENCE RESEARCH CENTRE SALISBURY					
				CHKD								
				APPD								
				CONTRACTOR			TITLE					
							BEARING BLOCK ASSEMBLY					
ISS		GRID	DESCRIPTION	AUTH NO	DRN	CHKD	APPD/DATE	CONTRACTORS DRG REF	CODE IDENT NO	DRG NO	SHEET SIZE	
									Z0004	014	A3	
DIMENSIONS IN mm		MATERIAL MILD STEEL						SECURITY CLASSIFICATION		SCALE 2:1	EST MASS	SH NO
TOLERANCES ±1		SPECIFICATION										
DRAWING STANDARD		FINISH PAINT, ZINC PRIMER										

2 3 4 5 6 7 8

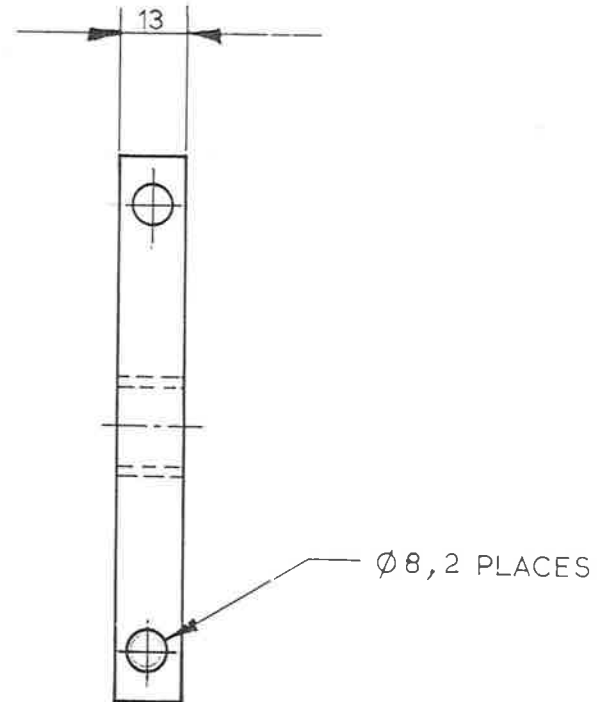
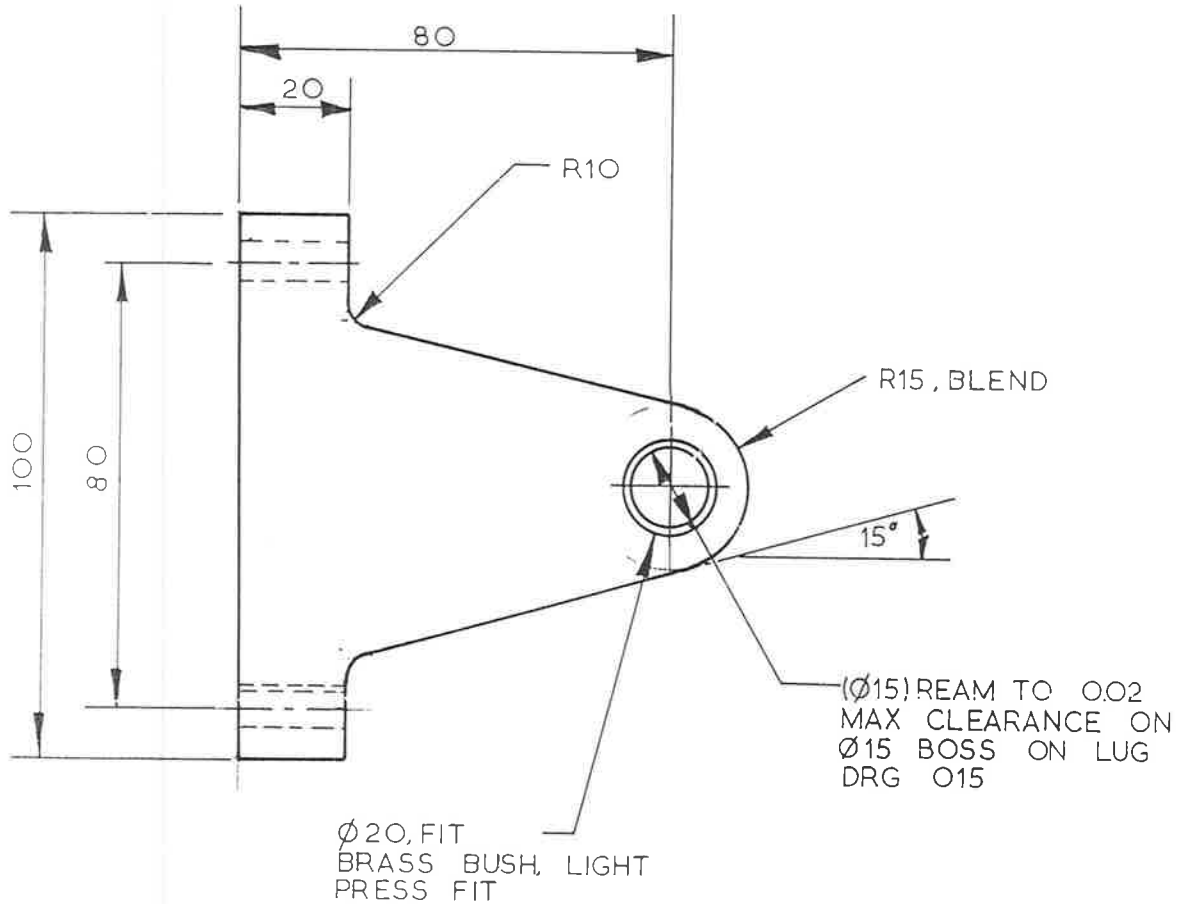
USED ON




2-13

					DRN	P. CHAPLIN		 DEFENCE RESEARCH CENTRE SALISBURY		
					CHKD					
					APPD			TITLE		
					CONTRACTOR			LUG		
DIMENSIONS IN mm		MATERIAL MILD STEEL			CONTRACTORS DRG REF		CODE IDENT NO	DRG NO	O15	SHEET SIZE
TOLERANCES ±1		SPECIFICATION			SECURITY CLASSIFICATION		Z0004			
DRAWING STANDARD		FINISH PAINT, ZINC-PRIMER (EXCEPT $\varnothing 15$)			SCALE 2:1		EST MASS	SH NO	A3	

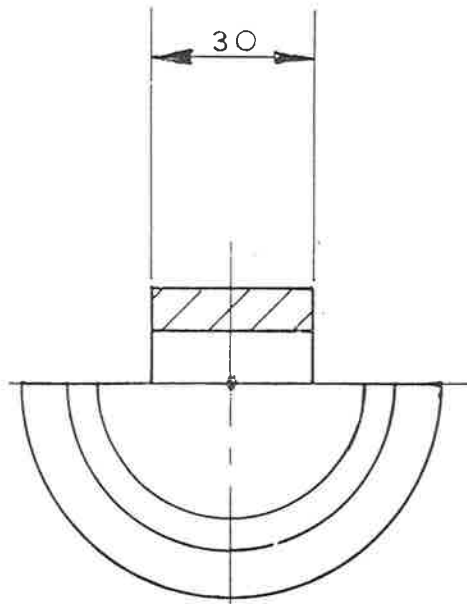
USED ON



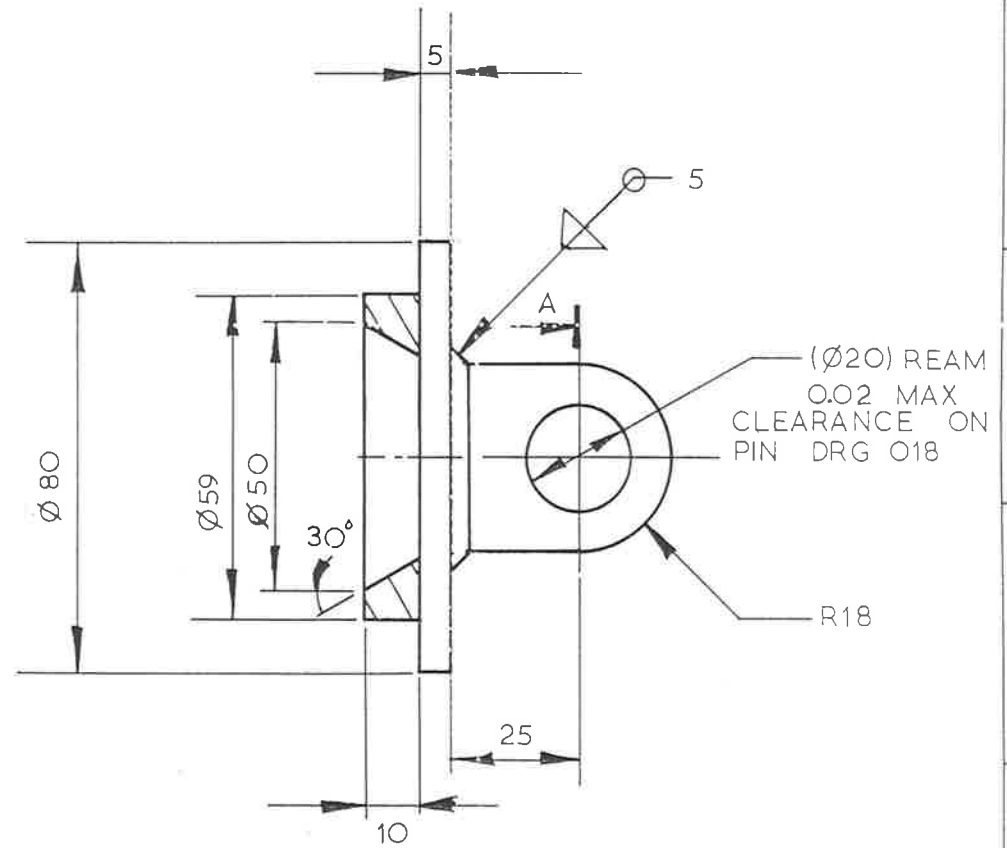
						DRN	P. CHAPLIN		 DEFENCE RESEARCH CENTRE SALISBURY																				
						CHKD																							
						APPD																							
						CONTRACTOR			TITLE																				
ISS GRID						DESCRIPTION			AUTH NO			DRN			CHKD			APPD/DATE											
DIMENSIONS IN mm						MATERIAL MILD STEEL						CONTRACTORS DRG REF						CODE IDENT NO			DRG NO			SHEET SIZE					
TOLERANCES						± 1						SPECIFICATION						Z0004			O16			A3					
DRAWING STANDARD						FINISH PAINT, ZINC PRIMER						SECURITY CLASSIFICATION						SCALE 1:1			EST MASS			SH NO					
2						3						4						5			6			7			8		

2-14


USED ON



SECTION A-A



2-15

				DRN	P. CHAPLIN		 DEFENCE RESEARCH CENTRE SALISBURY						
				CHKD									
				APPD									
				CONTRACTOR			TITLE						
							BASE						
ISS GRID		DESCRIPTION		AUTH NO		DRN	CHKD	APPD/DATE	CONTRACTORS DRG REF		CODE IDENT NO	DRG NO	SHEET SIZE
A											Z0004	O17	
DIMENSIONS IN mm		MATERIAL MILD STEEL							SECURITY CLASSIFICATION		SCALE 1 : 1	EST MASS	
TOLERANCES ±1		SPECIFICATION											A3
DRAWING STANDARD		FINISH PAINT , ZINC PRIMER											

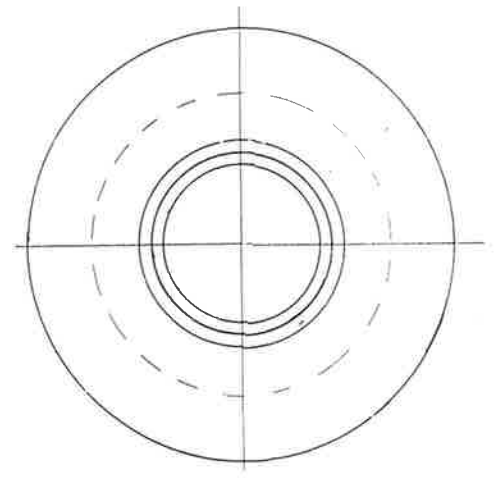
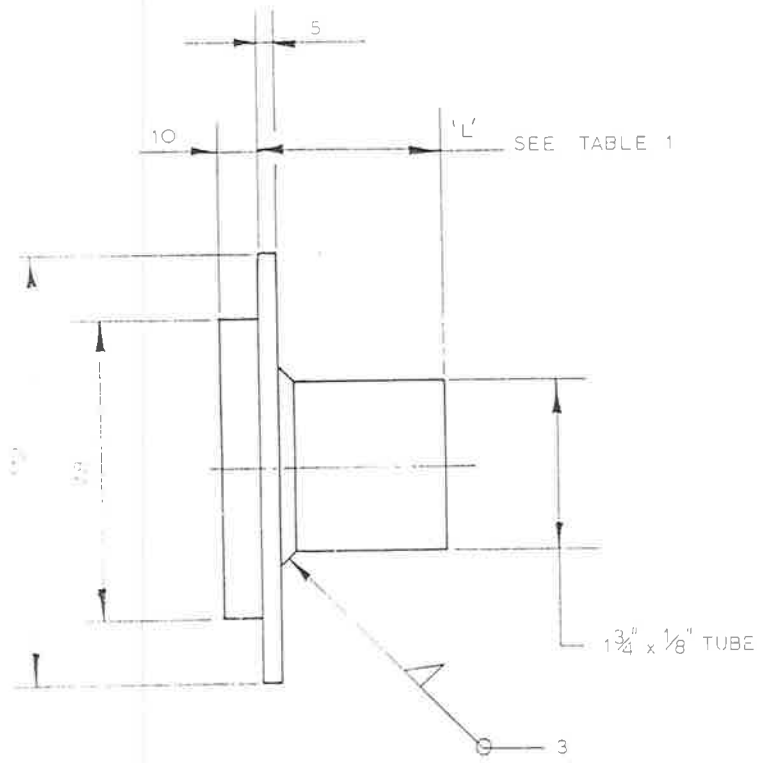
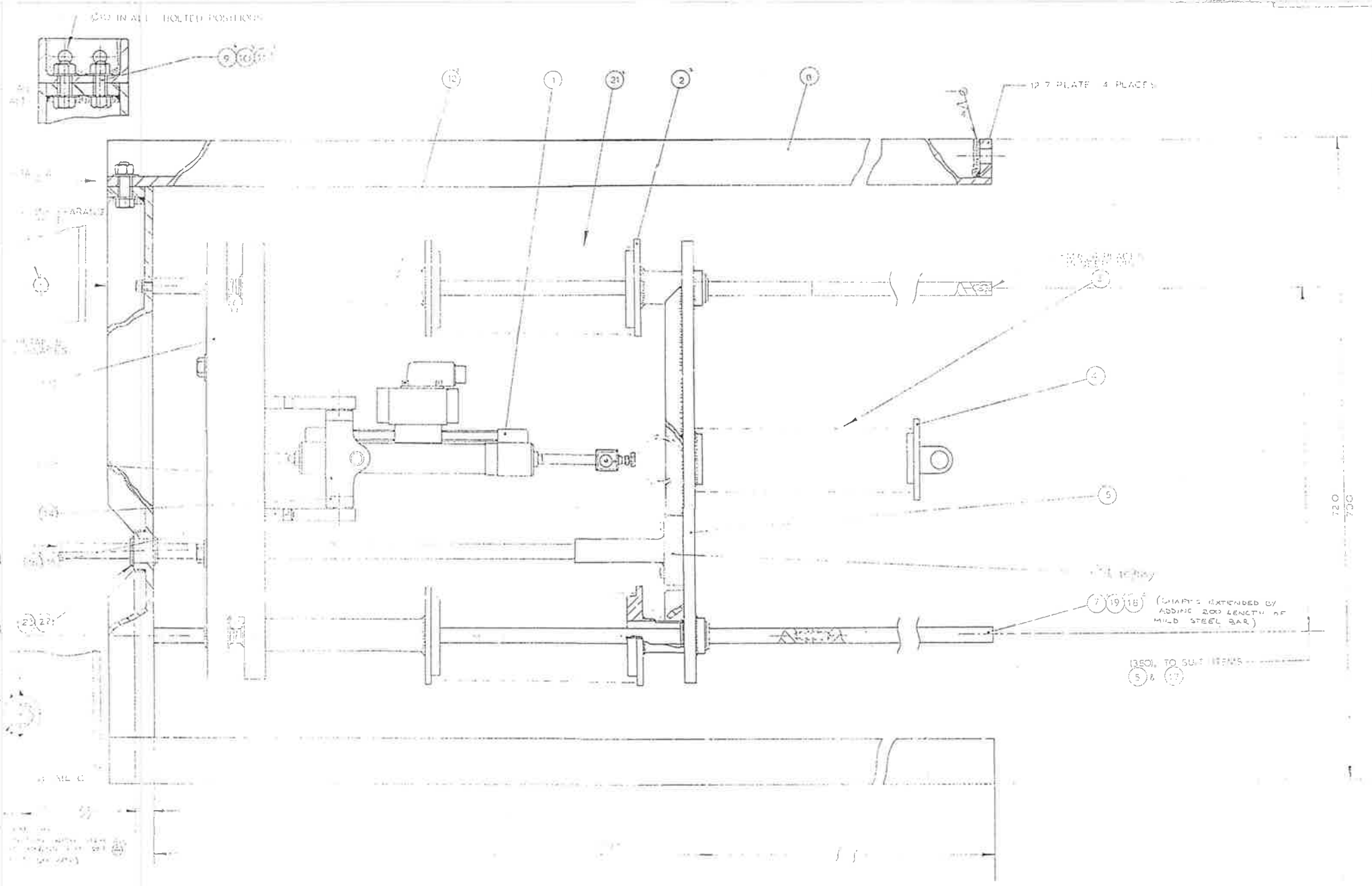


TABLE 1

PART NO.	DIM 'L'
O18-1	44
O18-2	174

						DIMENSIONS IN mm				TITLE	
						TOLERANCES ± 1		DEFENCE RESEARCH CENTRE SALISBURY		SPACER, LONG & SHOP	
						DRAWING STANDARD		MATERIAL MILD STEEL		CODE INVENT NO	
						PB NO		SPEC		Z0034	
						FINISH PAINT, ZINC PRIMER		DESIGNED BY P. CHAPLIN		O18-1 & -2	
DESCRIPTION		AUTH NO		DRG CHKD		APPD/DATE		SCALE 1:1		EST MASS	
1	2	3	4	5	6	7	8				

2-16



730
730

DIMENSIONS IN MM TOLERANCES				DEFENCE RESEARCH CENTRE SALISBURY		CONTRACTOR		TITLE ACTIVE SUSPENSION TEST RIG DETAIL - ASSEMBLY		SHEET SIZE
DRAWING STANDARD				MATERIAL		DRN P. CHAPLIN		CON. NO. AND REV.		
FINISH				SPEC		CHKD		SEC. IDENT. NO. Z0004		DRG NO. 010
APPR				FINISH		APPD		SECURITY CLASSIFICATION		
DESCRIPTION				AUTH. NO.		DRN. CHNO.		APPR. DATE		

Z0004

PND NUMBER	PART OR IDENTIFYING NUMBER	SHEET		CODE IDENT	DESCRIPTION	QUANTITY REQUIRED					
		SIZE	NO			a	b	c	d		
1	Q22				ACTUATOR ASSY			1			
2	Q18-2				SPACER, SHORT			2			
3	Q22				SPRING			1			
4	Q17				BASE			1			
5	Q20				PLATE - LOWER			1			
6	Q10				LOAD CELL ASSY			1			
7					SHAFT, THK BRG CO. TYPE SF 16 x 800			2			
8					STEEL CHANNEL, 100x50x8 (OR EQUIV)			as req'd			
9					M8 BOLT, 25mm LONG			8			
10					M8 NUT			8			
11					FLAT WASHER Ø9 ID.			16			
12	Q18-1				SPACER, LONG			2			
13	Q13				BEARING BLOCK ASSY			2			
14	Q15				LUG			2			
15	Q16				BRACKET			1			
16					M6 BOLT 30 mm LONG			4	6		
17					M6 BOLT 40 mm (min) LONG			2			
18					FLAT WASHER Ø7 ID.			6	8		
19					M6 BOLT 20 mm LONG			4			
20	Q23				PLATE - UPPER			1			
21	Q21				SPRING			2			
22					CIRCLIP, EXTERNAL FOR Ø26 SHAFT (24.2 FREE I.D.)			-	2		
23					LINEAR BRG, THK BRG CO LME-16			-	1		

2-18

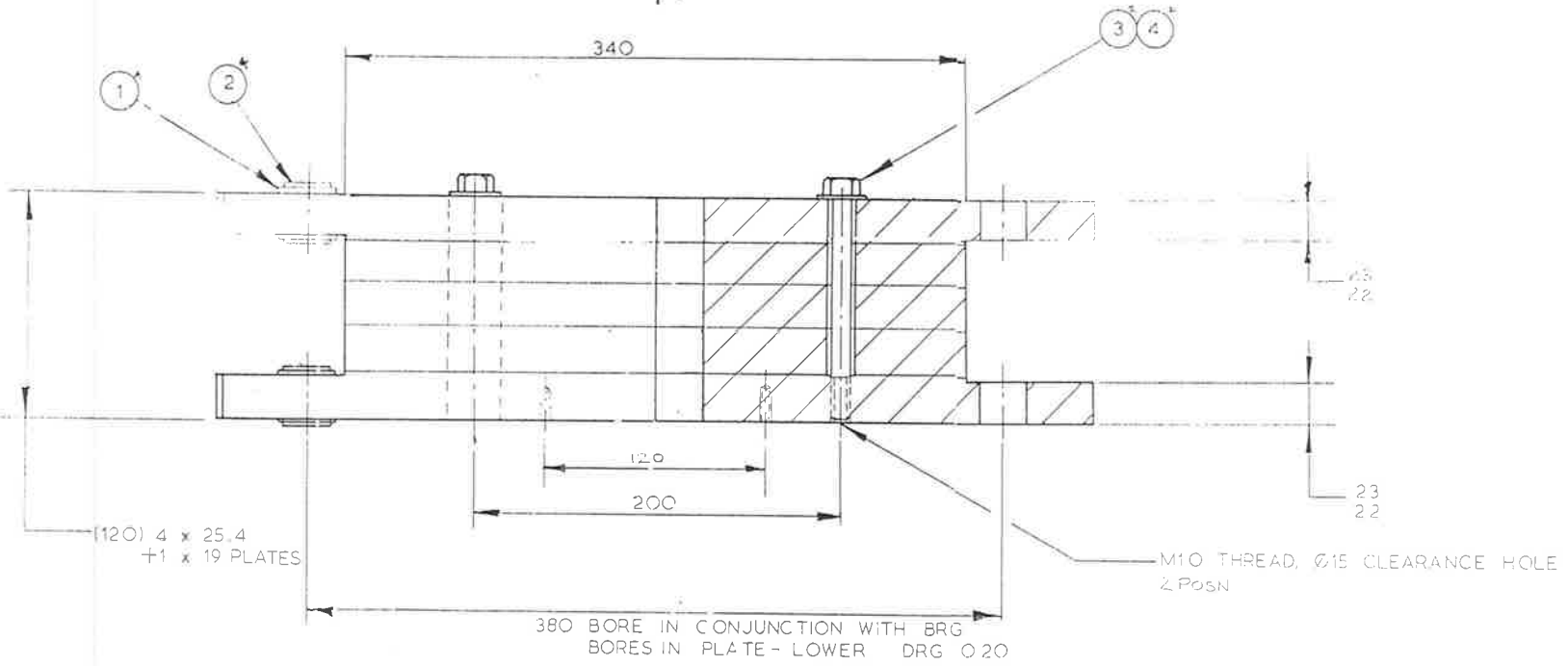
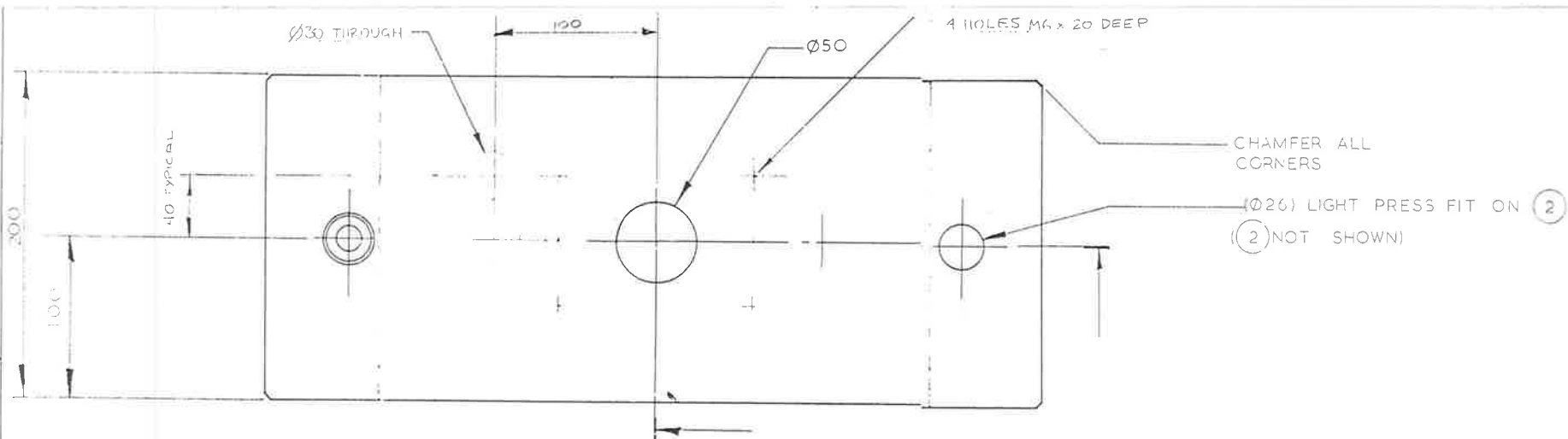
d	
c	
b	SEE SHEET 1
a	ORIGINAL


DEFENCE RESEARCH CENTRE SALISBURY

TITLE ACTIVE SUSPENSION TEST RIG

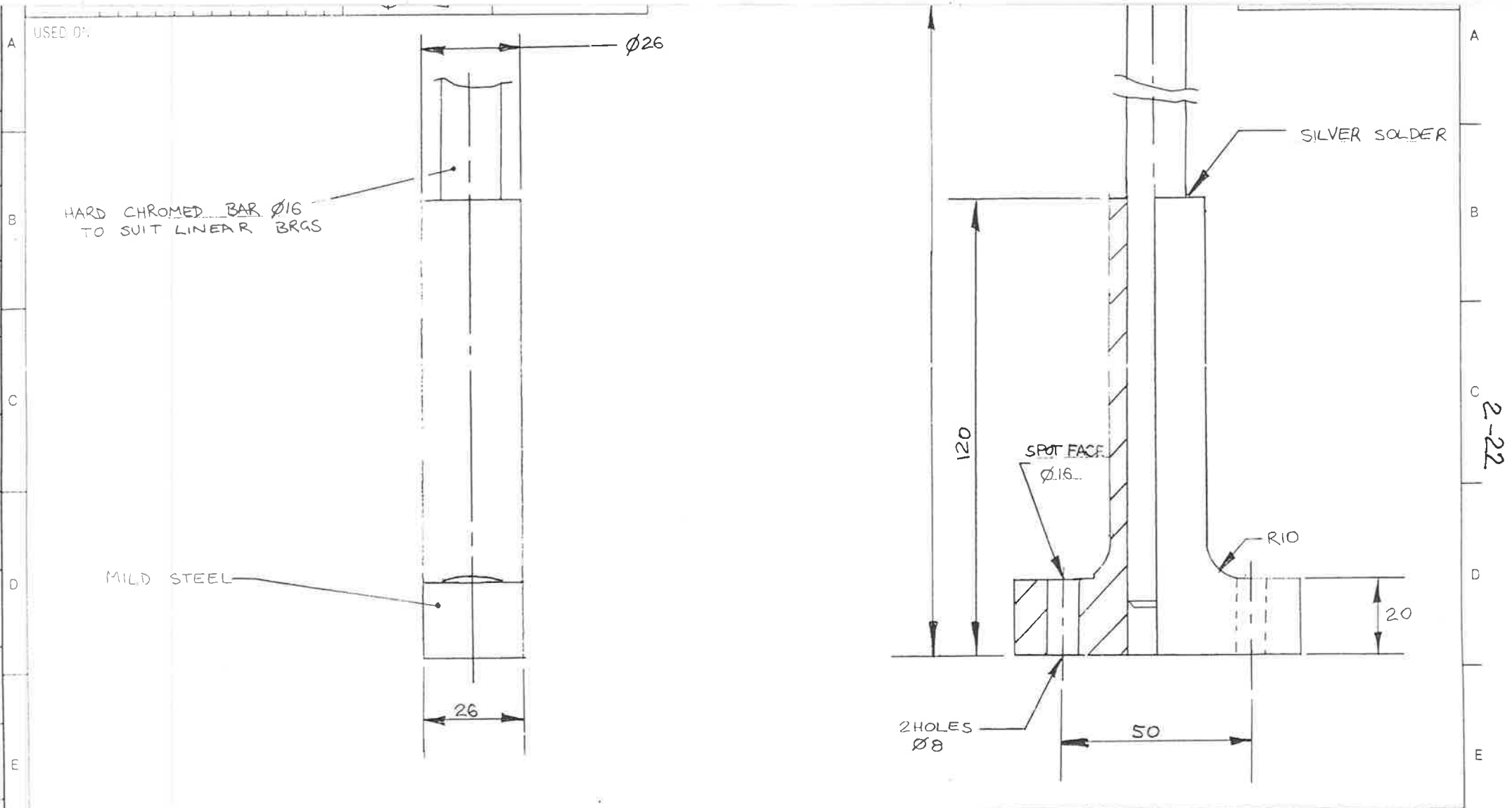
SECURITY CLASSIFICATION
CONTRACTORS DRG REF
DI SH NO


PARTS LIST



2-20

		DIMENSIONS IN mm		DEFENCE RESEARCH CENTRE SALISBURY		TITLE	
		TOLERANCES				PLATE - UPPER, DETAIL-ASSY	
		±5		DRAWING STANDARD		CODE IDENT NO	
				MATERIAL MILD STEEL		DRG NO	
				SPEC		Z0004	
				FINISH PAINT, ZINC PRIMER		O23	
DESCRIPTION		APP'D	CHK'D	APP'D/DATE	SCALE 1:2	EST. NO	70 1/2
UPPER BEARING PLATE ADDED BY 126 HOLES ADDED							



				DRN	PMC	 DEFENCE RESEARCH CENTRE SALISBURY		
				CHKD				
				APPD				
A - ORIGINAL				CONTRACTOR		TITLE GUIDE		
ISS GRID	DESCRIPTION	AUTH NO	DRN	CHKD	APP/DATE	CONTRACTORS DRF REF		
DIMENSIONS IN mm		MATERIAL AS SHOWN				CODE IDENT NO	DRG NO	SHEET SIZE A3
TOLERANCES ±1		SPECIFICATION				Z0004	024	
DRAWING STANDARD		FINISH ZINC PRIMER TO M.S.				SECURITY CLASSIFICATION	SCALE 1:1	EST MASS
1	2	3	4	5	6	7	8	

2-22

F

APPENDIX 3

PASCAL CODE FOR SOLUTION OF THE RICCATI EQUATION

```

program Riccati;
TYPE
  Matrix = ARRAY[1..9] OF ARRAY[1..9] OF REAL;
  Message=STRING[20];

VAR
  F,G,K,Ktrans,Q,P,R,Rinv,temp,next_F,Ereal,Eimag      :Matrix;
  check,old_check,diff                                 :REAL;
  M,N,I,J                                              :INTEGER;
  data                                                 :FILE OF REAL;
  error                                               :Message;
  answer                                              :CHAR;

LABEL The_End,input1,input2,input3,input4;

{$I Matprint }
{$I Matin }
{$I Multiply }
{$I Lyapunov }
{$I Transpose }
{$I Sum }
{$I Invert}
{$I QR }

BEGIN (* Riccati *)
  WriteLn('This program calculates the optimal feedback gains of a full state
  WriteLn('feedback system by solving the Riccati equation by Kleinmans method
  WriteLn(' system is:  $\dot{x} = Fx + Gu$ ,  $x(0) = x_0$ ,');
  WriteLn('           $u = Kx$ ');
  WriteLn;
  Assign(data,'ric.dta'); (* create a file called ric.dta before running this
  Reset(data);
  WriteLn('input the order of the system');
  ReadLn(N);
  WriteLn('input number of inputs');
  ReadLn(M);
  WriteLn('input new F?');
  input1:ReadLn(answer);
  CASE answer OF
    'Y','y':BEGIN
      WriteLn(' input F');
      Mat_input(N,N,F);
      FOR I:=1 TO N DO
        BEGIN
          FOR J:=1 TO N DO Write(data,F[I,J]);
        END;
      END;
    'N','n':BEGIN
      FOR J:=1 TO N DO
        BEGIN
          FOR J:=1 TO N DO Read(data,F[I,J]);
        END;
      END;
  ELSE
    WriteLn('input Y or N');
    GoTo input1;
  END;
  Mat_print(N,N,F);
  WriteLn('input new G?');
  input2:ReadLn(answer);
  CASE answer OF
    'Y','y':BEGIN
      WriteLn(' input G');
      Mat_input(N,M,G);
      FOR I:=1 TO N DO
        BEGIN

```

```

        FOR J:=1 TO M DO Write(data,G[I,J]);
    END;
END;
'N','n':BEGIN
    FOR I:=1 TO N DO
    BEGIN
        FOR J:=1 TO M DO Read(data,G[I,J]);
    END;
    END;
ELSE
    WriteLn('input Y or N');
    GoTo input2;
END;
Mat_print(N,M,G);
WriteLn('input new weighting matrix Q?');
input3:ReadLn(answer);
CASE answer OF
    'Y','y':BEGIN
        Mat_input(N,N,Q);
        FOR I:=1 TO N DO
        BEGIN
            FOR J:=1 TO N DO Write(data,Q[I,J]);
        END;
        END;
    'N','n':BEGIN
        FOR I:=1 TO N DO
        BEGIN
            FOR J:=1 TO N DO Read(data,Q[I,J]);
        END;
        END;
ELSE
    WriteLn('input Y or N');
    GoTo input3;
END;
Mat_print(N,N,Q);
WriteLn('input new weighting factor R?');
input4:ReadLn(answer);
CASE answer OF
    'Y','y':BEGIN
        Mat_input(M,M,R);
        FOR I:=1 TO M DO
        BEGIN
            FOR J:=1 TO M DO Write(data,R[I,J]);
        END;
        END;
    'N','n':BEGIN
        FOR I:=1 TO M DO
        BEGIN
            FOR J:=1 TO M DO Read(data,R[I,J]);
        END;
        END;
ELSE
    WriteLn('input Y or N');
    GoTo input4;
END;
Mat_print(M,M,R);
IF M=1 THEN      (* the invert routine won't handle 1x1 inverses! *)
BEGIN
    Rinv[1,1]:=1.0/R[1,1];
    WriteLn('Rinv=',Rinv[1,1]);
END
ELSE
BEGIN
    Invert(R,Rinv,M,error);
    Mat_print(M,M,R);
    IF error<>' ' THEN

```

```

BEGIN
  WriteLn(error);
  GoTo The_End;
END;
END;
WriteLn('input a starting feedback vector');
Mat_input(N,M,K);
Flush(data);
Close(data);
REPEAT
  Transpose(K,Ktrans,N,M);
  Multiply(G,Ktrans,temp,N,M,N);
  Sum(F,temp,next_F,N,N);
  QR(next_F,Ereal,Eimag,N); (* calc eigenvalues *)
  WriteLn;
  WriteLn('eigenvalues of closed loop system matrix:');
  FOR I:=1 TO N DO
  BEGIN
    WriteLn(Ereal[I,1]:10,' ',Eimag[I,1]:10);
  END;
  WriteLn;
  Multiply(K,R,temp,N,M,M);
  Multiply(temp,Ktrans,temp,N,M,N);
  Sum(Q,temp,temp,N,N);
  Lyapunov(next_F,P,temp,N);
  Multiply(P,G,temp,N,N,M);
  Multiply(temp,Rinv,temp,N,M,M);
  check:=0.0;
  FOR I:= 1 TO N DO
  BEGIN
    FOR J:=1 TO M DO
    BEGIN
      K[I,J]:=-temp[I,J];
      check:=check+Sqr(K[I,J]); (* 'check' is a measure of K's size *)
    END;
  END;
  diff:=old_check-check;
  old_check:=check;
  WriteLn('estimate of K is:');
  Mat_print(N,M,K);
UNTIL ABS(diff)<1E-3;
WriteLn('optimum feedback is:');
Mat_print(N,M,K);
The_End:END. (* Riccati *)

```